Title

Defining Metabolic Flexibility in Skin Carcinomas

Author

Galvan, Carlos

Publication Date

2024

Peer reviewed|Thesis/dissertation

UNIVERSITY OF CALIFORNIA

Los Angeles

Defining Metabolic Flexibility in Skin Carcinomas

A dissertation submitted in partial satisfaction of the requirements for the degree

Doctor of Philosophy in Molecular Biology

by

Carlos Galvan

2025

ABSTRACT OF THE DISSERTATION

Defining Metabolic Flexibility in Skin Carcinomas

by

Carlos Galvan

Doctor of Philosophy in Molecular Biology

University of California, Los Angeles, 2025

Professor William Edward Lowry, Chair

Among the numerous changes associated with the transformation to cancer, cellular metabolism is one of the first discovered and most prominent. Cancers were thought to be driven by metabolic changes including increased glycolysis and lactate generation. To that end, it was previously established that inhibition of pyruvate oxidation can promote glycolysis, and in some cases promote tumorigenesis. However, studies have identified cancers are metabolically flexible and can use multiple nutrients to sustain their growth. We previously showed that inhibition of glycolysis in cutaneous squamous cell carcinoma (SCC) initiating cells had no effect on tumorigenesis, despite the perceived ubiquity of the Warburg effect, which was thought to drive carcinogenesis. Instead, these SCCs were metabolically flexible and sustained growth through glutaminolysis, another metabolic process frequently implicated to fuel tumorigenesis in various cancers. Here we aim to understand metabolic flexibility in two types of skin cancer, SCC and melanoma. In SCC we focused on glutaminolysis and genetically blocked this process through glutaminase (GLS) deletion in SCC cells of origin. Genetic deletion of GLS had little effect on tumorigenesis due to the upregulated lactate consumption and utilization for the TCA cycle,

providing further evidence of metabolic flexibility. We went on to show that posttranscriptional regulation of nutrient transporters appears to mediate metabolic flexibility in this SCC model. To define the limits of this flexibility, we genetically blocked both glycolysis and glutaminolysis simultaneously and found that this abrogation of both of these carbon utilization pathways was enough to prevent both papilloma and frank carcinoma. In melanoma, we explored the role of pyruvate oxidation ability to drive melanoma formation through the deletion of mitochondrial pyruvate carrier 1 (Mpc1) in melanoma initiating cells. Using the Braf/Pten model, the best model available to study melanoma *in vivo*, we find that deletion of Mpc1 decreases melanoma formation. Although different models, these data point towards the treatment of cancer through metabolic manipulation and complete cancer abrogation will require multiple interventions on distinct pathways.

The dissertation of Carlos Galvan is approved.

Heather R. Christofk

David B. Shackelford

Brigitte N. Gomperts

Claudio Javier Villanueva

William Edward Lowry, Committee Chair

University of California, Los Angeles

2025

This dissertation is dedicated to my family for their continuous support, encouragement, and comfort throughout my academic journey.

My parents:

Norma Y. Galvan and Carlos M. Galvan

and to the first-generation Latino college students

TABLE OF CONTENTS

LIST OF FIGURES

Chapter 1

Chapter 2

Chapter 3

Chapter 4

List of tables

ACKNOWLEDGEMENTS

I would like to thank all the people that have encouraged and guided me throughout my academic journey. I joined the Lowry lab during the midst of the COVID-19 pandemic and appreciate Dr. William Lowry for taking me in and Dr. Aimee Flores for mentoring me during that time. The Lowry lab members have also been an essential part of my success as they have created a lab environment that I feel I can bring my whole self to. The thought provoking questions, mentorship, and support from my thesis committee was also key in the success of my projects in the lab. Furthermore, Dr. William Lowry has been understanding, empathetic, and allowed me to foster independence in the lab, as well as helped build my confidence as a scientist. My graduate program friends and the SACNAS at UCLA community have been an essential support system and motivation to continue to fulfill this degree. And of course, I'm so appreciative of my parents, sisters, cousins, tias and tios for always cheering me on and continuously telling me how proud they are of me.

Chapter 2, 3, 5 and Appendix is a version of Galvan C, Flores AA, Cerrillos V, Avila I, Murphy C, Zheng W, Christofk HR, Lowry WE. Defining metabolic flexibility in hair follicle stem cell induced squamous cell carcinoma. *Sci Adv*. 2024 Sep 20;10(38):eadn2806. doi: 10.1126/sciadv.adn2806. Epub 2024 Sep 20. PMID: 39303037; PMCID: PMC11414736.

Author contributions:

Conceptualization: C.G., W.E.L., H.R.C., A.A.F., W.Z., and I.A.

Methodology: C.G., W.E.L., V.C., A.A.F., and I.A.

Investigation: C.G., V.C., A.A.F., C.M., W.Z., and I.A.

Visualization: C.G., C.M., and I.A.

Supervision: C.G., W.E.L., and H.R.C.

Writing—original draft: C.G. and W.E.L.

Writing—review and editing: C.G., W.E.L., and I.A.

Funding: C.G. was supported by the Dermatological Scientist Training Program (NIH-NIAMS) T32AR071307. The project described was supported by award number R01AR070245 from the National Institute of Arthritis and Musculoskeletal and Skin Diseases and R01CA215185 from the National Cancer Institute. The content is solely the responsibility of the authors and does not necessarily represent the official views of the National Institutes of Health. C.G. was also supported by the UCLA Molecular Biology Interdepartmental Doctoral Program, the UCLA Eli and Edythe Broad Center of Regenerative Medicine, the Broad Stem Cell Research Training Program, and the Stem Cell Research Rose Hills Foundation Graduate Scholarship.

Chapter 4 and Appendix is a version of Seyran B*, Avila I*, Galvan C*, Robles G, Murphy C, Christofk H and Lowry WE. Inhibition of pyruvate oxidation diminishes melanoma progression. *Journal of Investigative Dermatology.* 2024 In Press.

Author contributions:

Conceptualization: WEL, BS

Investigation: CG, BS, IA, CM, GR

Data Curation: BS, IA, CG and HC

Supervision: WEL

Funding Acquisition: WEL and HC

Writing: BS,CG and WEL.

Funding: This work was funded by a BSCRC/Rose Hills Training Program to BS and CG, and by the NIH (R01AR070245-05).

We would also like to acknowledge the contributions of those that made this work possible, particularly the staff of core facilities at UCLA including the Genomics Core in the Department of Pathology, the Flow Cytometry Core in the Jonsson Comprehensive Cancer Center, and the Division of Laboratory Animal Medicine (DLAM). We would also like to thank members of the lab

and D. Shackelford for thoughtful comments on the manuscript. Schematic figures were created with BioRender.com.

VITA

EDUCATION

University of California, Los Angeles **2019-2025**
PhD Candidate, Molecular Biology (Cell and Developmental Biology)
University of California, Los Angeles **2015-2019**
B.S. Biochemistry

RESEARCH EXPERIENCE

University of California, Los Angeles **2019 – 2025**
Graduate Student Researcher; Advisor: William Lowry, PhD
University of California, Los Angeles **2016 – 2019**
Undergraduate Student Researcher; Advisor: Thomas Graeber, PhD
City of Hope **2018**
Intern Researcher; Advisor: Markus Müschen, PhD

PUBLICATIONS

Galvan C. and Lowry W. "Hangry hairs: intermittent fasting linked to hair loss" *Cell Research*, 2025.

Galvan C., Flores A., Cerrillos V., Avila I., Murphy C., Zheng W., Christofk H. and Lowry W. "Defining metabolic flexibility in hair follicle stem cell induced squamous cell carcinoma" *Science Advances*, 2024.

Seyran B.*, Avila I.*, **Galvan C.*,** Robles, G., Christofk H. and Lowry W. "Inhibition of pyruvate oxidation diminishes melanoma progression." *in Press at Journal of Investigative Dermatology*, 2024. *These authors contributed equally.

Galvan C. and Lowry W. "Yo-yoing stem cells defy differentiation dogma" *Nature News and Views,* 2023.

Galvan C., Tsoi J., Paraiso K., Graeber T.G. "IDH1 Metabolic Pathway Aids in Regulating Oxidative Stress" *UCLA Undergraduate Science Journal*, vol. 32, 2019.

Tsoi J., Robert L., Paraiso K., **Galvan C.,** Sheu K.M., Lay J., Wong D.J.L., Atefi M., Shirazi R., Wang X., Braas D., Grasso C.S., Palaskas N., Ribas A., and Graeber T.G. "Multi-stage Differentiation Defines Melanoma Subtypes with Differential Vulnerability to Drug-Induced Iron-Dependent Oxidative Stress." *Cancer Cell*. 2018;33(5):890-904.e5.

SELECTED HONORS AND AWARDS

***September 2024* - UCLA Molecular biology Institute Retreat Diversity, Equity, and Inclusion Award**

Award for individuals that have demonstrated a commitment to leadership, outreach, and service.

***December 2023* – UCLA Molecular, Cellular, and Developmental Biology Departmental Retreat Poster Award**

Poster: "Defining the Metabolic Flexibility of Hair Follicle Stem Cell Induced Squamous Cell Carcinoma.

***September 2023* – UCLA Molecular biology Institute Retreat Poster Award**

Poster: "Defining the Metabolic Flexibility of Hair Follicle Stem Cell Induced Squamous Cell Carcinoma.

***April 2023* – 2nd place in 2023 UCLA Broad Stem Cell Research Center Trainee Elevator Speech Contest**

Science in 60 seconds pitch explaining my research; developed skills necessary to talk about my research to any audience regardless of their level of scientific knowledge.

***October 2022* – Travel Award for the Society for Advancement of Chicanos and Native Americans in Science**

(SACNAS) Conference

Awarded travel award for SACNAS conference in San Juan, Puerto Rico. The SACNAS Conference focuses on National Diversity in STEM.

***September 2022 – Present* - UCLA Broad Stem Cell Research Center Fellow**

Training program for predoctoral students in the regenerative medicine and stem cell biology field.

***September 2022 – Present* – Rose Hills Foundation's Science and Engineering Scholar**

Nominated and awarded training program award to funding tuition and laboratory research supplies.

***February 2022* – Fontana Unified School District Article Feature**

Featured in the "Fontana Unified Alumnus Joins UCLA Doctoral Program to Pursue Cancer Research" article published by my K-12 school district describing my journey from Fontana to UCLA.

***November 2021* – UCLA Newsroom Feature**

Featured in the "'You belong': How first-gen students have succeeded in STEM" article touching on my experiences as a First-Generation student.

***July 2021 – July 2022* – UCLA Broad Stem Cell Research Center Fellow**

Training program for predoctoral students in the regenerative medicine and stem cell biology field.

***September 2020 – August 2021* – UCLA T32 Dermatology Scientist Trainee**

Training and career development program for predoctoral students pursuing career paths in investigative dermatology.

***June 2017 – June 2019* – Maximizing Access to Research Careers (MARC) Scholar**

Honors program that offers research training, financial support, mentoring, networking opportunities, and academic preparation.

***September 2015 – June 2016* - Program for Excellence in Education & Research in the Sciences (PEERS)**

Experience scientific poster sessions, lab tours, and panels with student researchers. Develop key strategies for success such as time management, effective study skills, and test preparation.

CHAPTER 1

INTRODUCTION

Cancer incidence, progression, treatments

Over the years cancer cases have increased due to several factors such as age, environmental exposures, or socioeconomic status. There were approximately 20 million new reported cancer cases in 2022, and 9.7 million deaths from cancer worldwide (1). This disease has become a global health issue, and the complexity of cancer requires a more complete understanding of exactly how cancer cells grow and become resistant to current treatments. In the United States, skin cancer is the most diagnosed type of cancer (2). There are multiple types of skin cancers, but the most common are squamous cell carcinoma (SCC) and basal cell carcinoma. The most deadly and invasive type of skin cancer is melanoma, which only accounts for 1% of all skin cancer cases. In the United States, however, melanoma accounts for the highest skin cancer related deaths and there are more than 8,000 people expected to die of melanoma in 2024 (3). All these skin cancers have similar risk factors such as chronic exposure to UV radiation, genetics, or increased age. Patients with skin cancers often have them surgically removed, however, upon late detection or if left untreated, cancer cells can spread throughout the body and become lethal. At times, surgical resection is not enough to fully eliminate the cancer, so they often need a more aggressive type of intervention such as radiation therapy, immune therapy or targeted drug therapy.

Here, we focused primarily on SCC and identify how this cancer is growing to target its metabolism as a potential therapeutic. Additionally, we include work on melanoma and how targeting metabolism in this cancer influences its progression and invasiveness. These studies demonstrate the effectiveness of manipulating metabolism in cancer and elucidate new therapeutic targets in skin cancers.

Squamous cell carcinoma – mutations, risks and stages

Squamous cell carcinoma (SCC) is known to initiate in the epidermis due to an accumulation of mutations in genes such as RAS, NOTCH, P53, CDKN2A, etc. (4–9). Hair follicle stem cells (HFSCs) are adult stem cells that reside in the epithelial bulge of the hair follicle and are normally quiescent (10). Although critical for maintaining hair growth, wound healing, and hair follicle formation in the skin, we and others showed that these cancers can arise due to transformation particularly of HFSCs using murine transgenic and chemically induced carcinogenesis protocols (11–13). Upon oncogenic mutations of p53 and Kras in various cells within the hair follicle, HFSCs were the only cells that had the capacity to initiate SCCs (12).

The most common risk factor for developing SCC is chronic exposure to ultraviolet (UV) radiation, typically causing SCC to develop in regions of the body that are exposed to the sun, such are head, neck, and limbs. There is also an increased risk of developing SCC with age or due to genetics. Usually, SCC are treated by surgical removal, however, SCC can metastasize at later stages making surgical removal not sufficient to eliminate the cancer. Additionally, after surgical removal of an SCC, the cancer can recur with a higher risk of metastasis to lymph nodes or other cutaneous areas such as ears and lip (14). SCC can also arise in or spread to other areas that are much more difficult to treat such as in the head and neck, leading to much higher rates of mortality (7,15). Interestingly, SCC is the most common cancer that develops in organ transplant patients. Typically, organ transplant patients have higher risk of SCC after their transplants due to immunosuppressive medication (16). Studies have found that this increase in SCC risk and development with immunosuppression can be due to the types of immunosuppressive drugs patients take such as azathioprine (17). This drug is primarily used to prevent transplant rejection; however, this drug can induce DNA damage and mutagenesis associated with SCC (18).

In patients, SCC are primarily staged 1-4 by histology based on the percentage of well-differentiated cells vs undifferentiated cells in the tumor (14). Well-differentiated cells in a cancer

setting can be described as cancer cells that look like cells from the normal tissue the cancer came from (19). Undifferentiated or poorly differentiated cells in cancer lack specialized structure or functions and have a better ability to grow and spread faster than well-differentiated cells (20). That said, when characterizing the histology of tumors, the higher the percentage of undifferentiated cells vs well-differentiated cells, the higher the stage of the SCC (14). Aside from the type of differentiated cells present in tumors, the location of tumors also plays a role in staging. A stage 1, SCC is observed in the epidermis or has spread to other layers of the skin. During stage 2 of SCC, the cancer spread into other layers of the skin, but cells have more characteristics that have the ability to spread to adjacent lymph nodes or other healthy organs (21). At stage 3, the cancer reaches lymph nodes in proximity but has not invaded other tissues (21). SCCs detected at stage 4 have spread to lymph nodes, but likely have also metastasized to other tissues such as brain, lung, or liver (21).

Melanoma – mutations, risks, and stages

Melanoma is highly mutated with common mutations being $BRAF^{V600}$, PTEN, NRAS, NF1, etc. (22). Melanocyte stem cells are cells that have the primary role of creating pigment producing cells called melanocytes (23). Melanocytes normally produce melanin, which is a brown pigment that gives skin its color and protects the skin from some of the sun's damaging effects (23). Upon oncogenic mutations, melanocytes grow uncontrollably and give rise to melanoma (23–26). Although a less common type of skin cancer, melanoma is the most deadly due to its increased ability to spread throughout the body (3).

Lighter skin individuals are more likely to develop melanoma. Increased age and genetics are also risk factors for developing melanoma (3). Like SCC, chronic exposure to UV radiation is linked with development of this cancer (3). Patients with melanoma can get the cancer surgically removed if detected early, but majority of the cases require more aggressive treatments due to the highly metastatic nature of the cancer. Therapies like immunotherapy and targeted drug

therapies have spiked in interest to treat this cancer (27). At times, the aggressiveness and plasticity of this cancer requires more than one therapy. For example, melanomas that are resistant to targeted therapies, have been found to be sensitive to another form of cell death called ferroptosis (28).

Melanoma in the clinic is classified in stages 0-4. During stages 0-2 the melanoma has not spread to distance lymph nodes and is subcategorized based on thickness or ulceration (29). Initially, the larger the tumor, measured by thickness, the higher the stage (29). However, in later stages such as 3 and 4, thickness is dispensable. Metastasis begins to occur in stage 3, as the melanoma spread to lymph nodes or neighboring areas in the skin, however, the cancer has not spread to other healthy tissues at this stage(29). Stage 4 is characterized like stage 3 but, the melanoma has spread to other tissues such as lungs, brain, and spinal cord (29).

Energy Metabolism and the Warburg Effect

Cells have demands for energy to survive and produce ATP to sustain themselves. During the process of cellular respiration, cells utilize glucose to generate large amounts of ATP in the presence of oxygen. Glucose is broken down through glycolysis, and then enters the TCA cycle to undergo oxidative phosphorylation leading to the generation of ATP. Although unfavorable, cells can also generate ATP via fermentation, which occurs in the absence of oxygen (anaerobic), and results in glucose being metabolized to produce lactate (30,31). This process is unfavorable because it produces a much lower amount of ATP compared to respiration.

For many years, the field of cancer metabolism revolved around a theory proposed by Otto Warburg, known as the Warburg Effect. He believed that cancer cells had defective mitochondria causing the shift from oxidative phosphorylation to glycolysis as their energy source in the presence or absence of oxygen (30,31). Furthermore, cancer cells exhibited a shift in their metabolism to favor glycolysis and lactate production (30). However, over the years,

studies have shown that in cancer cells, mitochondrial respiration remains functional while still exhibiting high glucose utilization for lactate production (32). Moreover, instead of switching from one pathway to another, cancer cells simply reprogram their metabolism for growth favoring glycolysis. The reprograming of metabolism in cancer cells has now become an emerging hallmark of cancer as it is essential for proliferation, tumorigenesis, and metastasis of cancer (33). Initially, lactate was thought to just be a “waste” product during glycolysis, however, recent studies have found that lactate can drive various processes that benefit cancer cells (34). The accumulation of lactate can acidify the tumor microenvironment which promotes angiogenesis, immune resistance, and metastasis (34). Additionally, cancer cells can take up and oxidize lactate to enter the TCA cycle as an energy source (35–38). Due to the new discoveries of cancer metabolism over the years, many studies have focused on nutrients that contribute to cancer growth and energy, primarily concentrating on glucose, lactate, and more recently, glutamine (Figure 1).

Glucose uptake and metabolism in cancer

Glucose is one of the main sources of energy for cancer cells and the increase in glucose uptake is facilitated by the increase expression of glucose transporters (GLUTs) (39). In normal physiology, there are 14 known GLUTs, however, GLUT1 has elevated expression levels in various cancer (Figure 1) (39,40). Once glucose enters the cells, it is metabolized via glycolysis using several enzymes that catalyze this process. Hexokinase (HK) catalyzes the first step of glycolysis and has four isoforms with HK2 being most prevalent in cancer (41). Enolase (ENO) is the enzyme that converts 2-phophoglycerate (2PG) to phosphoenolpyruvate (PEP). This reaction is at the latter half of glycolysis, but the overexpression of ENO has been linked to increased tumorigenesis, overall cancer survival, angiogenesis, and many more pro-tumorigenic properties (41). There are three isoforms of ENO, and each is overexpressed in cancers based on the type of cancer and tissue (42). Glucose is then metabolized into pyruvate,

and pyruvate can enter the TCA cycle via mitochondrial pyruvate carrier 1 (Mpc1) to further be used for oxidative phosphorylation (Figure 1). However, as previously mentioned, pyruvate generally favors producing lactate instead of entering the mitochondria for ATP production via TCA and oxidative phosphorylation.

Lactate generation and transport in cancer

Pyruvate and NADH can be converted into lactate and NAD+ by the enzyme Lactate dehydrogenase (LDH) (Figure 1) (43). LDH has multiple isoforms, but in tumors, LDHA is one of the most studied in cancer because it is overexpressed in nearly every solid tumor and is elevated in aggressive cancers (41). Interestingly, although not an energetically favorable reaction, LDHA can also catalyze the reversible reaction to convert lactate into pyruvate (44). This reverse conversion is typically observed in cases where cancers use lactate as an energy source and convert it to pyruvate to fuel the TCA cycle (45). Lactate is transported in and out of the cell using monocarboxylate transporters (MCTs). There are four MCT isoforms that can transport lactate, but MCT1 and MCT4 have been observed most dominant in cancer (Figure 1). It's also important to note that MCT1 can also facilitate pyruvate transport (46).

Glutaminolysis in cancer

A process known as glutaminolysis has been shown to replenish the TCA cycle in conditions where glucose metabolism favors lactate production instead of fueling the TCA cycle. During this process the amino acid glutamine is taken up by cells, converted to glutamate, and glutamate can then be converted to alpha-ketoglutarate and enter the TCA cycle (Figure 1) (47). This process has been seen in multiple cancers and show that glutamine can sustain cancer cell growth both *in vitro* and *in vivo* (48–51). Cancer cells take up glutamine using the transporter SLC1A5 (ASCT2) and once in the cell, glutamine enters the mitochondria to be converted into glutamate by the enzyme glutaminase (GLS) (52,53). From here, glutamate can

continue with glutaminolysis and be converted into alpha-ketoglutarate to fuel the TCA cycle using the enzyme glutamate dehydrogenase. Although essential for replenishing the TCA cycle in cancer, glutamate can also have other roles in the cell (52). Glutamate can be directed to produce non-essential amino acids such as alanine, aspartate, and phosphoserine. It can also generate glutathione (GSH) which plays a crucial role in redox homeostasis. Additionally, it can act as a signaling molecule to regulate pathways important for cancer maintenance such as mTOR. Although glutamate has essential roles in the cell, the generation of glutamate by glutamine is dependent on GLS. This enzyme has two isoforms, GLS1 and GLS2, with GLS1 generally being overexpressed in cancer and GLS2 being suppressed in cancers (47,54).

Measuring metabolic flux in cancer

The glucose transporter, GLUT1, is highly expressed in cancers and studies used this finding to create an imaging technique to readout glucose uptake *in vivo*, called Fluorodeoxyglucose-positron-emission tomography (FDG-PET) (55). This technique is used on patients to detect tissues or tumors that exhibit high amounts of glucose uptake. Patients are injected with the radiotracer, ^{18}F-FDG, and then scanned using PET. FDG is a glucose analog and can enter the cells via glucose transporters, however it cannot be metabolized like glucose and accumulates to give a readout of relative glucose uptake (56). In the lab, FDG-PET can also be used to understand glucose uptake in murine models, but because this technique only gives a readout of glucose uptake and not glucose metabolism.

Carbon-13 isotope tracing can be used *in vivo* or *in vitro* to understand the flux of metabolic pathways in cells, tissues, or cancer. In tumors, the most common carbon tracers used are ^{13}C-6 D-Glucose, ^{13}C-5 L-Glutamine, and ^{13}C-3-Lactate as these three nutrients are most prominent for energy generation in cancer cells. The labeled nutrient is introduced to cultured cells, organoids, or mouse models and can enter cells and be metabolized. The metabolite intermediates and products derived from labeled nutrients are labeled with the

carbon-13 isotope which can be detected through mass spectrometry. Glucose, glutamine, and lactate carbon labeling all give a deeper understanding of what pathways these nutrients contribute to cancer metabolism and during metabolic flexibility.

Metabolic flexibility in cancer

Metabolic reprograming has been established as a new hallmark of cancer as cancer cells are flexible and can adapt for survival (57). Studies have demonstrated evidence of metabolic flexibility when targeting glycolysis, the process that was believed to be the main fuel source for cancer cells. Studies in lung cancer have shown upon inhibition of glycolysis via mTOR manipulation, cancer cells adapt and use glutamine as a primary source for energy (58). Another study inhibited glycolysis using PI3K/mTOR inhibitors but found that cancer cells instead take up lactate and use it for the TCA cycle (59). Interestingly a study using lactate carbon-13 labeling in human patients with lung cancer showed that lactate contributed more to the TCA cycle than glucose metabolism (45). During metastasis, metabolic flexibility also comes into play. For example, a study focusing on breast cancer cell metastasis to the brain demonstrated that in the absence of glucose, cancer cells survived because of compensation from gluconeogenesis, glutamine, and branched chain amino acids (60). Gluconeogenesis uses lactate or other amino acids to generate glucose. This process has been observed in cancer and in some cases is key for metabolic flexibility.

The general theme with cancer survival and metabolism is that cancer cells adapt and use nutrients they have available to them. Since many studies have focused on targeting glycolysis, cancer cells have relied heavily on other nutrients like lactate or glutamine. This could be due to the increased concentration of these nutrients in cancer compared to physiological levels. Due to the increased production of lactate in cancer, the concentration of lactate in the blood increases to 10-30mM, where physiological concentration of lactate is 1.5-3mM (34). Of all circulating amino acids in plasma, glutamine is the most abundant at

concentrations of 0.6-0.9 mmol/l (61). Since glutamine can also fuel cancer cells, it's likely that availability of this amino acid in plasma plays a role in its increased use in cancer. Therefore, when studying metabolism in cancer, it is important to keep in mind that metabolic flexibility is likely to occur, and the model used should allow for this flexibility.

Modeling cancer *in vitro* and *in vivo*

For therapies to reach human subjects, therapies need to be tested in an *in vivo* system prior to clinical trials. Many times, discovery studies begin using *in vitro* cell culture where cancer cells are cultured in a dish as a two-dimensional layer (Figure 2A). Recently, organoids have become a revolutionary model to study cell-cell interactions in a disease environment. Organoids are also grown *in vitro* in a dish but employ a three-dimensional structure (Figure 2A). This framework has its advantages over two-dimensional culture for disease modeling due to their cellular complexity and similarities to disease environments and physiology. Using culture models has many advantages for cancer research such as the ease of controlling the environments of cells in a dish, ease of using multiple treatments/drugs screenings, and ability to genetically manipulate genes to study initiation or progression of cancer. However, the mammalian body is such an interconnected system that studying cancer using *in vivo* systems is essential to move forward with reproducibility and effectiveness in humans. Depending on the disease or condition studied, many *in vivo* models exist such as mice, drosophila, zebrafish, or *C.elegans*.

The best and most common model to study cancer are mouse models since they are genetically and biologically similar to humans (62). Due to significant effort in the field, genetically engineered mice and systems aid in recapitulating human mutations in mice (Figure 2A) (62). Since metabolism is required for growth and tumorigenesis, many studies have focused on identifying targets that manipulate metabolism in cancer to decrease proliferation or simply kill the cancer. However, most of the time small molecule inhibitors developed to target a

single pathway show promise in an *in vitro* model, but when used in an *in vivo* model, doesn't have the same effect. Many small molecule inhibitors targeting metabolism have failed *in vivo,* likely due to metabolic flexibility of cancer. *In vivo*, cancer cells potentially have access to a much more sophisticated environment due to the presence of vasculature, circulation, lymphatics, the nervous system, the immune system, etc. Therefore, it is possible that blockade of an individual pathway *in vitro* blocks cell growth simply because nutrients that allow for flexibility are not present in cell culture systems. Thus, it is important to model cancer using *in vivo* models when studying cancer metabolism so they can have access to circulating blood, or other ways to fulfill flexibility and survival.

Studies have also taken advantage of both *in vivo* and *in vitro* models in combination to further study disease. Both models can be used to study tumors derived from human patients. Because we can't test specific hypotheses on human patients, using human derived cells to culture in two- or three-dimensions and add to an *in vivo* model allows us to experiment using cells that are most accurately representing human cancer (Figure 2B). Additionally, it is advantageous to culture mouse derived tumor cells to model a more accurate profile of cells *in vivo*. Many times, aggressive cancers like melanoma develop so quickly that treatments and longitudinal studies can't be conducted because of overall mouse health and ethical regulations. Therefore, collecting the cancer cells from mice and culturing them captures cells with an *in vivo* background and allows for detailed experiments to fully characterize these cells and treatment approaches (Figure 2C).

Modeling Squamous Cell Carcinoma

Hair follicle stem cells (HFSCs) have been identified as cancer initiating cells in murine models upon oncogenic mutations like KRAS and p53 (12). Using a Keratin 15 (K15) promoter to target HFSCs specifically, we have been able to study SCC initiation and progression under wild-type and different knockout conditions. To grow SCC, we used a well-established skin

chemical carcinogenesis murine model of SCC to allow for the deletion of metabolic activity just prior to induction of oncogenesis in adult mice. The two-stage skin carcinogenesis utilizes a mutagen, 7,12-dimethylbenz-[a]- anthracene (DMBA), and a tumor growth-promoting agent, 12-*O*-tetradecanoylphorbol-13-acetate (TPA), to induce stimuli driving transformation (63,64). Shortly after topical application of DMBA onto the dorsal skin of mice, there are mutations in the RAS family of proto-oncogenes in the bulge region of the hair follicle (64). Then, after continual delivery of the TPA promoting agent, the stem cell region of the hair follicle increases DNA synthesis and cell proliferation, developing clonal outgrowths called papilloma (64). Papilloma then transform into SCC and at the genetic level, correlating with trisomy of chromosomes 6 and 7 and mutations in TP53 (64).

In vitro models have been used to study SCC, however, *in vivo* models have more of a resemblance to the human SCC and tumor microenvironment (65). The two-stage DMBA-TPA skin chemical carcinogenesis model we use is advantageous as it recapitulates mutations, pathology, and genetic changes seen in human SCCs. This process takes about 10-15 weeks to generate benign tumors and 20-30 weeks to generate SCC, so this model also allows us to study the entire initiation and progression of this cancer. Thus, aside from understanding how to target this cancer, we are able to understand the metabolism during the initiation and progression of SCC that can lead to therapeutics for the prevention of this cancer as well. Additionally, using this *in vivo* model recapitulates the architecture and cellular composition of the skin to tumor transition and elucidates the characteristics of natural regenerative properties in mammals to contribute to the overall knowledge of stem cell maintenance and reversibility.

Modeling Melanoma

Melanocyte stem cells (MeSCs) are adult stem cells that reside the hair follicle bulge and function to generate melanocytes for pigmentation (23). Upon oncogenic mutations in MeSCs, these cells give rise to melanoma. Over the years, scientists have used both *in vitro* and *in vivo*

models to study melanoma. Studies beginning to explore potential targets for melanoma usually being in two-dimensional cell culture but are not the most realistic model to study melanoma since done *in vitro* (Figure 2A) (66). Moreover, melanoma in culture is primarily used for high throughput screens that give insights to melanoma tumorigenesis or targeted therapies (66).

One of the most common *in vivo* models used to study melanoma is the BRAF/PTEN genetically engineered mice model (24). Human melanomas express the BRAF mutation and activation of pro-cancer kinases due to the silencing of tumor suppressor gene PTEN (26). With BRAF and PTEN mutations the most expressed mutations in melanoma, scientists have generated mouse models with Cre-inducible systems to induce the activation of the BRAF mutation and loss of PTEN specifically in cancer initiating melanocytes (Figure 2A) (26). This BRAF/PTEN mouse model also metastasizes to lymph nodes and other organs, similar to human melanoma (26). Histology of melanomas in the mouse model also exhibit proliferative characteristics and pathology as seen in human melanoma (26). Moreover, this *in vivo* mouse model exhibits genetic, pathological, and metastatic characteristics that recapitulate melanoma seen in human patients. Using these genetically engineered mice, genes can also be manipulated to study drug targets and sensitivity in different types of staged melanoma (66). Due to the aggressive nature of this cancer, ethical protocols, and lethality of melanoma in mice restrict the study of later stages of melanoma at times, melanoma cells from *in vivo* models are collected and cultured to study melanoma transformation and targets (Figure 2C). The advantage of collecting cells from an *in vivo* mouse model for culture is that the cancer cells have already become adjusted to the tumor microenvironment and can continue to exhibit the genetic manipulations done in the mouse. Another common approach to study anti-melanoma drugs is using Xenograft models (Figure 2B) (25). In these models, immunocompromised mice are injected with human melanoma cells giving researchers a model where the human derived melanoma can be studied in an *in vivo* setting where cells can interact with the tumor microenvironment and blood vessels in a mammalian system (66).

Preface

SCC demonstrates metabolic flexibility; however, the nature and limits of this flexibility are not fully understood. In melanoma, the metabolic flexibility and manipulation of metabolism by targeting pyruvate oxidation warrants further investigation. Work in Chapter 2 and 3 highlight key metabolic pathways cancer cells use to adapt and survive. Moreover, Chapter 3 focuses on how nutrient transporters are mediating this adaptability. The limits of metabolic flexibility in SCC have not been defined and Chapter 2 highlights a combination of targets to prevent SCC tumorigenesis. In Chapter 4, we explore how targeting metabolism in melanoma influences tumor progression and discover how effective the deletion of Mpc1 is in this cancer. The work from this thesis aims to address (1) how metabolically flexible these cancers are (2) mechanisms to metabolic flexibility (3) limits of metabolic flexibility and (4) elucidate new potential therapeutic targets for skin cancers.

FIGURES

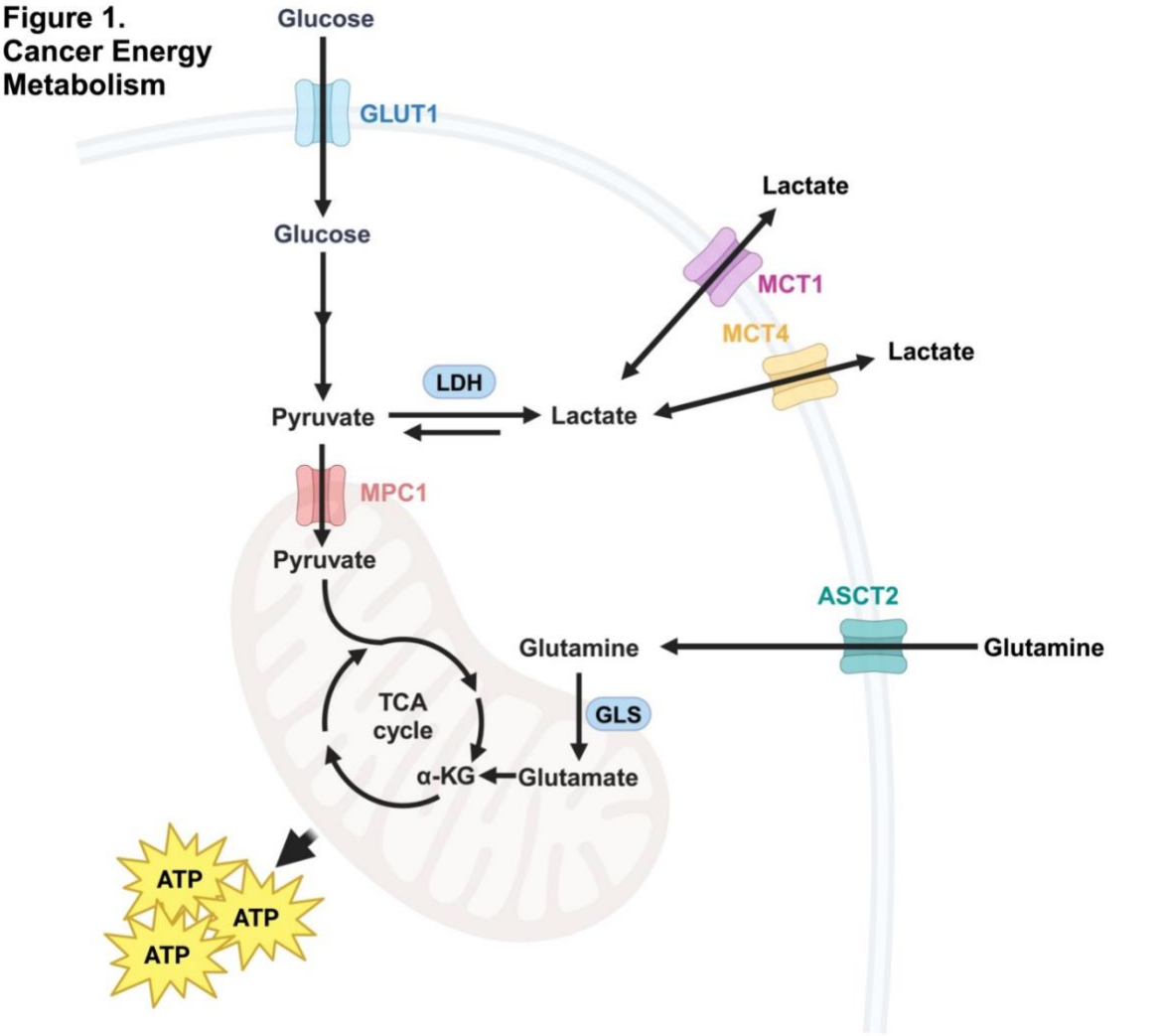

Figure 1 Cancer Energy Metabolism Glucose is transported into the cell through glucose transporter GLUT1 and undergoes glycolysis to produce pyruvate. Pyruvate can then produce Lactate through the enzyme Lactate Dehydrogenase (LDH), or it can enter the mitochondria via the Mitochondrial Pyruvate Carrier (MPC1) to then fuel the TCA cycle. Lactate can be transported in and out of the cell by monocarboxylate transporters 1 (MCT1) and 4 (MCT4). Glutamine can also enter the cell through Glutamine transporter ASCT2, and then enter the mitochondria to be converted to Glutamate via Glutaminase (GLS). That Glutamate can then be converted int alpha-ketoglutarate (a-KG) to fuel the TCA cycle and generate ATP.

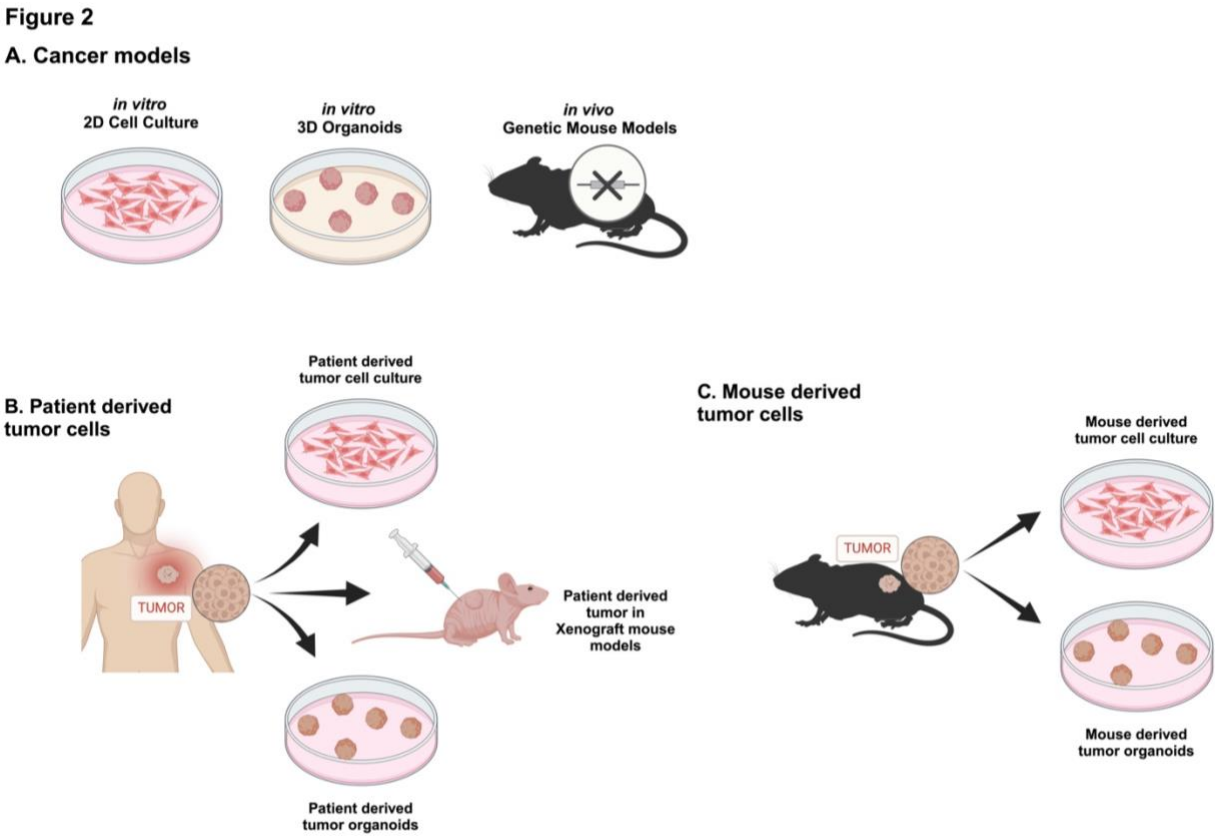

Figure 2 Models to study cancer

A. Cells can be cultured in a two-dimensional layer or in three dimensional organoids *in vitro*. Genetic mouse models are *in vivo* models that can manipulate genes to study the effects of those genes in disease. **B.** Tumor cells can also be derived from patients and be cultured in a two-dimensional layer or as organoids *in vitro*. Patient derived tumor cells can also be administered into *in vivo* Xenograft mouse models. **C.** Tumor cells generated on mice can be collected for *in vitro* culture as well.

REFERENCES

1. Bray Bsc F, Laversanne | Mathieu, Hyuna |, Phd S, Ferlay J, Siegel Mph RL, et al. Global cancer statistics 2022: GLOBOCAN estimates of incidence and mortality worldwide for 36 cancers in 185 countries. CA Cancer J Clin [Internet]. 2024 May 1 [cited 2024 Oct 1];74(3):229–63. Available from: https://onlinelibrary.wiley.com/doi/full/10.3322/caac.21834
2. Cancer Facts & Figures 2024 | American Cancer Society [Internet]. [cited 2024 Oct 1]. Available from: https://www.cancer.org/research/cancer-facts-statistics/all-cancer-facts-figures/2024-cancer-facts-figures.html
3. What Is Melanoma Skin Cancer? About Melanoma Skin Cancer.
4. van der Schroeff JG, Evers LM, Boot AJM, Bos JL. Ras Oncogene Mutations in Basal Cell Carcinomas and Squamous Cell Carcinomas of Human Skin. Journal of Investigative Dermatology. 1990 Apr 1;94(4):423–5.
5. Pierceall WE, Mukhopadhyay T, Goldberg LH, Ananthaswamy HN. Mutations in the p53 tumor suppressor gene in human cutaneous squamous cell carcinomas. Mol Carcinog [Internet]. 1991 Jan 1 [cited 2024 Oct 2];4(6):445–9. Available from: https://onlinelibrary.wiley.com/doi/full/10.1002/mc.2940040606
6. Nassar D, Latil M, Boeckx B, Lambrechts D, Blanpain C. Genomic landscape of carcinogen-induced and genetically induced mouse skin squamous cell carcinoma. Nature Medicine 2015 21:8 [Internet]. 2015 Jul 13 [cited 2024 Oct 2];21(8):946–54. Available from: https://www.nature.com/articles/nm.3878
7. Prevalence of RAS oncogene mutation in head and neck carcinomas - PubMed [Internet]. [cited 2024 Oct 2]. Available from: https://pubmed.ncbi.nlm.nih.gov/1361585/
8. Chang D, Shain AH. The landscape of driver mutations in cutaneous squamous cell carcinoma. npj Genomic Medicine 2021 6:1 [Internet]. 2021 Jul 16 [cited 2024 Oct 2];6(1):1–10. Available from: https://www.nature.com/articles/s41525-021-00226-4

9. Nichols AC, Yoo J, Palma DA, Fung K, Franklin JH, Koropatnick J, et al. Frequent Mutations in TP53 and CDKN2A Found by Next-Generation Sequencing of Head and Neck Cancer Cell Lines. Arch Otolaryngol Head Neck Surg [Internet]. 2012 Aug 1 [cited 2024 Oct 6];138(8):732–9. Available from: https://jamanetwork.com/journals/jamaotolaryngology/fullarticle/1351925

10. Flores A, Schell J, Krall AS, Jelinek D, Miranda M, Grigorian M, et al. Lactate dehydrogenase activity drives hair follicle stem cell activation. Nature Cell Biology 2017 19:9 [Internet]. 2017 Aug 14 [cited 2024 Oct 6];19(9):1017–26. Available from: https://www.nature.com/articles/ncb3575

11. Lapouge G, Youssef KK, Vokaer B, Achouri Y, Michaux C, Sotiropoulou PA, et al. Identifying the cellular origin of squamous skin tumors. Proc Natl Acad Sci U S A [Internet]. 2011 May 3 [cited 2024 Oct 6];108(18):7431–6. Available from: https://www.pnas.org/doi/abs/10.1073/pnas.1012720108

12. White AC, Tran K, Khuu J, Dang C, Cui Y, Binder SW, et al. Defining the origins of Ras/p53-mediated squamous cell carcinoma. Proc Natl Acad Sci U S A [Internet]. 2011 May 3 [cited 2024 Oct 6];108(18):7425–30. Available from: https://www.pnas.org/doi/abs/10.1073/pnas.1012670108

13. Li S, Park H, Trempus CS, Gordon D, Liu Y, Cotsarelis G, et al. A keratin 15 containing stem cell population from the hair follicle contributes to squamous papilloma development in the mouse. Mol Carcinog [Internet]. 2013 Oct [cited 2024 Oct 6];52(10):751. Available from: /pmc/articles/PMC3424369/

14. Que SKT, Zwald FO, Schmults CD. Cutaneous squamous cell carcinoma: Incidence, risk factors, diagnosis, and staging. J Am Acad Dermatol [Internet]. 2018 Feb 1 [cited 2024 Oct 6];78(2):237–47. Available from: http://www.jaad.org/article/S0190962217323253/fulltext

15. Prince MEP, Ailles LE. Cancer stem cells in head and neck squamous cell cancer. Journal of Clinical Oncology [Internet]. 2008 [cited 2024 Oct 6];26(17):2871–5. Available from: https://ascopubs.org/doi/10.1200/JCO.2007.15.1613

16. Garrett GL, Blanc PD, Boscardin J, Lloyd AA, Ahmed RL, Anthony T, et al. Incidence of and Risk Factors for Skin Cancer in Organ Transplant Recipients in the United States. JAMA Dermatol [Internet]. 2017 Mar 1 [cited 2024 Oct 2];153(3):296–303. Available from: https://jamanetwork.com/journals/jamadermatology/fullarticle/2596399

17. Blue ED, Freeman SC, Lobl MB, Clarey DD, Fredrick RL, Wysong A, et al. Cutaneous Squamous Cell Carcinoma Arising in Immunosuppressed Patients: A Systematic Review of Tumor Profiling Studies. JID Innov. 2022 Jul 1;2(4):100126.

18. Jiyad Z, Olsen CM, Burke MT, Isbel NM, Green AC. Azathioprine and Risk of Skin Cancer in Organ Transplant Recipients: Systematic Review and Meta-Analysis. American Journal of Transplantation. 2016 Dec 1;16(12):3490–503.

19. Definition of differentiation - NCI Dictionary of Cancer Terms - NCI [Internet]. [cited 2024 Oct 6]. Available from: https://www.cancer.gov/publications/dictionaries/cancer-terms/def/differentiation

20. Definition of undifferentiated - NCI Dictionary of Cancer Terms - NCI [Internet]. [cited 2024 Oct 6]. Available from: https://www.cancer.gov/publications/dictionaries/cancer-terms/def/undifferentiated

21. Squamous Cell Carcinoma Stages | Moffitt [Internet]. [cited 2024 Oct 6]. Available from: https://www.moffitt.org/cancers/squamous-cell-carcinoma/diagnosis/stages/

22. Davis EJ, Johnson DB, Sosman JA, Chandra S. Melanoma: What do all the mutations mean? Cancer [Internet]. 2018 Sep 9 [cited 2024 Oct 6];124(17):3490. Available from: /pmc/articles/PMC6191351/

23. Lang D, Mascarenhas JB, Shea CR. Melanocytes, melanocyte stem cells, and melanoma stem cells. Clin Dermatol [Internet]. 2013 Mar [cited 2024 Oct 6];31(2):166. Available from: /pmc/articles/PMC3582991/

24. Damsky WE, Bosenberg M. Mouse melanoma models and cell lines. Pigment Cell Melanoma Res [Internet]. 2010 Dec 1 [cited 2024 Oct 6];23(6):853–9. Available from: https://onlinelibrary.wiley.com/doi/full/10.1111/j.1755-148X.2010.00777.x

25. Kuzu OF, Nguyen FD, Noory MA, Sharma A. Current State of Animal (Mouse) Modeling in Melanoma Research. Cancer Growth Metastasis [Internet]. 2015 Jan [cited 2024 Oct 6];8(Suppl 1):81. Available from: /pmc/articles/PMC4597587/

26. Dankort D, Curley DP, Cartlidge RA, Nelson B, Karnezis AN, Damsky WE, et al. BrafV600E cooperates with Pten loss to induce metastatic melanoma. Nature Genetics 2009 41:5 [Internet]. 2009 Mar 12 [cited 2024 Oct 6];41(5):544–52. Available from: https://www.nature.com/articles/ng.356

27. Rashid S, Shaughnessy M, Tsao H. Melanoma classification and management in the era of molecular medicine. Dermatol Clin [Internet]. 2023 Jan 1 [cited 2024 Oct 6];41(1):49–63. Available from: https://www.mayoclinic.org/diseases-conditions/melanoma/symptoms-causes/syc-20374884

28. Tsoi J, Robert L, Paraiso K, Galvan C, Sheu KM, Lay J, et al. Multi-stage Differentiation Defines Melanoma Subtypes with Differential Vulnerability to Drug-Induced Iron-Dependent Oxidative Stress. Cancer Cell. 2018 May 14;33(5):890-904.e5.

29. Stages of Melanoma Skin Cancer | American Cancer Society [Internet]. [cited 2024 Oct 6]. Available from: https://www.cancer.org/cancer/types/melanoma-skin-cancer/detection-diagnosis-staging/melanoma-skin-cancer-stages.html

30. WARBURG O. On the origin of cancer cells. Science. 1956 Feb 24;123(3191):309–14.

31. WARBURG O. On respiratory impairment in cancer cells. Science. 1956 Aug 10;124(3215):269–70.

32. Koppenol WH, Bounds PL, Dang C V. Otto Warburg's contributions to current concepts of cancer metabolism. Nature Reviews Cancer 2011 11:5 [Internet]. 2011 Apr 14 [cited 2024 Oct 2];11(5):325–37. Available from: https://www.nature.com/articles/nrc3038

33. Hanahan D, Weinberg RA. Hallmarks of cancer: The next generation. Cell [Internet]. 2011 Mar 4 [cited 2024 Oct 2];144(5):646–74. Available from: http://www.cell.com/article/S0092867411001279/fulltext

34. de la Cruz-López KG, Castro-Muñoz LJ, Reyes-Hernández DO, García-Carrancá A, Manzo-Merino J. Lactate in the Regulation of Tumor Microenvironment and Therapeutic Approaches. Front Oncol [Internet]. 2019 Nov 1 [cited 2024 Sep 30];9:492088. Available from: www.frontiersin.org

35. Hui S, Ghergurovich JM, Morscher RJ, Jang C, Teng X, Lu W, et al. Glucose feeds the TCA cycle via circulating lactate. Nature 2017 551:7678 [Internet]. 2017 Oct 18 [cited 2024 Sep 30];551(7678):115–8. Available from: https://www.nature.com/articles/nature24057

36. Faubert B, Li KY, Cai L, Hensley CT, Kim J, Zacharias LG, et al. Lactate Metabolism in Human Lung Tumors. Cell [Internet]. 2017 Oct 5 [cited 2024 Sep 30];171(2):358-371.e9. Available from: http://www.cell.com/article/S0092867417310681/fulltext

37. Park S, Chang CY, Safi R, Liu X, Baldi R, Jasper JS, et al. ERRα-Regulated Lactate Metabolism Contributes to Resistance to Targeted Therapies in Breast Cancer. Cell Rep. 2016 Apr 12;15(2):323–35.

38. Sonveaux P, Végran F, Schroeder T, Wergin MC, Verrax J, Rabbani ZN, et al. Targeting lactate-fueled respiration selectively kills hypoxic tumor cells in mice. J Clin Invest [Internet]. 2008 Dec 1 [cited 2024 Sep 30];118(12):3930–42. Available from: http://www.jci.org

39. Adekola K, Rosen ST, Shanmugam M. Glucose transporters in cancer metabolism. Curr Opin Oncol [Internet]. 2012 Nov [cited 2024 Oct 1];24(6):650. Available from: /pmc/articles/PMC6392426/

40. Navale AM, Paranjape AN. Glucose transporters: physiological and pathological roles. Biophys Rev [Internet]. 2016 Mar 1 [cited 2024 Oct 1];8(1):5. Available from: /pmc/articles/PMC5425736/

41. Chelakkot C, Chelakkot VS, Shin Y, Song K. Modulating Glycolysis to Improve Cancer Therapy. Int J Mol Sci [Internet]. 2023 Feb 1 [cited 2024 Oct 1];24(3). Available from: /pmc/articles/PMC9916680/

42. Ni J, Huang Y, Li C, Yin Q, Ying J. Beyond ENO1, emerging roles and targeting strategies of other enolases in cancers. Mol Ther Oncolytics. 2023 Dec 19;31:100750.

43. Olson KA, Schell JC, Rutter J. Pyruvate and Metabolic Flexibility: Illuminating a path toward selective cancer therapies. Trends Biochem Sci [Internet]. 2016 Mar 1 [cited 2024 Oct 1];41(3):219. Available from: /pmc/articles/PMC4783264/

44. Valvona CJ, Fillmore HL, Nunn PB, Pilkington GJ. The Regulation and Function of Lactate Dehydrogenase A: Therapeutic Potential in Brain Tumor. Brain Pathology [Internet]. 2015 Jan 1 [cited 2024 Oct 15];26(1):3. Available from: https://pmc.ncbi.nlm.nih.gov/articles/PMC8029296/

45. Faubert B, Li KY, Cai L, Hensley CT, Kim J, Zacharias LG, et al. Lactate Metabolism in Human Lung Tumors. Cell [Internet]. 2017 Oct 5 [cited 2024 Oct 1];171(2):358-371.e9. Available from: http://www.cell.com/article/S0092867417310681/fulltext

46. Pérez-Tomás R, Pérez-Guillén I. Lactate in the Tumor Microenvironment: An Essential Molecule in Cancer Progression and Treatment. Cancers (Basel) [Internet]. 2020 Nov 1 [cited 2024 Oct 1];12(11):1–29. Available from: /pmc/articles/PMC7693872/

47. Wang Z, Liu F, Fan N, Zhou C, Li D, Macvicar T, et al. Targeting Glutaminolysis: New Perspectives to Understand Cancer Development and Novel Strategies for Potential

Target Therapies. Front Oncol [Internet]. 2020 Oct 26 [cited 2024 Oct 1];10:589508. Available from: www.frontiersin.org

48. Zhao Y, Zhao X, Chen V, Feng Y, Wang L, Croniger C, et al. Colorectal cancers utilize glutamine as an anaplerotic substrate of the TCA cycle in vivo. Scientific Reports 2019 9:1 [Internet]. 2019 Dec 16 [cited 2024 Oct 1];9(1):1–9. Available from: https://www.nature.com/articles/s41598-019-55718-2

49. Le A, Lane AN, Hamaker M, Bose S, Gouw A, Barbi J, et al. Glucose-independent glutamine metabolism via TCA cycling for proliferation and survival in b cells. Cell Metab [Internet]. 2012 Jan 4 [cited 2024 Oct 1];15(1):110–21. Available from: http://www.cell.com/article/S1550413111004682/fulltext

50. DeBerardinis RJ, Mancuso A, Daikhin E, Nissim I, Yudkoff M, Wehrli S, et al. Beyond aerobic glycolysis: Transformed cells can engage in glutamine metabolism that exceeds the requirement for protein and nucleotide synthesis. Proc Natl Acad Sci U S A [Internet]. 2007 Dec 4 [cited 2024 Oct 1];104(49):19345–50. Available from: https://www.pnas.org/doi/abs/10.1073/pnas.0709747104

51. Gaglio D, Metallo CM, Gameiro PA, Hiller K, Danna LS, Balestrieri C, et al. Oncogenic K-Ras decouples glucose and glutamine metabolism to support cancer cell growth. Mol Syst Biol [Internet]. 2011 Aug 16 [cited 2024 Oct 1];7(523). Available from: https://www.embopress.org/doi/10.1038/msb.2011.56

52. Jin J, Byun JK, Choi YK, Park KG. Targeting glutamine metabolism as a therapeutic strategy for cancer. Experimental & Molecular Medicine 2023 55:4 [Internet]. 2023 Apr 3 [cited 2024 Oct 1];55(4):706–15. Available from: https://www.nature.com/articles/s12276-023-00971-9

53. Zhang Z, Liu R, Shuai Y, Huang Y, Jin R, Wang X, et al. ASCT2 (SLC1A5)-dependent glutamine uptake is involved in the progression of head and neck squamous cell

carcinoma. British Journal of Cancer 2019 122:1 [Internet]. 2019 Dec 10 [cited 2024 Oct 1];122(1):82–93. Available from: https://www.nature.com/articles/s41416-019-0637-9

54. Katt WP, Lukey MJ, Cerione RA. A tale of two glutaminases: homologous enzymes with distinct roles in tumorigenesis. Future Med Chem [Internet]. 2017 Feb 1 [cited 2024 Oct 1];9(2):223–43. Available from: https://pubmed.ncbi.nlm.nih.gov/28111979/

55. Meyer HJ, Wienke A, Surov A. Associations between GLUT expression and SUV values derived from FDG-PET in different tumors—A systematic review and meta analysis. PLoS One [Internet]. 2019 Jun 1 [cited 2024 Oct 1];14(6):e0217781. Available from: https://journals.plos.org/plosone/article?id=10.1371/journal.pone.0217781

56. Ashraf MA, Goyal A. Fludeoxyglucose (18F). StatPearls [Internet]. 2023 Aug 28 [cited 2024 Oct 1]; Available from: https://www.ncbi.nlm.nih.gov/books/NBK557653/

57. Mosier JA, Schwager SC, Boyajian DA, Reinhart-King CA. Cancer cell metabolic plasticity in migration and metastasis. Clinical & Experimental Metastasis 2021 38:4 [Internet]. 2021 Jun 2 [cited 2024 Oct 1];38(4):343–59. Available from: https://link.springer.com/article/10.1007/s10585-021-10102-1

58. Momcilovic M, Bailey ST, Lee JT, Fishbein MC, Braas D, Go J, et al. The GSK3 signaling axis regulates adaptive glutamine metabolism in lung squamous cell carcinoma. Cancer Cell [Internet]. 2018 May 5 [cited 2024 Oct 1];33(5):905. Available from: /pmc/articles/PMC6451645/

59. Park S, Chang CY, Safi R, Liu X, Baldi R, Jasper JS, et al. ERRα-Regulated Lactate Metabolism Contributes to Resistance to Targeted Therapies in Breast Cancer. Cell Rep [Internet]. 2016 Apr 12 [cited 2024 Oct 1];15(2):323–35. Available from: http://www.cell.com/article/S2211124716302820/fulltext

60. Chen J, Lee HJ, Wu X, Huo L, Kim SJ, Xu L, et al. Gain of glucose-independent growth upon metastasis of breast cancer cells to the brain. Cancer Res [Internet]. 2015 Feb 1

[cited 2024 Oct 1];75(3):554–65. Available from: /cancerres/article/75/3/554/606669/Gain-of-Glucose-Independent-Growth-upon-Metastasis

61. Hensley CT, Wasti AT, DeBerardinis RJ. Glutamine and cancer: cell biology, physiology, and clinical opportunities. J Clin Invest [Internet]. 2013 Sep 3 [cited 2024 Oct 1];123(9):3678–84. Available from: http://www.jci.orgVolume123

62. Why Mice for Biomedical Research? [Internet]. [cited 2024 Oct 1]. Available from: https://www.jax.org/about-us/why-mice

63. Vähätupa M, Pemmari T, Junttila I, Pesu M, Järvinen TAH. Chemical-Induced Skin Carcinogenesis Model Using Dimethylbenz[a]Anthracene and 12-O-Tetradecanoyl Phorbol-13-Acetate (DMBA-TPA). J Vis Exp [Internet]. 2019 Dec 19 [cited 2024 Oct 6];2019(154):e60445. Available from: https://app.jove.com/t/60445

64. Abel EL, Angel JM, Kiguchi K, DiGiovanni J. Multi-stage chemical carcinogenesis in mouse skin: Fundamentals and applications. Nat Protoc [Internet]. 2009 [cited 2024 Oct 6];4(9):1350. Available from: /pmc/articles/PMC3213400/

65. Chaves P, Garrido M, Oliver J, Pérez-Ruiz E, Barragan I, Rueda-Domínguez A. Preclinical models in head and neck squamous cell carcinoma. Br J Cancer [Internet]. 2023 May 5 [cited 2024 Oct 6];128(10):1819. Available from: /pmc/articles/PMC10147614/

66. Beaumont KA, Mohana-Kumaran N, Haass NK. Modeling Melanoma In Vitro and In Vivo. Healthcare [Internet]. 2014 Mar 1 [cited 2024 Oct 6];2(1):27. Available from: /pmc/articles/PMC4934492/

CHAPTER 2

Metabolic flexibility in Squamous Cell Carcinoma

INTRODUCTION

SCC and essentially every other solid tumor are known to show evidence of a metabolic transition known as the Warburg effect where cancer cells choose to increase glucose uptake as a nutrient and use it to produce lactate leading to acidification of tissue, a process also known as aerobic glycolysis (1, 2). This observation has led to serious effort to block various targets in the glucose utilization pathway for the treatment of cancer. However, to date, these approaches have not been successful (3). We previously showed that genetic deletion of lactate dehydrogenase A (LDHA) in cancer initiating cells of the epidermis led to a marked decrease in the Warburg effect as measured by glucose uptake and lactate production (4). However, SCC formed despite lack of LDHA, suggesting that cancer cells do not necessarily rely on glucose metabolism for their growth and transformation. Instead, these data raised the possibility that cancer cells show metabolic flexibility which allows them to grow by up-regulating alternative pathways that generate adenosine triphosphate (ATP) and biosynthesis of key materials to allow for increased proliferation. As potential evidence of flexibility, we also showed that tumors lacking LDHA activity exhibited increased glutamine consumption (4); however, we did not experimentally investigate in the previous study whether this increased glutamine metabolism enabled tumor growth in the absence of LDHA.

Glutaminolysis has also emerged as a key metabolic pathway in a variety of cancer models (5,6). Glutamine is imported into cells via plasma membrane glutamine transporters and can be converted to glutamate through the action of glutaminase (GLS) enzymes in the cytoplasm or mitochondria (7). Glutamate can be converted to alpha-ketoglutarate which can enter into the tricarboxylic acid (TCA) cycle to power oxidative phosphorylation and production of ATP in the mitochondria. In addition, recent data show that many human tumors consume lactate through monocarboxylate transporters, and convert it into pyruvate by lactate

dehydrogenase, and then use that pyruvate anapleurotically in the TCA cycle (8). Therefore, cancer cells can acquire carbon-based nutrients to power the TCA cycle either through uptake of glucose, lactate, or glutamine, all of which have been shown to be up-regulated in many human cancers. Despite numerous studies suggesting that glutaminolysis could be a driver of tumorigenesis, this has yet to be tested genetically *in vivo* in murine cancer models, particularly in SCC. To date, efforts to block glutaminolysis with small-molecule inhibition of GLS activity have not yet led to clinically available therapies for patients despite intense effort (6, 9-11).

In the current study, we use a well-established murine model of SCC coupled with genetic deletion of LDHA and GLS to test the limits of cancer metabolic flexibility (12, 13). In this model, genetic manipulation is inducible in HFSCs, which are known to initiate SCC in murine epidermis (14, 15). Coupled with chemical carcinogenesis, this model allows for the deletion of metabolic activity just before induction of oncogenesis in adult mice. Because the tumorigenesis begins at the skin surface, the entire process is tractable over time allowing for detailed quantification of oncogenesis and precise measurement of the role various metabolic pathways play in this process. We exploited this model to probe the role of glutaminolysis in SCC initiation or progression and, in doing so, define metabolic flexibility in SCC as well as the limits of that flexibility.

RESULTS

Glutamine metabolism (Fig. 1A) has previously been implicated as a key metabolic activity in tumor progression in a variety of cancer models (11, 16, 17, 18-20). Here, we sought to understand whether glutamine metabolism plays a role in tumor initiation or progression of SCC. We previously demonstrated that HFSCs serve as cells of origin for SCC and that the tumors formed share many physiological and metabolic similarities with SCC formed in human skin (14, 21, 22). We acquired transcriptome data from dimethylbenz[*a*]anthracene (DMBA)/12-*O*-tetradecanoylphorbol 13-acetate (TPA)–induced SCC to determine which metabolic pathway genes were altered at the RNA level. We found that many of the genes involved in

glutaminolysis and glutamine metabolism elevated in murine SCC derived from HFSCs (Fig. 1A). An ontological analysis for metabolic substrates showed a robust enrichment in gene expression for genes related to mostly glycolysis and glutaminolysis, as expected (Fig. 1B). Ontological analysis for biological processes increased in SCC compared to normal skin demonstrate classical transformations in cancer such as promotion and enhancement of cell division, cell migration, and signaling pathways (Fig. S1A), consistent with transcriptome transformation in cancer. We then examined cancer genome data (Gene Expression database of Normal and Tumor tissues, GENT2) to assess the relative mRNA levels in normal versus tumorigenic human tissues, which pointed toward higher expression of GLS, the enzyme that converts glutamine to glutamate as the first step of glutaminolysis, and other enzymes involved in glutamine metabolism in many tumor types (Fig. S1, B and C). Next, we performed liquid chromatography mass spectrometry (LCMS)–based metabolomics to measure the relative levels of metabolites in HFSC-induced SCC and found elevated levels of several metabolites involved in glutamine metabolism (Fig. 1C). In addition, in a model of HFSC-induced tumorigenesis, we found that deletion of LDHA did not markedly affect tumor production but did show evidence of metabolic compensation by glutaminolysis (Fig. 1, D to F). On the other hand, transcriptional analysis of LDHA-null tumors did not show changes in expression of genes related to glutaminolysis raising the question of how this compensation was mediated (Fig. S1D).

Since SCC tumors showed increased glutaminolysis-related gene expression, we sought to determine the role of glutaminolysis in the initiation or progression of SCC through deletion of GLS in HFSCs before initiating tumorigenesis. Crossing mice floxed for GLS (GLS1 fl/fl, the Jackson Laboratory) with mice transgenic for K15-CrePR allowed for an inducible deletion of GLS in HFSCs upon administration of the progesterone inhibitor mifepristone (Fig. 2A). To induce tumorigenesis, we relied on the established chemical carcinogenesis protocol using DMBA as a mutagen followed by repeated stimulation of proliferation by TPA (13).

Both *WT* and *GLS*^{KO} models produced papilloma, well-differentiated SCC, moderately differentiated SCC, and keratoacanthoma (Fig. 2B). We quantified time to tumor formation, number of tumors, and volume of tumors but did not detect any statistically significant differences in cancer formation in mice with or without GLS expression in cancer cells of origin (Fig. 2C). On the other hand, we did find that 6% of tumors that formed in mice with GLS deletion in cancer cells of origin became necrotic, which we did not observe in animals with GLS activity (Fig. 2C).

To examine whether the genetic deletion of GLS in HFSCs effectively created tumors lacking GLS activity, we used immunostaining, GLS activity assays, and LCMS-based metabolomics. Immunostaining of *WT* tumors showed high GLS expression particularly on the epithelial edge of tumors formed after DMBA/TPA, whereas immunostaining of *GLS*^{KO} tumors resulted in negligible GLS staining (Fig. 3A). We also used a GLS activity assay to measure the relative activity of the enzyme in protein lysates generated from *WT* and *GLS*^{KO} tumors and found a decrease in GLS activity in the *GLS*^{KO} tumors (Fig. 3A). While it is clear that our genetic strategy to eliminate GLS activity from cancer cells of origin and subsequent tumors was successful, we did find cells that were strongly positive for GLS expression in the mesenchyme surrounding the nascent tumors (Fig. S2A). These CD45^{+} cells were also positive for CD11b, suggesting that they are macrophages (Fig. S2, B and C). Because our genetic strategy was not designed to target immune cells, it is not unexpected to find GLS-positive cells within the mesenchyme, and these will be the subject of future investigation.

To investigate whether GLS-deleted tumors show evidence of metabolic changes despite relative lack of phenotypic change, we performed metabolic tracing with ^{13}C-glutamine and LCMS-based metabolomics. Tumors with labeled glutamine showed that both the oxidative and reductive pathways for glutamine utilization were abrogated in GLS-deleted tumors (Fig. 3B), consistent with a loss of GLS activity. On the other hand, metabolomics also showed

consistent decreases in glucose conversion to pyruvate and lactate in the absence of GLS in papilloma, but not in SCC (Fig. 3C).

RNA sequencing (RNA-seq) of *WT* and *GLS*^{KO} tumors showed a relatively small number of gene expression differences caused by loss of GLS activity. When looking particularly at genes related to proliferation, epithelial-mesenchymal transition (EMT), or stemness, there were no significant changes (Fig. 3D). Immunostaining for Ki67, proliferation marker, and cleaved caspase 3, apoptosis marker, also showed no changes between *WT* and *GLS*^{KO} tumors (Fig. S3, A and B). Because the activity of GLS was previously linked to hypoxia signaling, we looked at hypoxia-inducible factor target genes but did not find any differences (Fig. S3C). Furthermore, ontological analysis showed that several pathways appeared to be enriched; however, the enrichment was driven by a small number of genes mostly related to ECM and did not point to obvious physiological changes caused by the deletion of GLS (Fig. S3D).

Since ^{13}C-glutamine and ^{13}C-glucose tracing in *GLS*^{KO} tumors revealed decreased glutamine and glucose consumption, we examined whether *GLS*^{KO} tumors increased consumption of lactate, another abundant nutrient in circulation. ^{13}C-lactate tracing revealed a large increase in lactate uptake in *GLS*^{KO} tumors (Fig. 4A) and TCA cycle products, suggesting that increased lactate uptake was able to power the TCA cycle to compensate for the loss of glutaminolysis.

As described previously, *LDHA*^{KO} tumors appeared pathologically identical to tumors expressing LDHA (Fig. 1E). We pulsed mice bearing *LDHA*^{KO} tumors with ^{13}C-labeled glucose before tumor harvesting and as expected, found diminished tumor glucose uptake, conversion of glucose to lactate, and decreased tumor levels of glucose and lactate, confirming abrogation of glucose metabolism in the absence of LDHA activity described in our previous study (Fig. 5, A and B). In addition, we reexamined metabolomic data from tumors generated by HFSCs lacking the mitochondrial pyruvate carrier (MPC). In this model, tumorigenesis was also unaffected by blocking pyruvate oxidation, providing yet another example of metabolic flexibility (4). Increased

glucose, lactate, glutamine, and glutamate levels in MPC-null tumors suggested a potential up-regulation of glycolysis and glutaminolysis (Fig. 5C).

The data from Figs. 4 to 6 suggest that SCC-initiating cells have metabolic flexibility for carbon sources to power metabolic pathways, so we hypothesized that perhaps deletion of two carbon sources might be sufficient to starve cells attempting transformation. To test this hypothesis, we crossed animals floxed for both LDHA and GLS with K15-CrePR transgenic mice in an attempt to abrogate both glucose utilization and glutaminolysis (Fig. 7A). We then treated double-floxed mice with DMBA/TPA to induce tumorigenesis. After 10 to 20 weeks, we routinely detected papilloma in all genotypes (Fig. 7B) but never observed the formation of an SCC in $GLS^{KO}LDHA^{KO}$ mice. By the end of the experiment, when the control animals had to be euthanized, there were no papilloma or SCC that lacked both LDHA activity and GLS expression in any of the $GLS^{KO}LDHA^{KO}$ mice (Fig. 7B). This suggests that those papilloma that lacked both LDHA and GLS that might have formed in $GLS^{KO}LDHA^{KO}$ mice probably underwent regression. Careful chronological examination of tumorigenesis in the *WT*, GLS^{KO}, $LDHA^{KO}$, and $GLS^{KO}LDHA^{KO}$ tumors showed that all tumors formed in $GLS^{KO}LDHA^{KO}$ mice were benign papilloma, which then either underwent necrosis or regression (Fig. 7, B to D).

Previous studies indicate that SCCs do not rely on glycolysis and lactate production for their growth and instead rely on glutamine metabolism. Here, although we targeted glutamine metabolism, cancer cells continued to grow as they are flexible and use lactate to grow. When targeting both GLS and LDHA to ultimately starve the cancer cells from their carbon sources, the cells fail to transform into SCC. This work elucidates how adaptable cancer cells are and the importance of targeting metabolism in combination. The identification of the two enzymes essential for SCC tumorigenesis allows us to explore the therapeutic potential of these targets using small molecule inhibitors to recapitulate our genetic results.

FIGURES

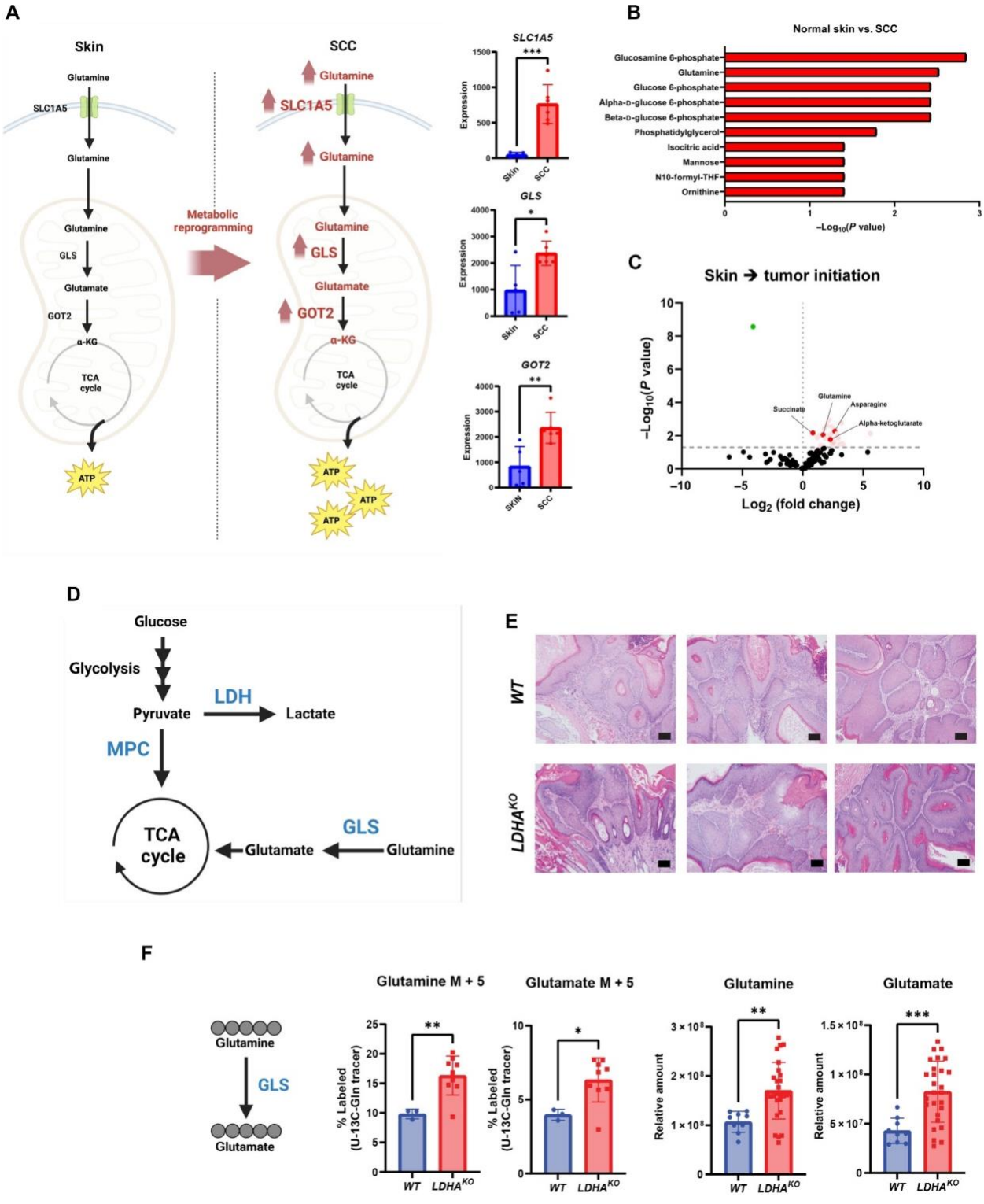
A
Skin
SCC
Glutamine
SLC1A5
Glutamine
Glutamine
GLS
Glutamate
GOT2
α-KG
TCA cycle
ATP
Metabolic reprogramming
Glutamine
SLC1A5
Glutamine
Glutamine
GLS
Glutamate
GOT2
α-KG
TCA cycle
ATP
ATP
ATP
SLC1A5
GLS
GOT2
Expression
Skin
SCC
B
Normal skin vs. SCC
Glucosamine 6-phosphate
Glutamine
Glucose 6-phosphate
Alpha-D-glucose 6-phosphate
Beta-D-glucose 6-phosphate
Phosphatidylglycerol
Isocitric acid
Mannose
N10-formyl-THF
Ornithine
−Log10(P value)
C
Skin → tumor initiation
−Log10(P value)
Log2 (fold change)
Succinate
Glutamine
Asparagine
Alpha-ketoglutarate
D
Glucose
Glycolysis
Pyruvate
LDH
Lactate
MPC
TCA cycle
GLS
Glutamate
Glutamine
E
WT
LDHAKO
F
Glutamine
GLS
Glutamate
Glutamine M + 5
Glutamate M + 5
Glutamine
Glutamate
% Labeled (U-13C-Gln tracer)
Relative amount
WT
LDHAKO

Fig. 1. Glutamine metabolism is up-regulated in SCC.

(A) Schematic showing metabolic reprogramming in glutamine metabolism from normal skin to SCC. Glutamine is metabolized into TCA cycle, and ATP is synthesized from TCA cycle–derived glutamine. ASCT2 (SLC1A5), GLS, and GOT2 gene expression in skin (n = 5) and SCC (n = 6). Statistical significance (*P < 0.05, **P < 0.01, and ***P < 0.001) was calculated using a two-tailed t test. (**B**) Ontological analysis from metabolomics workbench for metabolic substrates increased in SCC compared to normal skin. THF, tetrahydrofolate. (**C**) Metabolomic pool volcano plot of normal skin versus papilloma (benign tumor) initiated by DMBA/TPA skin chemical carcinogenesis. Dashed lines indicate adjusted $P \leq 0.05$ or $\log_2$(fold change) of ≥0 or ≤0. Colored dots represent metabolites significantly increasing (red) or decreasing (green) during the skin to tumor transition. (**D**) Schematic of enzymes used in glycolysis, lactate production, and glutaminolysis. (**E**) Tumors from *WT* and *LDHA*^{KO} mice stained for hematoxylin and eosin (H&E). Scale bars, 10 μm. (**F**) Schematic of fully labeled glutamine isotopomer conversion. Data represent percent of M5-labeled glutamine and M5-labeled glutamate in tumors [n = 3 (*WT*), n = 9 (*LDHA*^{KO})] after $^{13}C_5$-glutamine infusion. Metabolic pool data representing relative amounts of glutamine and glutamate in tumors [n = 9 (*WT*), n = 27 (*LDHA*^{KO})]. Statistical significance (*P < 0.05, **P < 0.01, ***P < 0.001, and ****P < 0.0001) was calculated using a two-tailed t test. Figure 1 (A, D, and F) were produced using BioRender.

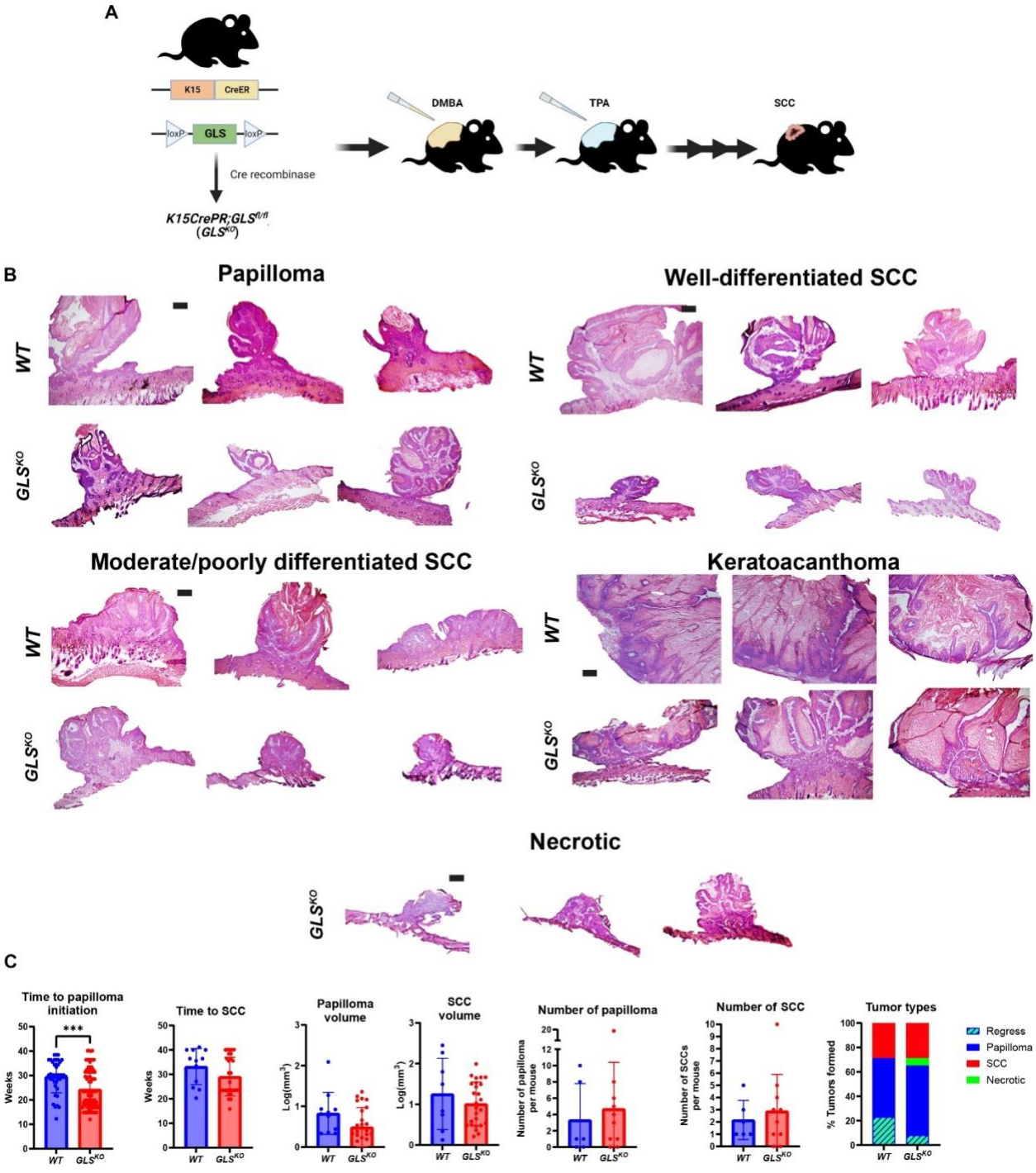

Fig. 2. Loss of GLS does not affect SCC initiation, progression, or pathology.

(**A**) Schematic of transgenic mice used to knock out GLS in HFSCs coupled with topical SCC chemical carcinogenesis using DMBA and TPA. Figures 2A was produced using BioRender. (**B**) Dorsal tumors from *WT* and *GLS*^{KO} mice stained for H&E. Scale bars, 50 μm. (**C**) Quantification

of time to papilloma [*n* = 40 (*WT*), *n* = 88 (GLS^{KO})] initiation and SCC [*n* = 12 (*WT*), *n* = 29 (GLS^{KO})] formation. Each data point represents a tumor of that genotype. Quantification of volume of papilloma [*n* = 11 (*WT*), *n* = 25 (GLS^{KO})] and SCC [*n* = 8 (*WT*), *n* = 26 (GLS^{KO})]. Each data point represents a tumor of that genotype. Quantification of the number of papilloma [*n* = 6 (*WT*), *n* = 10 (GLS^{KO})] and SCC [*n* = 6 (*WT*), *n* = 10 (GLS^{KO})] formed per mice. Each data point represents a mouse of that genotype. Data shown represent tumors present at the end of the experiment. Quantification of percent and types of tumors formed per genotype: *WT* (papilloma = 48%; SCC = 30%; regress = 23%; necrotic = 0%) and GLS^{KO} (papilloma = 57%; SCC = 30%; regress = 8%; necrotic = 6%). Data shown represent tumor quantifications from the beginning to the end of the experiment.

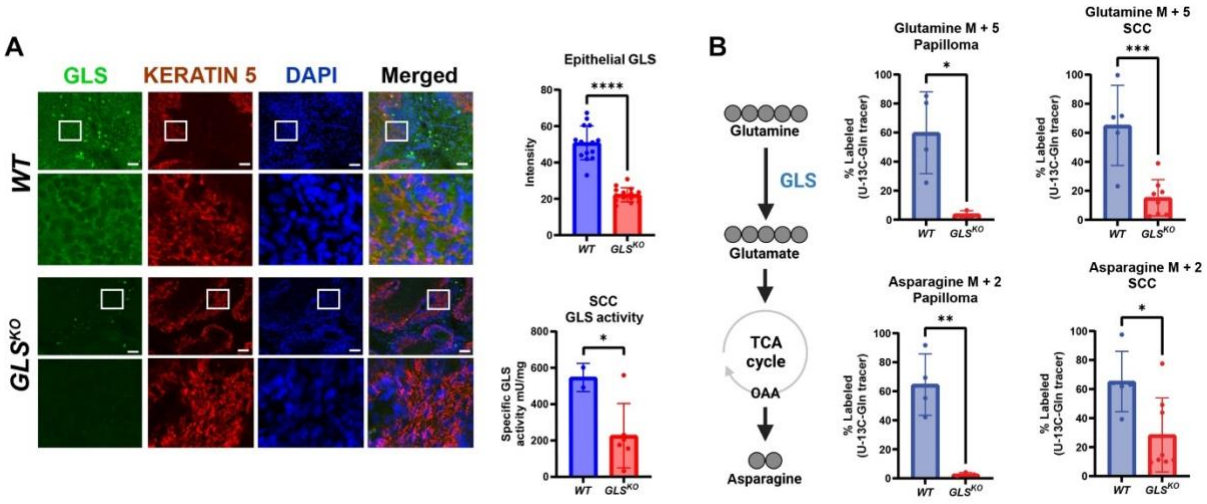

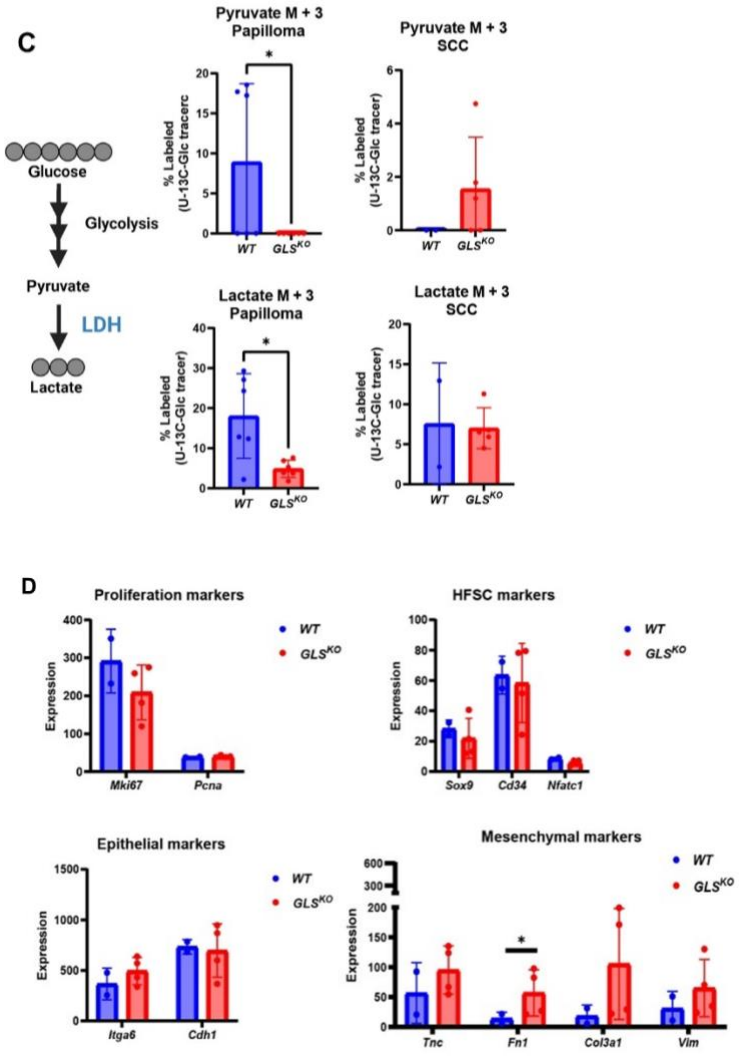

Fig. 3. Loss of GLS in tumors alters glutamine and glucose metabolism.

(**A**) *WT* or *GLS*^{KO} SCC immunostaining for GLS and KERATIN 5, an epidermal marker. Cell nuclei were stained with 4′,6-diamidino-2-phenylindole (DAPI). Quantification of mean intensity epithelial GLS fluorescence in *WT* (*n* = 15) and *GLS*^{KO} (*n* = 15) SCCs. GLS activity in *WT* (*n* = 2) and *GLS*^{KO} (*n* = 6) SCC lysates. (**B**) Schematic of fully labeled glutamine isotopomer conversion. Data represent percent of M5-labeled glutamine and M2-labeled asparagine in papilloma [*n* = 4 (*WT*), *n* = 3 (*GLS*^{KO})] and SCC [*n* = 5 (*WT*), *n* = 8 (*GLS*^{KO})] after $^{13}C_5$-glutamine infusion. OAA, oxaloacetate. (**C**) Schematic of fully labeled glucose isotopomer conversion. Data represent percent of M3-labeled pyruvate and M3-labeled lactate in papilloma [*n* = 6

(*WT*), *n* = 6 (*GLS*^{KO})] and SCC [*n* = 2 (*WT*), *n* = 5 (*GLS*^{KO})] after $^{13}C_6$-glucose infusion. (**D**) RNA-seq data of *WT* (*n* = 2) or *GLS*^{KO} (*n* = 5) tumors showing transcription levels of proliferation, HFSC, epithelial, and mesenchymal markers. Figure 3 (B and C) was produced using BioRender. Statistical significance (**P* < 0.05, ***P* < 0.01, ****P* < 0.001, and *****P* < 0.0001) for (A) to (D) was calculated using a two-tailed *t* test.

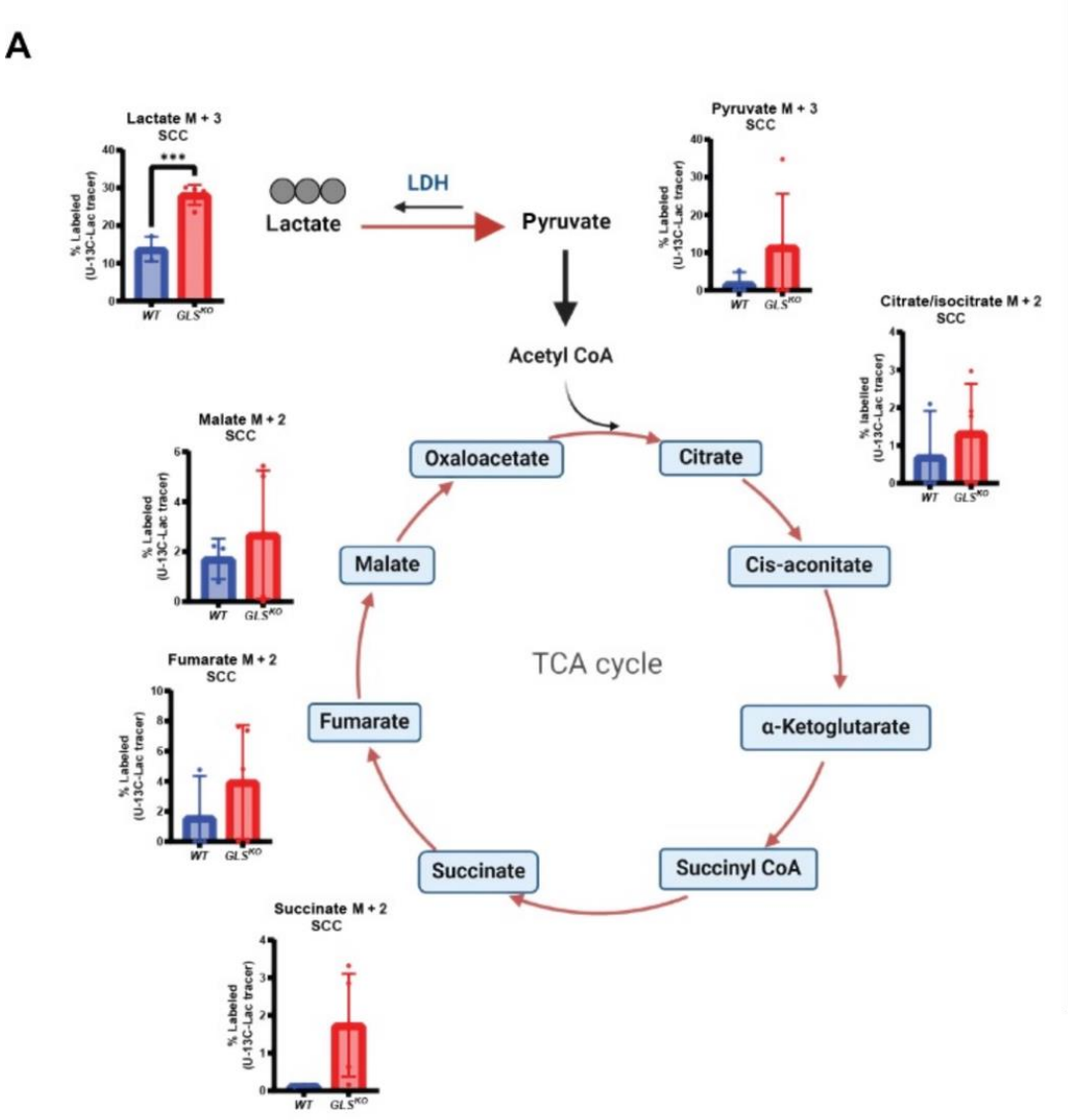

Fig. 4. Increased lactate transporter and uptake in *GLS*^{KO} SCC.

(**A**) Schematic of fully labeled lactate isotopomer conversion. Data represent percent of M3-labeled lactate, M2-labeled citrate/isocitrate, M2-labeled succinate, M2-labeled fumarate, and

M2-labeled malate in SCCs [n = 3 (*WT*), n = 5 (GLS^{KO})] after $^{13}C_3$-lactate infusion. Statistical significance (***P < 0.001) was calculated using a two-tailed t test. CoA, coenzyme A. Figure 4A was produced using BioRender. Statistical significance (****P < 0.0001) was calculated using a two-tailed t test.

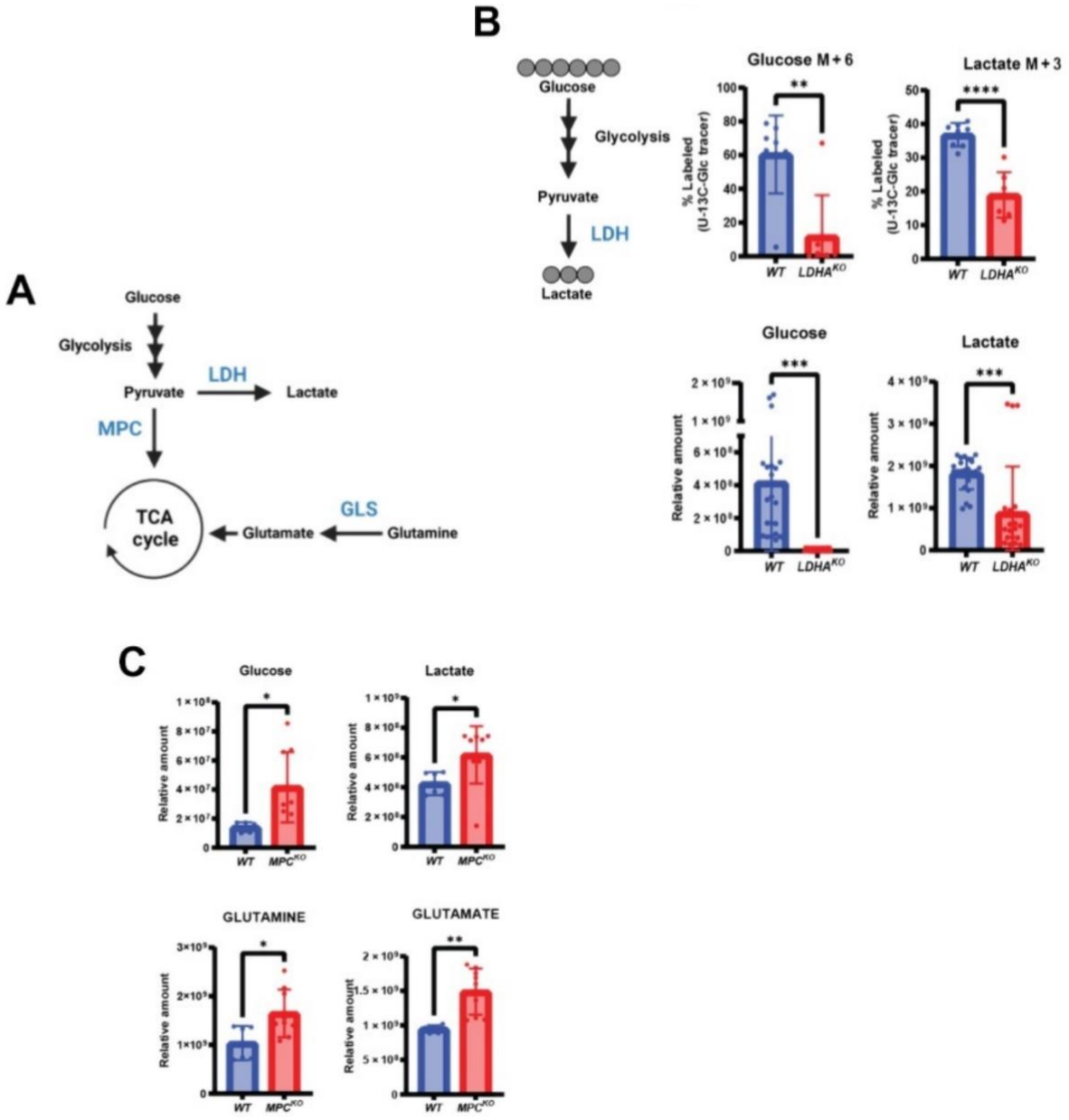

Fig. 5. Posttranscriptional increased glucose transporter at the cell surface.

(**A**) Schematic of glycolysis, lactate production, and glutaminolysis. (**B**) Schematic of fully labeled glucose isotopomer conversion. Data represent percent of M6-labeled glucose and M3-labeled lactate in tumors [n = 8 (*WT*), n = 7 ($LDHA^{KO}$)] after $^{13}C_6$-glucose infusion. Metabolic pool data representing relative amounts of glucose and lactate in tumors [n = 24 (*WT*), n = 21 ($LDHA^{KO}$)]. (**C**) Metabolic pool data representing relative amounts of glucose, lactate, glutamine, and glutamate in tumors [n = 6 (*WT*), n = 9 (MPC^{KO})]. Figure 5 (A and B) was produced using BioRender. Statistical significance (*P < 0.05, **P < 0.01, ***P < 0.001, and ****P < 0.0001) for (B) and (C) was calculated using a two-tailed t test.

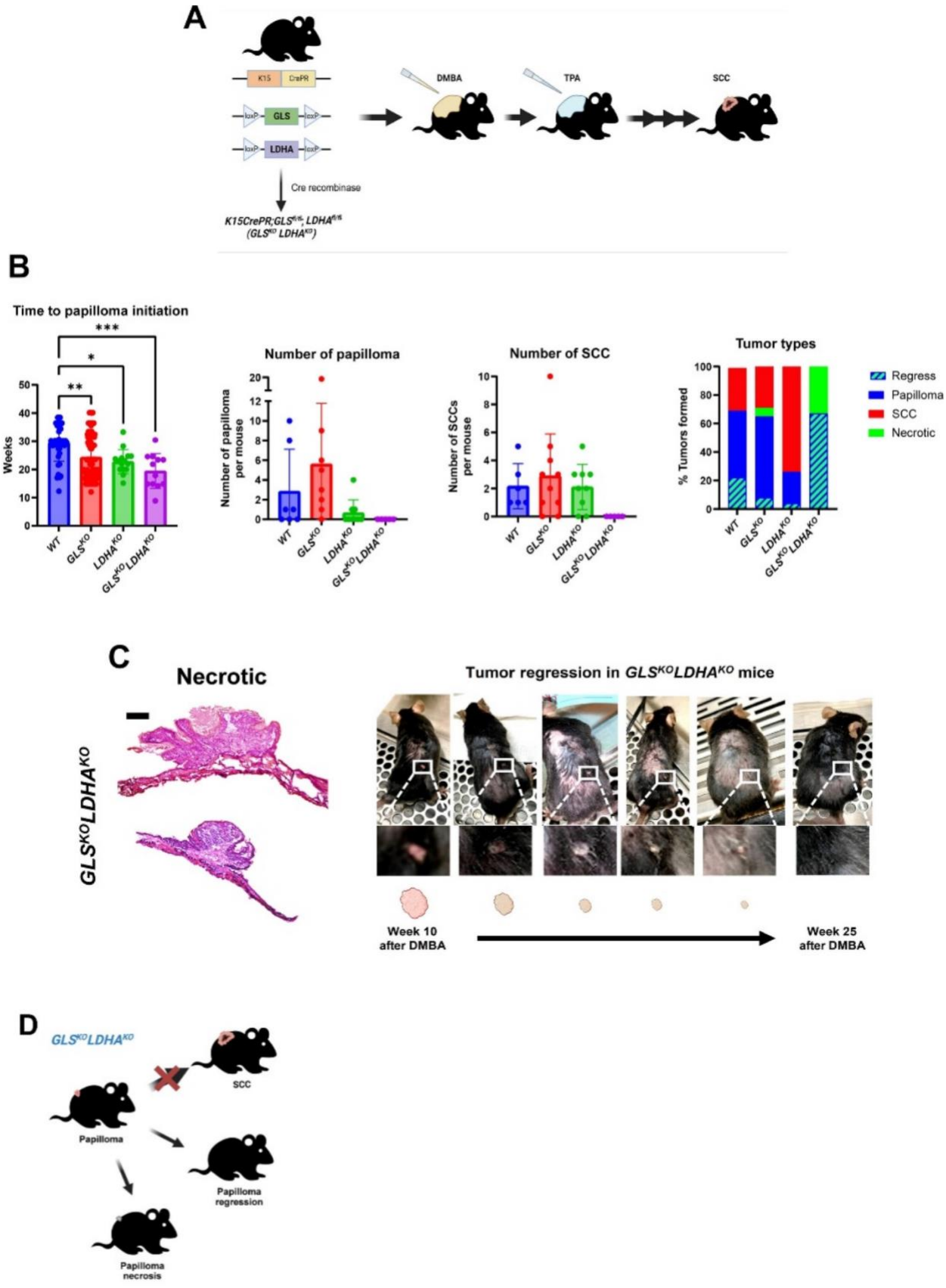
A
K15
CrePR
GLS
LDHA
loxP
Cre recombinase
DMBA
TPA
SCC
B
Time to papilloma initiation
Weeks
Number of papilloma
Number of papilloma per mouse
Number of SCC
Number of SCCs per mouse
Tumor types
% Tumors formed
Regress
Papilloma
SCC
Necrotic
WT
GLS^KO
LDHA^KO
GLS^KO LDHA^KO
C
Necrotic
GLS^KO LDHA^KO
Tumor regression in GLS^KO LDHA^KO mice
Week 10 after DMBA
Week 25 after DMBA
D
GLS^KO LDHA^KO
SCC
Papilloma
Papilloma regression
Papilloma necrosis

Fig. 7. Targeting both glutaminolysis and glycolysis in SCC.

(**A**) Schematic of transgenic mice used to knock out GLS and LDHA in HFSCs coupled with topical SCC chemical carcinogenesis using DMBA and TPA. (**B**) Quantification of time to papilloma n = 40 (*WT*), n = 88 (GLS^{KO}), n = 15 ($LDHA^{KO}$), and n = 12 ($GLS^{KO}LDHA^{KO}$) initiation. Each data point represents a tumor of that genotype. Quantification of the number of papilloma [n = 6 (*WT*), n = 10 (GLS^{KO}), n = 6 ($LDHA^{KO}$), n = 5 ($GLS^{KO}LDHA^{KO}$)] and SCC [n = 6 (*WT*), n = 10 (GLS^{KO}), n = 6 ($LDHA^{KO}$), n = 5 ($GLS^{KO}LDHA^{KO}$)]. Each data point represents a mouse of that genotype. Data shown represent tumors present at the end of the experiment. Quantification of percent and types of tumors formed per genotype: *WT* (papilloma = 48%; SCC = 30%; regress = 23%; necrotic = 0%), GLS^{KO} (papilloma = 57%; SCC = 30%; regress = 8%; necrotic = 6%), $LDHA^{KO}$ (papilloma = 41%; SCC = 55%; regress = 4%; necrotic = 0%), and $GLS^{KO}LDHA^{KO}$ (papilloma = 0%; SCC = 0%; regress = 67%; necrotic = 33%). (**C**) Necrotic tumors from $GLS^{KO}LDHA^{KO}$ mice stained for H&E. Scale bar, 50 μm. Images of $GLS^{KO}LDHA^{KO}$ mouse over time undergoing papilloma regression. (**D**) Schematic of summary of phenotypic results for $GLS^{KO}LDHA^{KO}$ mice. Figure 7 (A, C, and D) was produced using BioRender.

SUPPLEMENTAL FIGURES

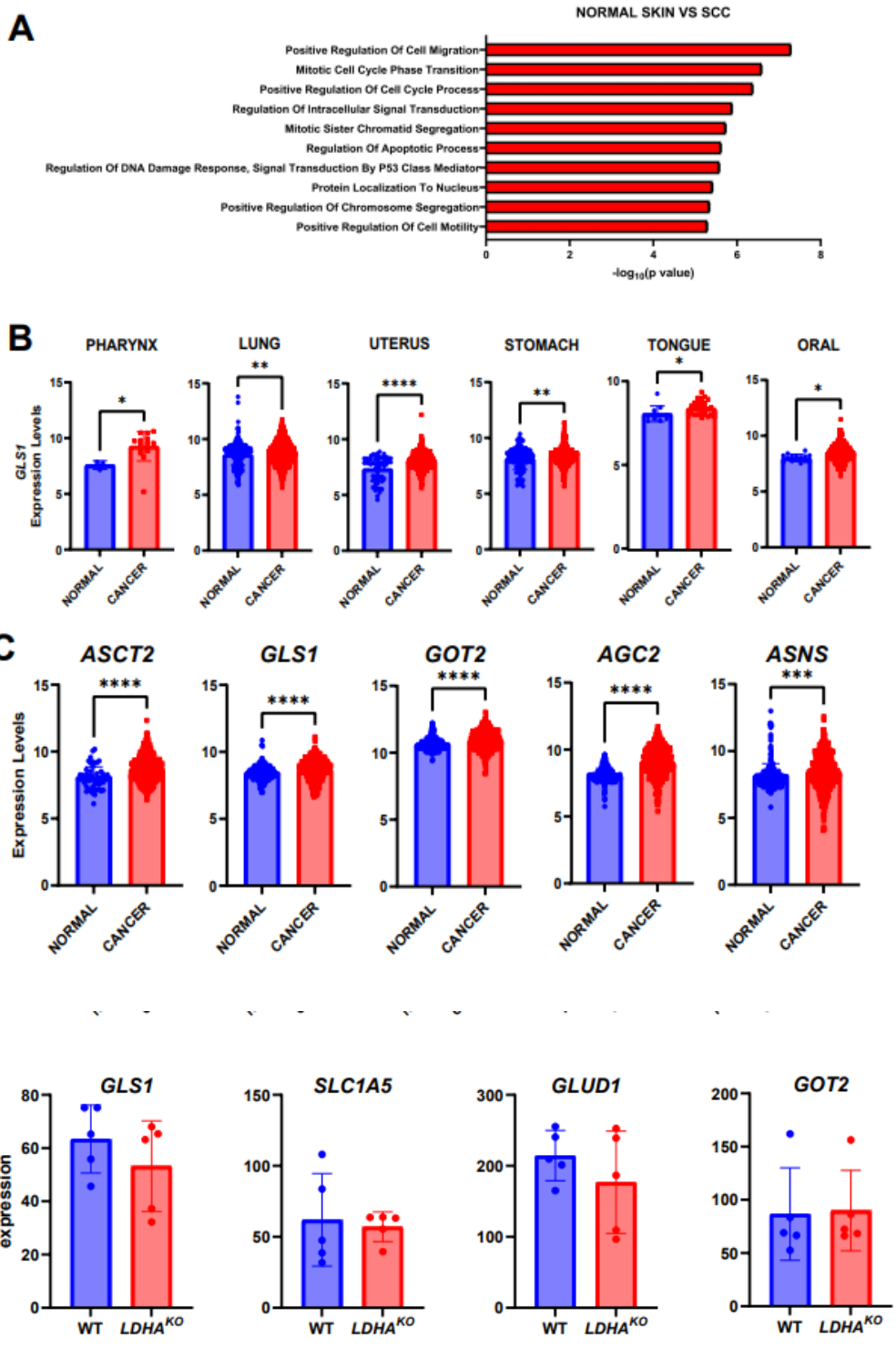

Fig S1. Metabolism is increased broadly in cancers

(**A**) Ontological analysis for biological processes increased in SCC compared to normal skin. (**B**) GLS gene expression in pharynx n = 3 (normal), n = 15 (cancer); lung n = 508 (normal), n = 2362 (cancer); uterus n = 58 (normal), n = 432 (cancer); stomach n = 117 (normal), n = 1028 (cancer); tongue n = 11 (normal), n = 30 (cancer); oral n = 15 (normal), n = 371 (cancer) based on the Gene Expression database of Normal and Tumor tissue 2 (GENT2) data analysis. Statistical significance (*p<0.05; **p<0.01; ***<0.001; ****p<0.0001) was calculated using a two-tailed t test. (**C**) ASCT2, GLS, GOT2, AGC2, and ASNS gene expression in skin n = 263 (normal), n = 547 (cancer) based on GENT2 data analysis. Statistical significance (*p<0.05; **p<0.01; ***<0.001; ****p<0.0001) was calculated using a two-tailed t test. (**D**) RNA-seq data of *WT* (n=5) or $LDHA^{KO}$ (n=5) tumors showing transcription levels of genes related to glutaminolysis.

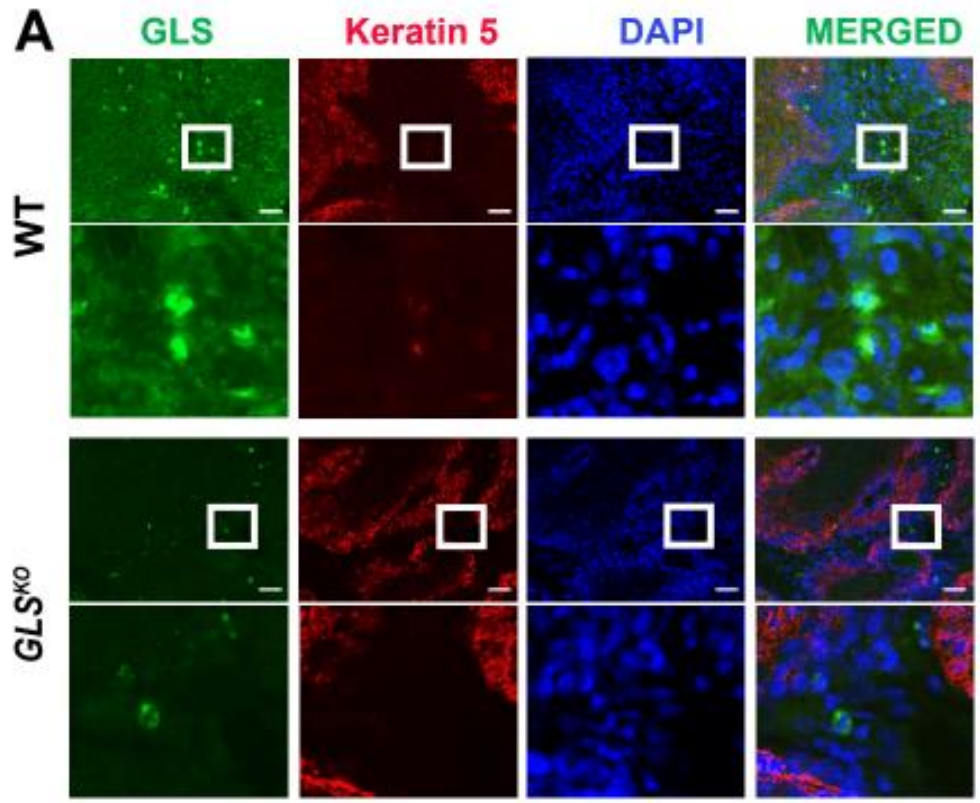
A
GLS
Keratin 5
DAPI
MERGED
WT
GLSKO

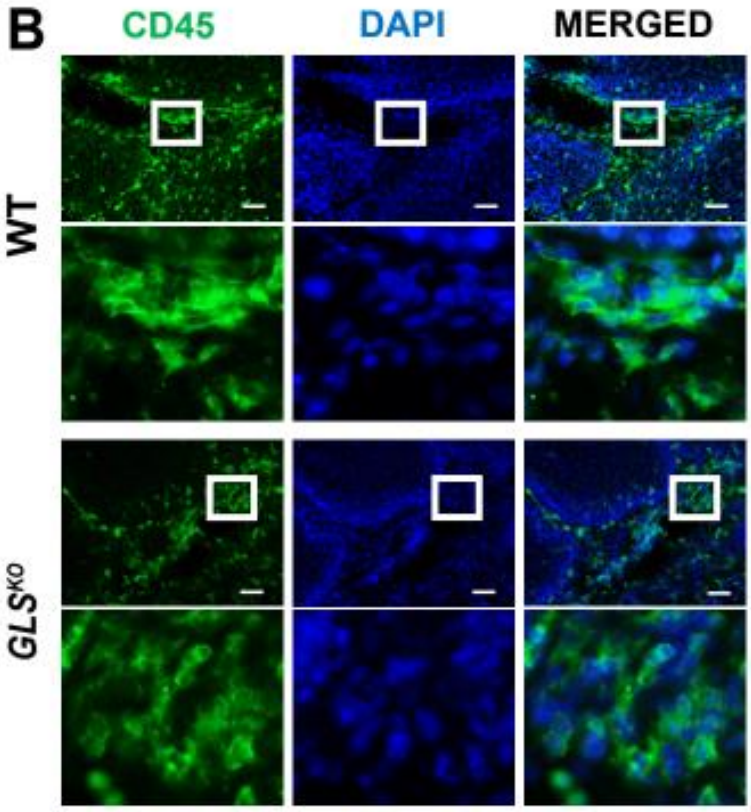
B
CD45
DAPI
MERGED
WT
GLSKO

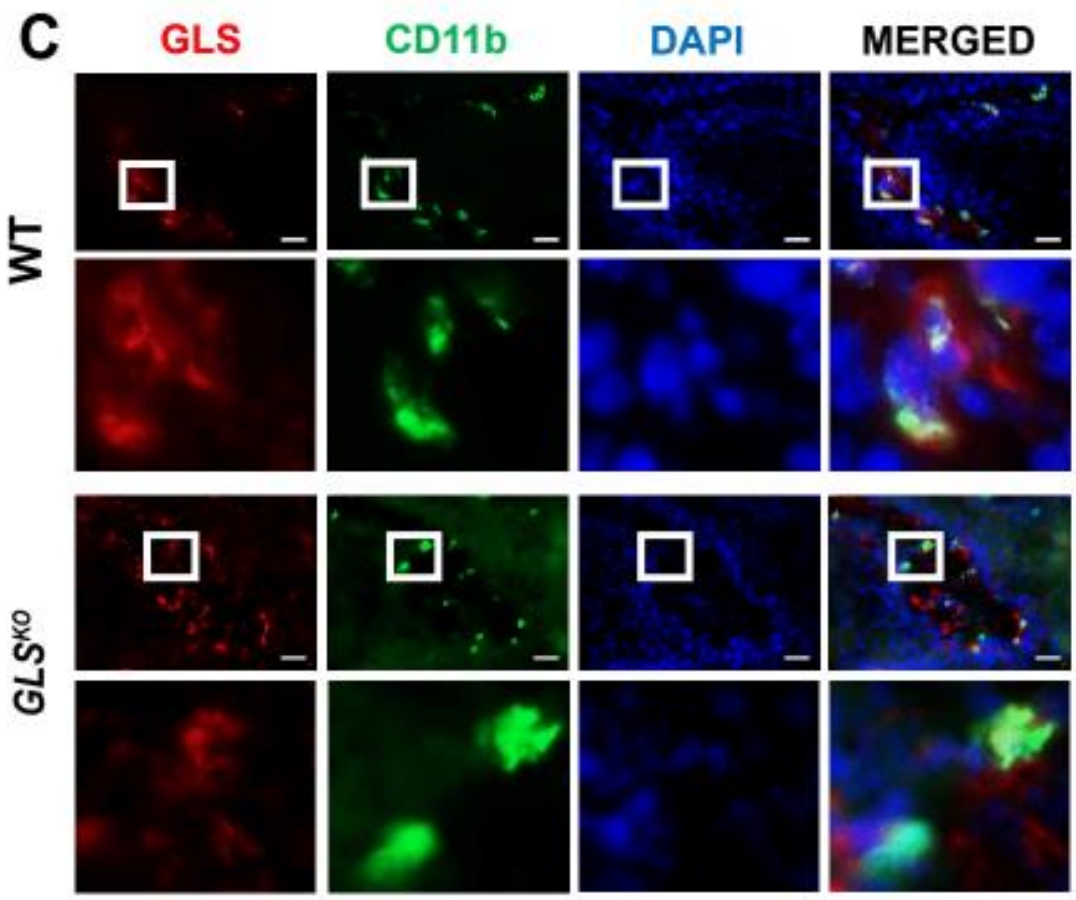

Fig S2. GLS+ are present in immune cells in tumor mesenchyme

(**A**) WT or GLSKO SCC immunostaining for GLS and KERATIN5, an epidermal marker. Magnified images of strong GLS positive cells in mesenchyme of tumor. Scale bar, 100μm. (**B**) WT or GLSKO SCC immunostaining for immune cell surface marker CD45. Magnified images of strong CD45 positive cells in mesenchyme of tumor. Cell nuclei were stained with DAPI. Scale bar, 100μm. (**C**) WT or GLSKO SCC immunostaining for macrophage marker CD11b. Magnified images of strong CD11b positive cells in mesenchyme of tumor. Cell nuclei were stained with DAPI. Scale bar, 100μm.

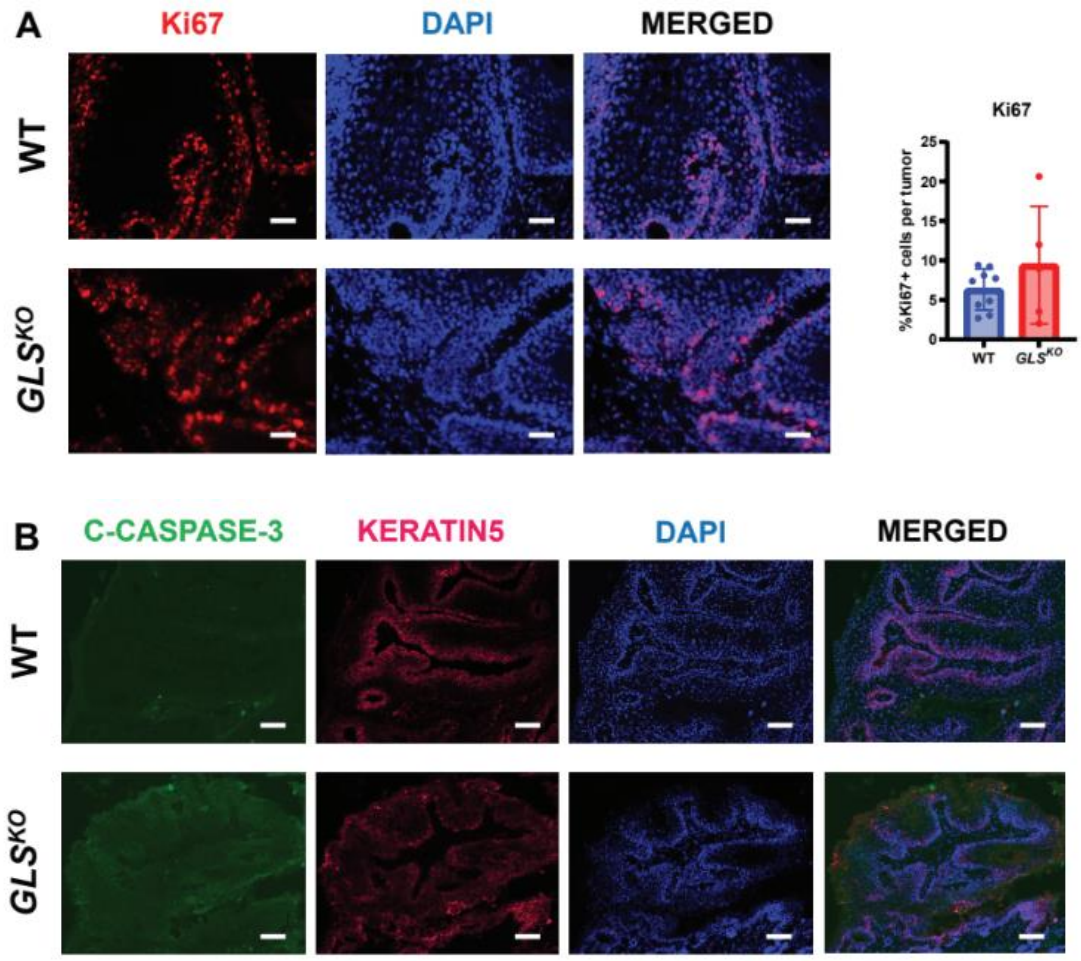
A
Ki67
DAPI
MERGED
WT
GLS^KO
Ki67
%Ki67+ cells per tumor
25
20
15
10
5
0
WT
GLS^KO
B
C-CASPASE-3
KERATIN5
DAPI
MERGED
WT
GLS^KO

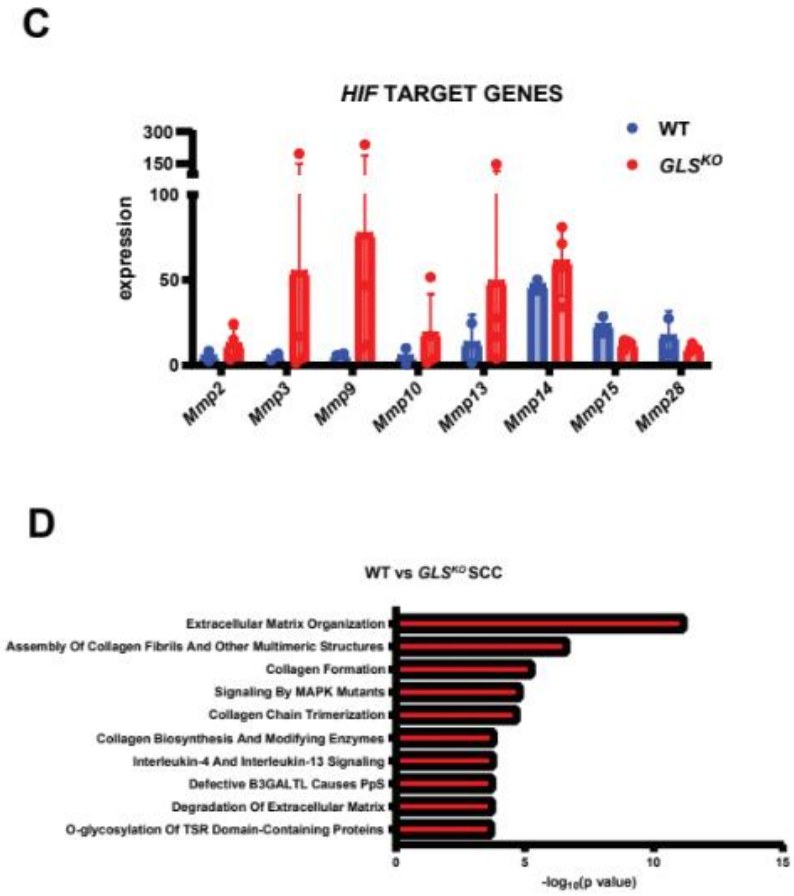

Fig S3 Extended characterization of GLS-deleted tumors

(**A**) WT or GLSKO SCC immunostaining for Ki67, a proliferation marker, and DAPI for cell nuclei. Quantification of percentage of Ki67 positive cells in WT (n=9) and GLSKO (n=5) SCCs. Scale bar, 100μm. (**B**) WT or GLSKO SCC immunostaining for Cleave-Caspase-3, an apoptosis marker, and DAPI for cell nuclei. Quantification of percentage of Cleave-Caspase-3 positive cells in WT (n=11) and GLSKO (n=5) SCCs. Scale bar, 100μm. (**C**) RNA-seq data of WT (n=2) or GLSKO (n=5) tumors showing transcription levels of HIF target genes. (**D**) Ontological analysis for biological processes increased in GLSKO SCCs compared to WT SCCs.

REFERENCES

1. O. Warburg, On respiratory impairment in cancer cells. Science 124, 269–270 (1956).
2. O. Warburg, On the origin of cancer cells. Science 123, 309–314 (1956).
3. K. Kozal, P. Jozwiak, A. Krzeslak, Contemporary Perspectives on the Warburg Effect Inhibition in Cancer Therapy. Cancer Control 28, 10732748211041243 (2021).
4. A. Flores, S. Sandoval-Gonzalez, R. Takahashi, A. Krall, L. Sathe, L. Wei, C. Radu, J. H. Joly, N. A. Graham, H. R. Christofk, W. E. Lowry, Increased lactate dehydrogenase activity is dispensable in squamous carcinoma cells of origin. Nat. Commun. 10, 91 (2019).
5. T. Li, C. Copeland, A. Le, Glutamine metabolism in cancer. Adv. Exp. Med. Biol. 1311, 17–38 (2021).
6. W. Yu, X. Yang, Q. Zhang, L. Sun, S. Yuan, Y. Xin, Targeting GLS1 to cancer therapy through glutamine metabolism. Clin. Transl. Oncol. 23, 2253–2268 (2021).
7. T. Kealey, R. Williams, M. P. Philpott, The human hair follicle engages in glutaminolysis and aerobic glycolysis: Implications for skin, splanchnic and neoplastic metabolism. Skin Pharmacol. 7, 41–46 (1994)
8. S. Hui, J. M. Ghergurovich, R. J. Morscher, C. Jang, X. Teng, W. Lu, L. A. Esparza, T. Reya, Z. Le, J. Yanxiang Guo, E. White, J. D. Rabinowitz, Glucose feeds the TCA cycle
9. S. Han, L. Zhu, Y. Zhu, Y. Meng, J. Li, P. Song, N. A. Yousafzai, L. Feng, M. Chen, Y. Wang, H. Jin, X. Wang, Targeting ATF4-dependent pro-survival autophagy to synergize glutaminolysis inhibition. Theranostics 11, 8464–8479 (2021).
10. H. Jin, S. Wang, E. A. Zaal, C. Wang, H. Wu, A. Bosma, F. Jochems, N. Isima, G. Jin, C. Lieftink, R. Beijersbergen, C. R. Berkers, W. Qin, R. Bernards, A powerful drug combination strategy targeting glutamine addiction for the treatment of human liver cancer. eLife 9, e56749 (2020).
11. P. Korangath, W. W. Teo, H. Sadik, L. Han, N. Mori, C. M. Huijts, F. Wildes, S. Bharti, Z. Zhang, C. A. Santa-Maria, H. Tsai, C. V. Dang, V. Stearns, Z. M. Bhujwalla, S. Sukumar, Targeting

glutamine metabolism in breast cancer with aminooxyacetate. Clin. Cancer Res. 21, 3263–3273 (2015).

12. C. Lasne, A. Gentil, I. Chouroulinkov, Two-stage carcinogenesis with rat embryo cells in tissue culture. *Br. J. Cancer* **35**, 722–729 (1977).
13. K. Goerttler, H. Loehrke, Improved tumour yields by means of a TPA-DMBA-TPA variation of the Berenrlum-Mottram experiment on the back skin of NMRI mice. The effect of stationary hyperplasia without inflammation. *Exp. Pathol.* **12**, 336–341 (1976).
14. A. C. White, K. Tran, J. Khuu, C. Dang, Y. Cui, S. W. Binder, W. E. Lowry, Defining the origins of Ras/p53-mediated squamous cell carcinoma. *Proc. Natl. Acad. Sci. U.S.A.* **108**, 7425–7430 (2011).
15. G. Lapouge, K. K. Youssef, B. Vokaer, Y. Achouri, C. Michaux, P. A. Sotiropoulou, C. Blanpain, Identifying the cellular origin of squamous skin tumors. *Proc. Natl. Acad. Sci. U.S.A.* **108**, 7431–7436 (2011).
16. T. Li, C. Copeland, A. Le, Glutamine metabolism in cancer. *Adv. Exp. Med. Biol.* **1311**, 17–38 (2021).
17. H. Jin, S. Wang, E. A. Zaal, C. Wang, H. Wu, A. Bosma, F. Jochems, N. Isima, G. Jin, C. Lieftink, R. Beijersbergen, C. R. Berkers, W. Qin, R. Bernards, A powerful drug combination strategy targeting glutamine addiction for the treatment of human liver cancer. *eLife* **9**, e56749 (2020).
18. K. Vanhove, E. Derveaux, G. J. Graulus, L. Mesotten, M. Thomeer, J. P. Noben, W. Guedens, P. Adriaensens, Glutamine addiction and therapeutic strategies in lung cancer. *Int. J. Mol. Sci.* **20**, 252 (2019).
19. T. Li, A. Le, Glutamine metabolism in cancer. *Adv. Exp. Med. Biol.* **1063**, 13–32 (2018).
20. J. Marquez, F. J. Alonso, J. M. Mates, J. A. Segura, M. Martin-Rufian, J. A. Campos-Sandoval, Glutamine addiction in gliomas. *Neurochem. Res.* **42**, 1735–1746 (2017).

21. A. C. White, W. E. Lowry, Refining the role for adult stem cells as cancer cells of origin. *Trends Cell Biol.* **25**, 11–20 (2015).
22. A. C. White, J. K. Khuu, C. Y. Dang, J. Hu, K. V. Tran, A. Liu, S. Gomez, Z. Zhang, R. Yi, P. Scumpia, M. Grigorian, W. E. Lowry, Stem cell quiescence acts as a tumour suppressor in squamous tumours. *Nat. Cell Biol.* **16**, 99–107 (2014).
23. K. Goerttler, H. Loehrke, Improved tumour yields by means of a TPA-DMBA-TPA variation of the Berenrlum-Mottram experiment on the back skin of NMRI mice. The effect of stationary hyperplasia without inflammation. *Exp. Pathol.* **12**, 336–341 (1976).

CHAPTER 3

Mechanisms of nutrient transporter in response to metabolic flexibility

INTRODUCTION

Transporters for nutrients are upregulated in cancers and go hand in hand with upregulation of their respective metabolic pathways. As demonstrated in Chapter 2, upon targeting of an enzyme in a single metabolic pathway, cancer cells are flexible to use another nutrient for their growth. Transgenic mice were used to knockout enzymes facilitating metabolism and growth in cancer, such as lactate dehydrogenase a (LDHA) and glutaminase (GLS). When knocking out these enzymes in cancer initiating cells for SCC, each single knockout condition resulted in metabolic flexibility facilitated by nutrient transporters like GLUT1 (glucose), ASCT2 (glutamine), and MCT1/4 (lactate). In this chapter, we examine the mechanisms of metabolic flexibility focusing on nutrient transporters and their regulation of growth in SCC.

RESULTS

To being to understand how glucose metabolism is influenced in GLS^{KO} SCC, we immunostained for GLUT1, a glucose transporter known to be up-regulated in SCC, and found diminished expression in GLS^{KO} tumors (Fig. 1A). Furthermore, fluorodeoxyglucose (FDG)–positron emission tomography (PET) imaging, which measures the rate of FDG uptake as a proxy for glucose uptake in tumors of live animals, also showed signs of decreased glucose uptake in the absence of GLS specifically in papilloma (Fig 1B) (1). Since there was elevated lactate metabolism in the GLS^{KO} tumors independent of glycolysis, we looked for evidence of changes in lactate transporter expression in GLS^{KO} tumors by staining for monocarboxylate transporter 1 (MCT1) and monocarboxylate transporter 4 (MCT4). These two transporters are known to allow both lactate and pyruvate to traverse the plasma membrane in both directions as needed (2). We found that MCT1 expression was unchanged in GLS^{KO} tumors, but MCT4 was up-regulated in GLS^{KO} tumors, providing an explanation for the increased lactate uptake and

utilization in *GLS*^{KO} tumors (Fig 2A and B). However, neither MCT1 nor MCT4 was differentially expressed at the RNA level, consistent with a posttranscriptional mechanism by which MCT4 protein is changed in these tumors (Fig 2C).

These results suggesting metabolic flexibility in *GLS*^{KO} tumors and capability to switch to a different carbon source through altering expression of nutrient transporters, in particular MCT4, prompted us to reexamine metabolic flexibility and nutrient transporter expression in tumors initiated by HFSCs lacking LDHA. These data, coupled with our observations about lactate transporter, MCT4, prompted us to ask whether glucose transporters are potentially dynamically regulated to mediate metabolic flexibility. We therefore immunostained for GLUT1, the glucose transporter, and found that GLUT1 protein expression at the cell membrane was strongly down-regulated in *LDHA*^{KO} tumors but up-regulated in *MPC*^{KO} tumors (Fig 3A and B).

Again, RNA-seq showed no changes in the expression of glucose transporter in LDHA-null tumors (Fig 3C) suggesting a posttranscriptional mechanism for the changes in GLUT1 protein levels. To identify such a mechanism, we looked at expression of thioredoxin-interacting protein (TXNIP), which is known to regulate GLUT1 levels at the plasma membrane (Fig 3D) (3). We stained for these two proteins in the various tumor models described here to see whether a correlation of expression of these proteins could serve to explain the membrane up- or down-regulation of metabolite transporters in response to genetic manipulation of LDHA or MPC. Immunohistochemistry (IHC) for TXNIP and GLUT1 showed a remarkable anticorrelation as previously described, and quantification of total expression for both of these proteins showed that TXNIP is expressed much lower in MPC-null tumors, and the converse was true in LDHA-null tumors (Fig 3E).

We next immunostained for ASCT2, a plasma membrane glutamine transporter, in our models of tumors initiated by HFSCs. *GLS*^{KO} tumors showed a significant decrease in ASCT2 protein consistent with the decrease in glutamine uptake and metabolism in these tumors (Fig 4A). ASCT2 protein at the membrane showed a strong increase in LDHA-null tumors, providing

a potential mechanism by which glutaminolysis was induced in these tumors (Fig 4B). Profiling multiple *WT* and *GLS*^{KO} tumors using RNA-seq analysis showed that neither ASCT2 nor other relevant transporters were differentially expressed (Fig 4C). ASCT2 is thought to form a complex with activated epidermal growth factor receptor (EGFR) (4), which is also known to be highly active in Ras-driven SCC (5, 6). We immunostained for active phosphorylated EGFR (pEGFR) and indeed found strong expression at the cell membrane in SCC driven by DMBA/TPA (Fig 4D), consistent with high EGF signaling activity. In tumors generated by *GLS*^{KO} HFSCs, pEGFR expression appeared to be localized to the cytoplasm rather than the plasma membrane, as shown by high-resolution confocal microscopy (Fig 4E and F). When looking at RNA-seq analysis for several pathways of downstream EGFR signaling such as mitogen-activated protein kinase (MAPK), phosphoinositide 3-kinase-protein kinase B (PI3K-AKT), and phospholipase C gamma (PLCg), there were scattered differentially expressed genes, but none of the pathways examined pointed to a change in signaling overall (Fig. S1A). Moreover, to probe for changes in EGFR signaling at the protein level, we also carried out a series of Western blots and immunostains for antibodies that recognize activity of signaling proteins (fig. S1, B and C). We found that there was an elevation of pEGFR expression in the *GLS*^{KO} tumors, despite the fact that there was diminished EGFR enrichment at the cell membrane. Downstream signaling of EGFR, however, was not consistent with the elevated EGFR expression seen in *GLS*^{KO} tumors. Despite elevation of EGFR activity as measured by this antibody, this did not correlate with increased tumor progression, perhaps because of the localization of the activity within the cell as opposed to just the overall activity. On the other hand, in tumors from the *LDHA*^{KO} background, the pEGFR was at the membrane and expressed at a higher level, similar to what was observed for ASCT2 (Fig 4G). Therefore, the elevated glutaminolysis observed in *LDHA*^{KO} tumors and diminished glutamine uptake observed in *GLS*^{KO} tumors could be due to dynamic regulation of active EGFR with ASCT2 at the membrane (Fig 4H).

The fact that genetic abrogation of two metabolic pathways blocked cancer formation and the intriguing pattern of nutrient transporter expression in single pathway deletions led us to hypothesize that perhaps coupling genetic blockade of glutaminolysis with small-molecule inhibition of lactate uptake could diminish tumor progression in the DMBA/TPA model. AZD0095 is an established inhibitor of MCT4, the transporter we showed that was up-regulated in GLS^{KO} tumors (Fig 2B). We treated both *WT* and GLS^{KO} tumor model mice with this inhibitor to test whether blocking the primary means of metabolic flexibility would have an effect on GLS^{KO} tumors. We tracked tumor formation and progression in *WT* and GLS^{KO} models before and after treatment with AZD0095 and found that, once lactate uptake was inhibited by AZD0095, the trajectory of tumorigenesis was diminished, specifically in tumors arising from deletion of GLS in cancer cells of origin (Fig 5A and B). Therefore, these data point toward the utility of blocking multiple metabolic pathways to treat cancer and demonstrate the importance of nutrient transporter regulation as a key mediator of metabolic flexibility.

Our data also show that when LDHA activity is blocked, an increase of glutamine uptake coincides with the up-regulation of the ASCT2 transporter (Fig 5C). Conversely, when GLS activity was genetically blocked, lactate uptake was increased along with expression of MCT4 transporter at the cell membrane (Fig 5C). Furthermore, we expanded previous findings to demonstrate that the GLUT1 transporter is key to the promotion and diminution of glycolytic activity observed in LDHA- and MPC-deleted tumors (Fig 3). The regulation of these transporters did not appear to be at the transcriptional level, as RNA-seq failed to identify changes in RNA expression of any of these transporters. These results suggest that interactions between these transporters and proteins, such as EGFR and TXNIP, mediate the regulation of cell membrane localization of these transporters, which then appear to drive metabolic flexibility (Fig 5C). We have yet to identify a mechanism for regulation of MCT4 at the membrane which can explain the increase in lactate uptake in the absence of GLS, but this will be an active area of investigation going forward. The mechanisms proposed here demonstrate that cancer cells

have a rather elegant means with which to compensate for loss of function of a metabolic pathway by simply putting more transporter at the membrane for an alternate pathway. Another outstanding question from this study is how cells appear to sense a deficiency in nutrient uptake from one pathway to then up-regulate alternative transporter concentration at the membrane.

FIGURES

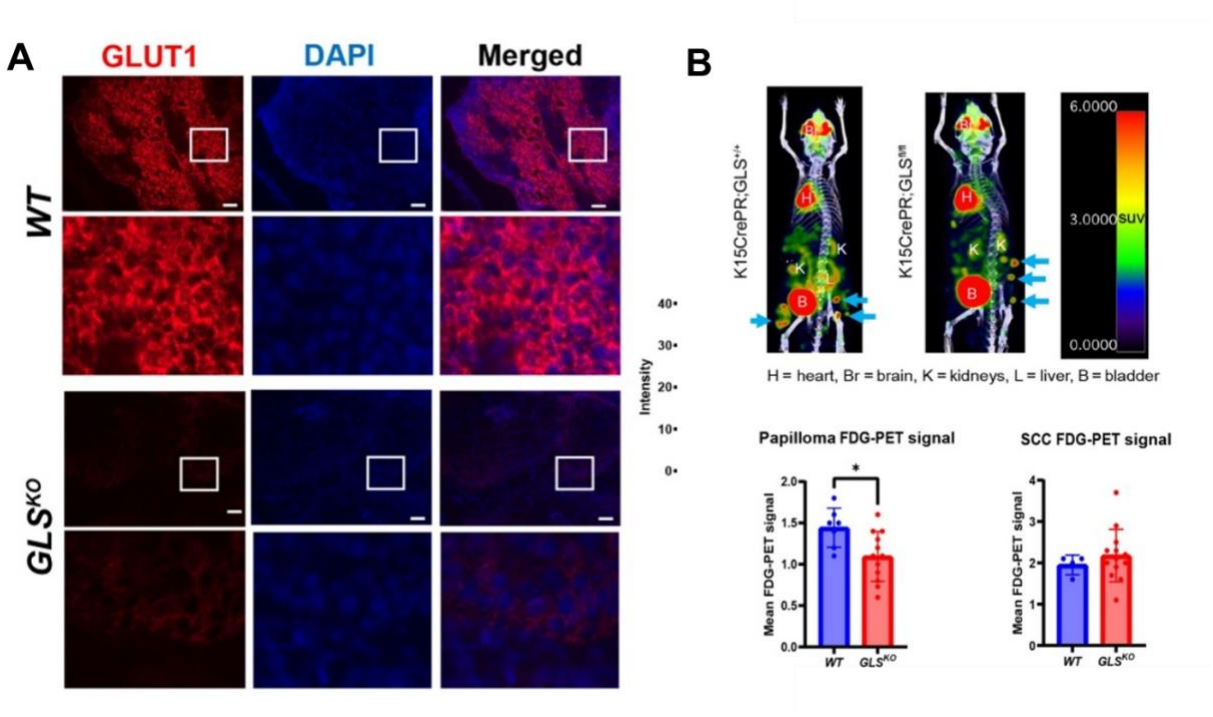

Fig. 1. Loss of GLS in tumors alters glutamine and glucose metabolism.

(**A**) *WT* or *GLS*^{KO} SCC immunostaining for glucose transporter, GLUT1. Cell nuclei were stained with DAPI. Quantification of mean intensity GLUT1 fluorescence in *WT* (*n* = 91) and *GLS*^{KO} (*n* = 56) SCCs. Scale bars, 100 μm. (**B**) Mean ^{18}F-FDG SUV signal of papilloma [*n* = 7 (*WT*), *n* = 12 (*GLS*^{KO})] and SCC [*n* = 4 (*WT*), *n* = 15 (*GLS*^{KO})]. H, heart; Br, brain; K, kidneys; L, liver; B, bladder. Statistical significance (**P* < 0.05, ***P* < 0.01, ****P* < 0.001, and *****P* < 0.0001) for (A) and (B) was calculated using a two-tailed *t* test.

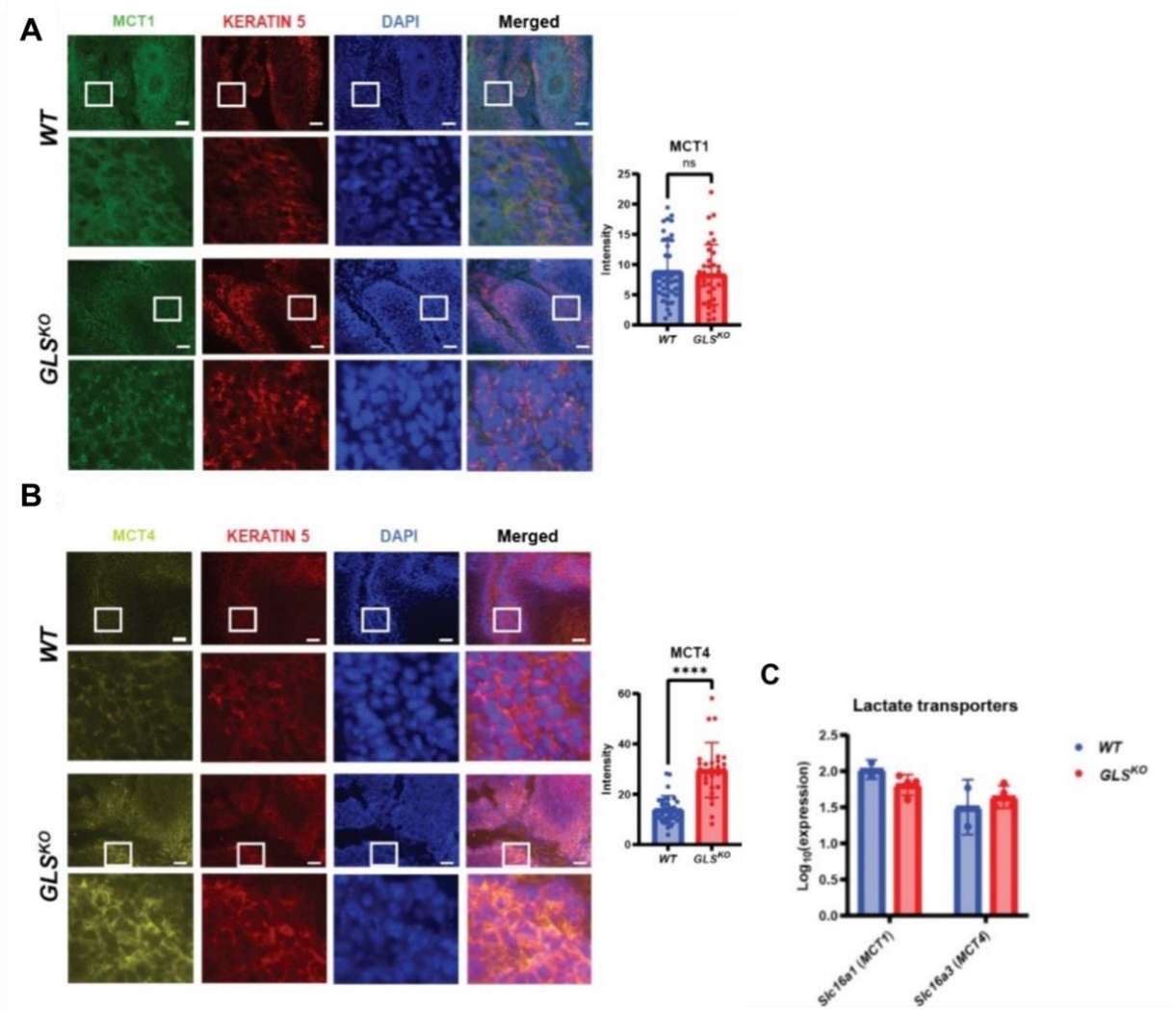

Fig. 2. Increased lactate transporter and uptake in *GLS*^{KO} SCC.

(**A**) *WT* or *GLS*^{KO} SCC immunostaining for lactate transporter, MCT1. Cell nuclei were stained with DAPI. Quantification of mean intensity MCT1 fluorescence in *WT* (*n* = 39) and *GLS*^{KO} (*n* = 36) SCCs. ns, not significant. Scale bars, 100 μm. (**B**) *WT* or *GLS*^{KO} SCC immunostaining for lactate transporter, MCT4. Cell nuclei were stained with DAPI. Quantification of mean intensity MCT4 fluorescence in *WT* (*n* = 33) and *GLS*^{KO} (*n* = 27) SCCs. Statistical significance (****$P <$ 0.0001) was calculated using a two-tailed *t* test. Scale bars, 100 μm. (**C**) RNA-seq data of *WT* (*n* = 2) or *GLS*^{KO} (*n* = 5) tumors showing transcription levels of lactate transporters.

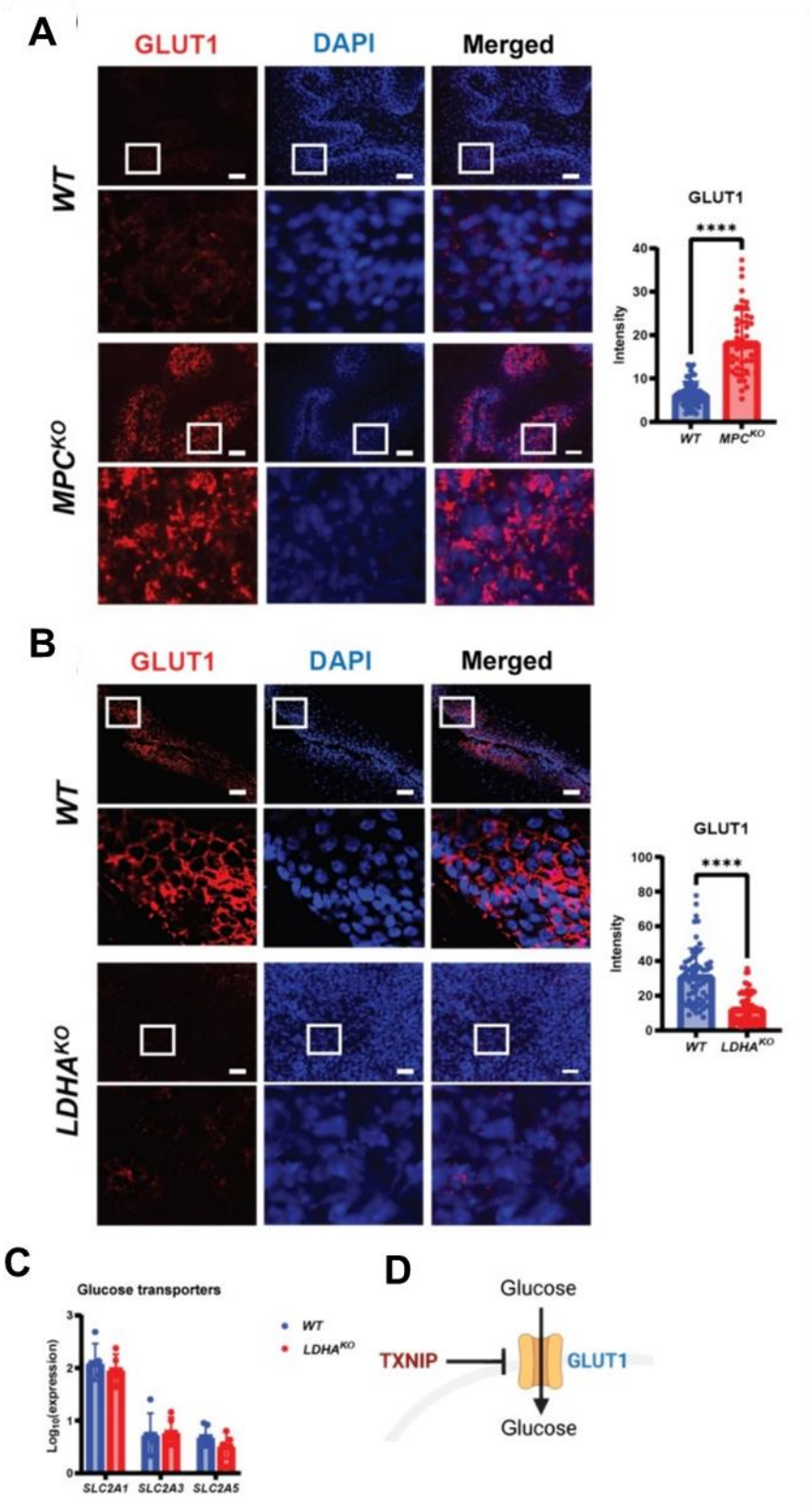
A
GLUT1
DAPI
Merged
WT
MPC^KO
GLUT1
****
Intensity
WT
MPC^KO
B
GLUT1
DAPI
Merged
WT
LDHA^KO
GLUT1
****
Intensity
WT
LDHA^KO
C
Glucose transporters
WT
LDHA^KO
Log10(expression)
SLC2A1
SLC2A3
SLC2A5
D
Glucose
TXNIP
GLUT1
Glucose

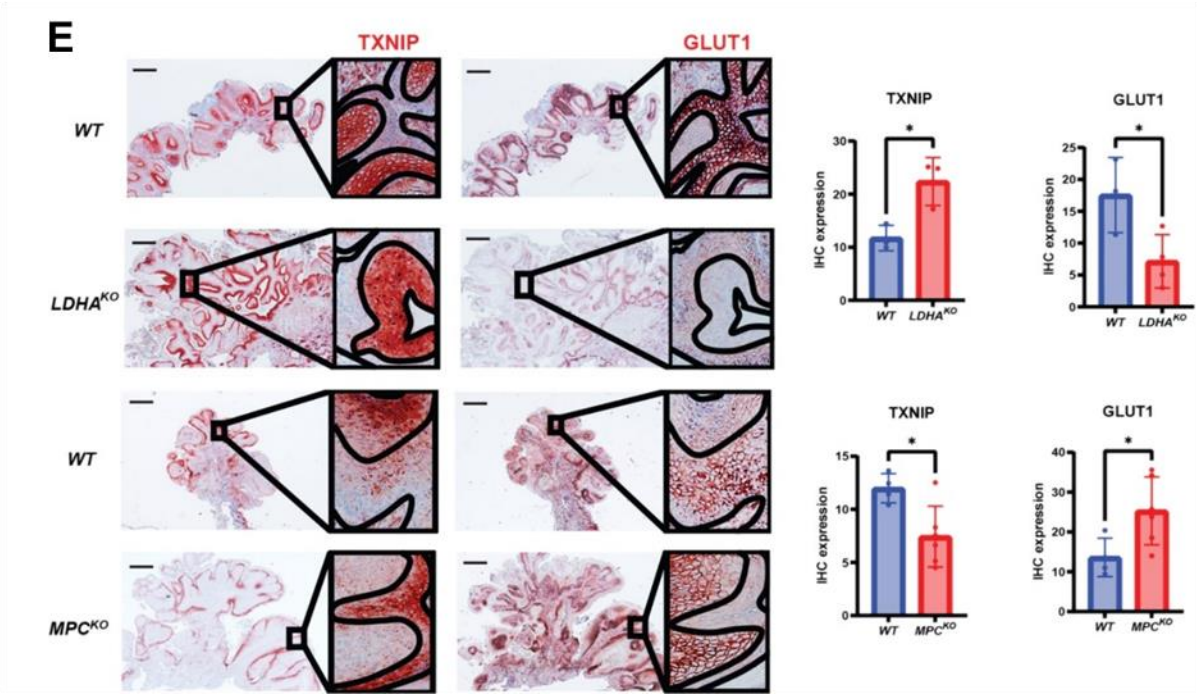

Fig. 3. Posttranscriptional increased glucose transporter at the cell surface.

(**A**) *WT* or *MPC*^{KO} SCC immunostaining for glucose transporter, GLUT1. Cell nuclei were stained with DAPI. Quantification of mean intensity GLUT1 fluorescence in *WT* (*n* = 56) and *MPC*^{KO} (*n* = 49) SCCs. Scale bars, 100 μm. (**B**) *WT* or *LDHA*^{KO} SCC immunostaining for glucose transporter, GLUT1. Cell nuclei were stained with DAPI. Quantification of mean intensity GLUT1 fluorescence in *WT* (*n* = 61) and *LDHA*^{KO} (*n* = 65) SCCs. Scale bars, 100 μm. (**C**) RNA-seq data of *WT* (*n* = 5) or *LDHA*^{KO} (*n* = 5) tumors showing transcription levels of glucose transporters. (**D**) Schematic of TXNIP inhibiting GLUT1. (**E**) *WT*, *LDHA*^{KO}, or *MPC*^{KO} tumor serial sections were probed for TXNIP and GLUT1. Lines in zoomed images mark boundaries of tissue structures and highlight anticorrelation between TXNIP and GLUT1. Quantification of TXNIP expression [*n* = 3 (*WT*), *n* = 3 (*LDHA*^{KO})] and [*n* = 4 (*WT*), *n* = 6 (*MPC*^{KO})] SCCs. Quantification of GLUT1 expression [*n* = 3 (*WT*), *n* = 4 (*LDHA*^{KO})] and [*n* = 4 (*WT*), *n* = 6 (*MPC*^{KO})] SCCs. Scale bars, 50 μm. Figure 3D was produced using BioRender. Statistical significance (*P < 0.05, **P < 0.01, ***P < 0.001, and ****P < 0.0001) for (A), (B), and (E) was calculated using a two-tailed *t* test.

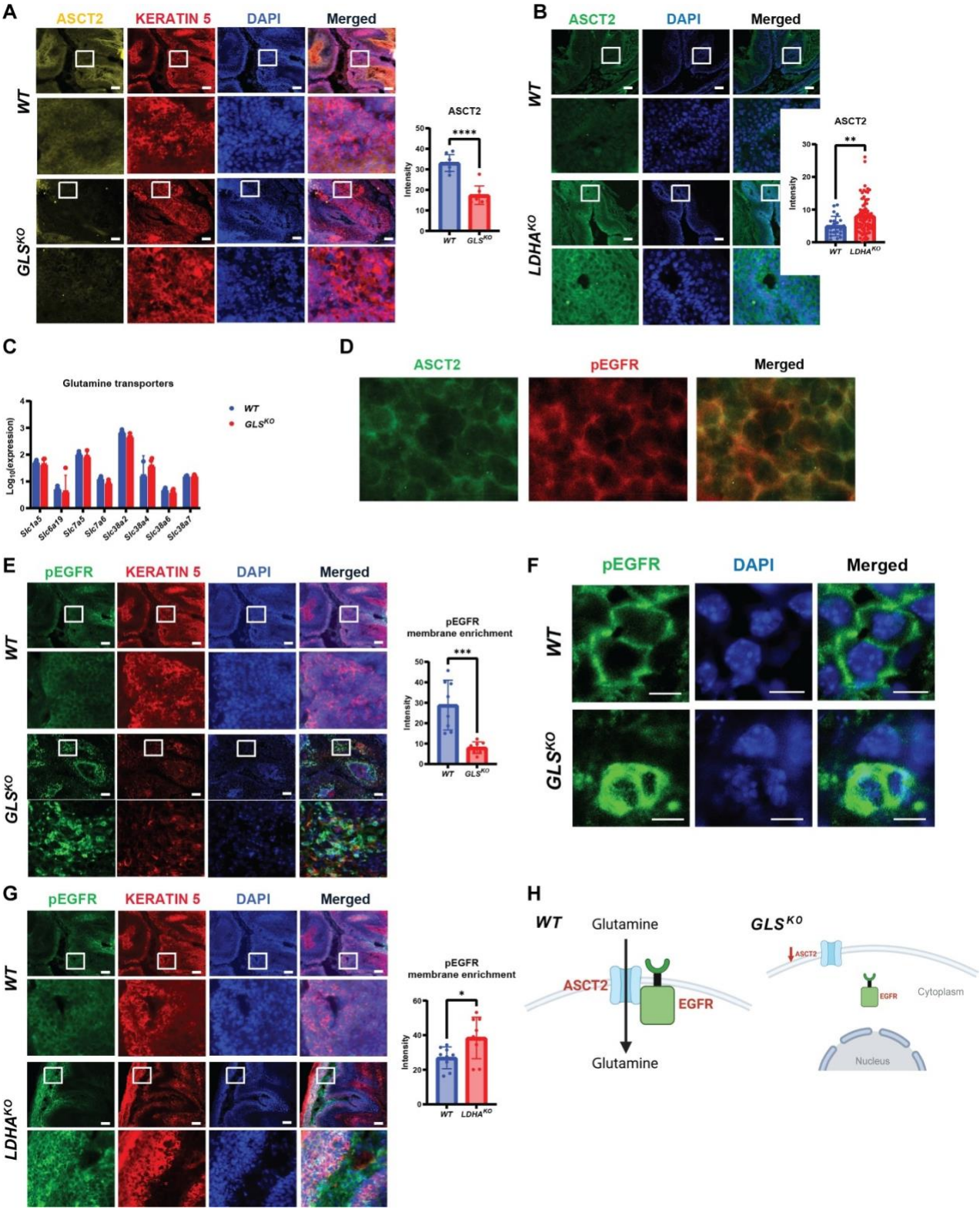
A
ASCT2
KERATIN 5
DAPI
Merged
WT
GLS^KO
ASCT2
****
Intensity
WT
GLS^KO
B
ASCT2
DAPI
Merged
WT
LDHA^KO
ASCT2
**
Intensity
WT
LDHA^KO
C
Glutamine transporters
Log10(expression)
WT
GLS^KO
Slc1a5
Slc6a19
Slc7a5
Slc7a6
Slc38a2
Slc38a4
Slc38a6
Slc38a7
D
ASCT2
pEGFR
Merged
E
pEGFR
KERATIN 5
DAPI
Merged
WT
GLS^KO
pEGFR
membrane enrichment
***
Intensity
WT
GLS^KO
F
pEGFR
DAPI
Merged
WT
GLS^KO
G
pEGFR
KERATIN 5
DAPI
Merged
WT
LDHA^KO
pEGFR
membrane enrichment
*
Intensity
WT
LDHA^KO
H
WT
Glutamine
ASCT2
EGFR
Glutamine
GLS^KO
ASCT2
EGFR
Cytoplasm
Nucleus

Fig. 4. Inhibition of the Warburg effect drives increase in glutamine transporter and uptake.

(A) *WT* or GLS^{KO} SCC immunostaining for glutamine transporter, ASCT2. Cell nuclei were stained with DAPI. Quantification of mean intensity ASCT2 fluorescence in *WT* (n = 8) and GLS^{KO} (n = 8) SCCs. Statistical significance (****P < 0.0001) was calculated using a two-tailed t test. Scale bars, 100 μm. (B) *WT* or $LDHA^{KO}$ SCC immunostaining for glutamine transporter, ASCT2. Cell nuclei were stained with DAPI. Quantification of mean intensity ASCT2 fluorescence in *WT* (n = 23) and $LDHA^{KO}$ (n = 74) SCCs. Statistical significance (**P < 0.01) was calculated using a two-tailed t test. Scale bars, 100 μm. (C) RNA-seq data of *WT* (n = 2) or GLS^{KO} (n = 5) tumors showing transcription levels of glutamine transporters. (D) Confocal microscopy for *WT* SCC immunostaining for ASCT2 and pEGFR. Scale bar, 20 μm. (E) *WT* or GLS^{KO} SCC immunostaining for pEGFR. Cell nuclei were stained with DAPI. Quantification of pEGFR membrane enrichment in *WT* (n = 8) and GLS^{KO} (n = 8) SCCs. Statistical significance (***P < 0.001) was calculated using a two-tailed t test. Scale bars, 100 μm. (F) Confocal microscopy of *WT* or GLS^{KO} SCC immunostaining for pEGFR. Scale bar, 10 μm. (G) *WT* or $LDHA^{KO}$ SCC immunostaining for pEGFR. Cell nuclei were stained with DAPI. Quantification of pEGFR membrane enrichment in *WT* (n = 9) and $LDHA^{KO}$ (n = 9) SCCs. Statistical significance (*P < 0.05) was calculated using a two-tailed t test. Scale bars, 100 μm. (H) Schematic proposing ASCT2 and EGFR localizations in *WT* and GLS^{KO} SCCs. Figure 4H was produced using BioRender.

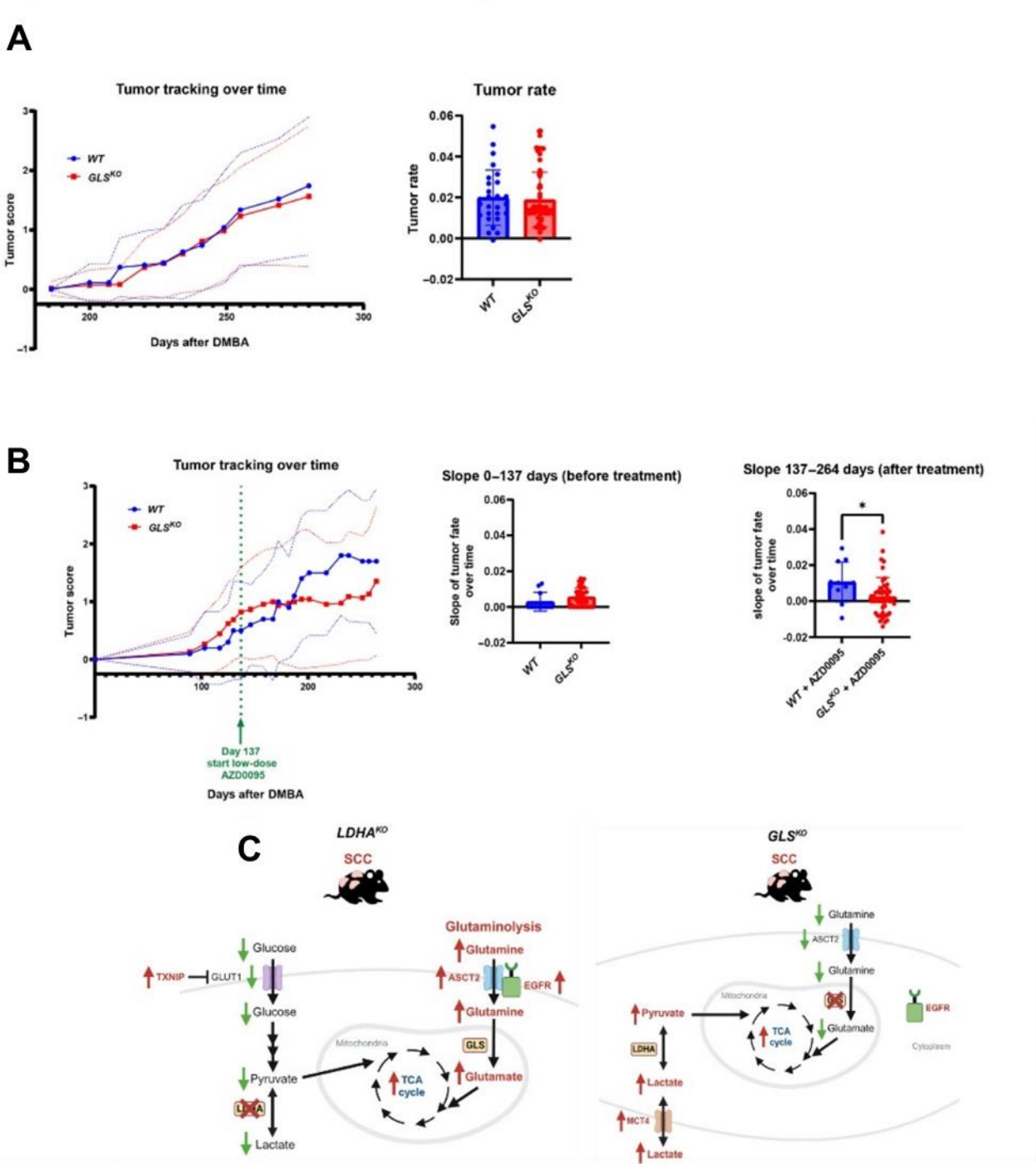

Fig. 5. Targeting both glutaminolysis and glycolysis in SCC.

(**A**) Tumor rates for *WT* (*n* = 26) and *GLS*^{KO} (*n* = 73) tumors during DMBA/TPA chemical carcinogenesis. (**B**) Tumor rates for *WT* (*n* = 11) and *GLS*^{KO} (*n* = 45) tumors treated with AZD0095 on day 137. Rates quantified before and after AZD0095 treatments. (**C**) Schematic of

proposed mechanisms of metabolic flexibility in *LDHA*^{KO} and *GLS*^{KO} HFSC-induced SCCs. Figure 5C was produced using BioRender.

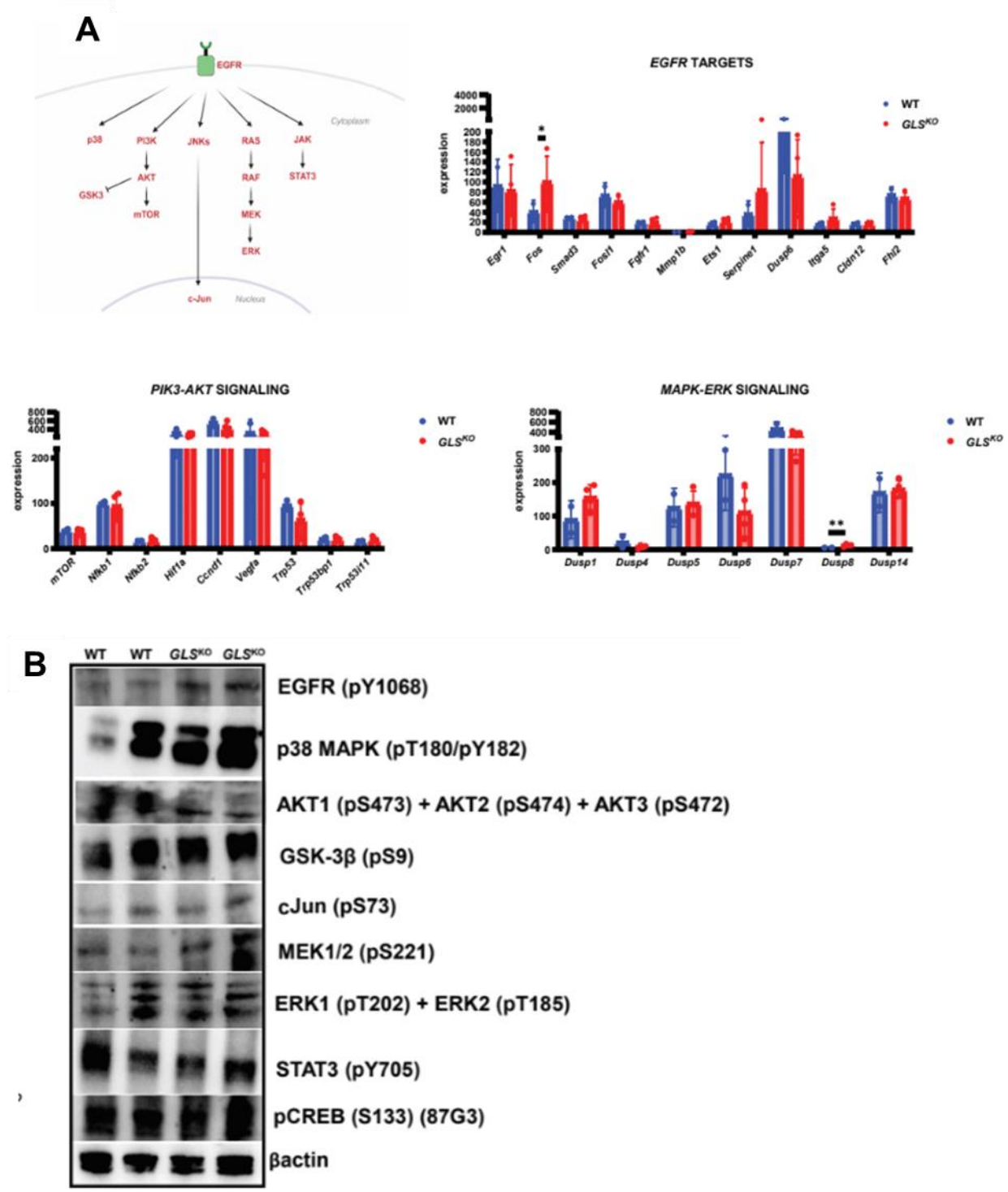

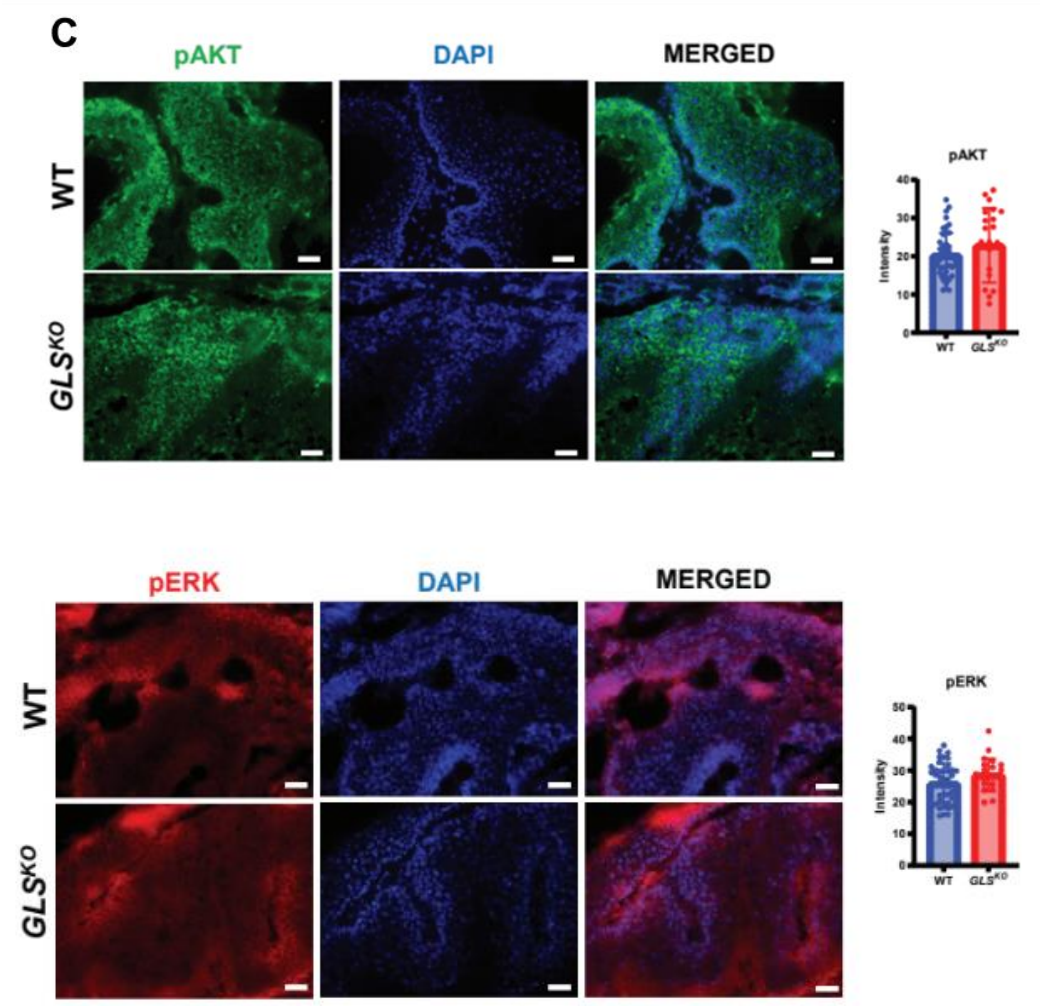

Figure S1 EGFR Signaling in *GLS*^{KO} tumors

(**A**) Schematic of EGFR downstream signaling and RNA-seq data of *WT* (n=2) or *GLS*^{KO} (n=5) tumors showing transcription levels of EGF target genes: EGFR, PIK3-AKT, and MAPK-ERK target genes. Statistical significance (*p<0.05; **p<0.01; ***<0.001; ****p<0.0001) was calculated using a two-tailed t test. Figure 3A was produced using Biorender.(**B**) Western blots of *WT* and *GLS*^{KO} SCCs probed for proteins associated with activated EGFR signaling. (**C**) *WT* or *GLS*^{KO} SCC immunostaining for downstream EGFR signaling, pAKT and pERK. Cell nuclei were stained with DAPI. Quantification of mean fluorescence intensity of pAKT, *WT* (n=46) and *GLS*^{KO} (n=22), and pERK, *WT* (n=41) and *GLS*^{KO} (n=22), in SCCs. Scale bar, 100μm.

REFERENCES

1. A. Flores, S. Sandoval-Gonzalez, R. Takahashi, A. Krall, L. Sathe, L. Wei, C. Radu, J. H. Joly, N. A. Graham, H. R. Christofk, W. E. Lowry, Increased lactate dehydrogenase activity is dispensable in squamous carcinoma cells of origin. Nat. Commun. 10, 91 (2019).
2. C. S. Hong, N. A. Graham, W. Gu, C. Espindola Camacho, V. Mah, E. L. Maresh, M. Alavi, L. Bagryanova, P. A. L. Krotee, B. K. Gardner, I. S. Behbahan, S. Horvath, D. Chia, I. K. Mellinghoff, S. A. Hurvitz, S. M. Dubinett, S. E. Critchlow, S. K. Kurdistani, L. Goodglick, D. Braas, T. G. Graeber, H. R. Christofk, MCT1 modulates cancer cell pyruvate export and growth of tumors that co-express MCT1 and MCT4. *Cell Rep.* 14, 1590–1601 (2016).
3. W. J. Sullivan, P. J. Mullen, E. W. Schmid, A. Flores, M. Momcilovic, M. S. Sharpley, D. Jelinek, A. E. Whiteley, M. B. Maxwell, B. R. Wilde, U. Banerjee, H. A. Coller, D. B. Shackelford, D. Braas, D. E. Ayer, T. Q. de Aguiar Vallim, W. E. Lowry, H. R. Christofk, Extracellular matrix remodeling regulates glucose metabolism through TXNIP destabilization. *Cell* 175, 117–132 e121 (2018).
4. H. Lu, X. Li, Y. Lu, S. Qiu, Z. Fan, ASCT2 (SLC1A5) is an EGFR-associated protein that can be co-targeted by cetuximab to sensitize cancer cells to ROS-induced apoptosis. *Cancer Lett.* 381, 23–30 (2016).
5. M. Watanabe, A. Nobuta, J. Tanaka, M. Asaka, An effect of K-ras gene mutation on epidermal growth factor receptor signal transduction in PANC-1 pancreatic carcinoma cells. *Int. J. Cancer* 67, 264–268 (1996).
6. J. DiGiovanni, O. Rho, W. Xian, L. Beltran, Role of the epidermal growth factor receptor and transforming growth factor alpha in mouse skin carcinogenesis. *Prog. Clin. Biol. Res.* 387, 113–138 (1994).

CHAPTER 4

Inhibition of pyruvate oxidation diminishes melanoma progression

INTRODUCTION

Emerging evidence suggests that cell fate can be influenced by changes in metabolic flux. For example, the activation of stem cells in the hair follicle, intestine and brain has been shown to be regulated by pyruvate oxidation [1]. In addition, there is extensive evidence that stem cells can serve as cancer cells of origin, and tumor cells are well-established to show profound metabolic changes that are thought to drive proliferation and metastasis [2]. One common metabolic change associated with cancer is increased glycolysis, namely the Warburg effect [3]. It was previously established that inhibition of pyruvate oxidation can promote glycolysis, and in some cases promote tumorigenesis [4]. Here we explored a role for pyruvate oxidation in melanocyte stem cell regulation and their ability to drive melanoma formation. Melanocyte Stem Cells (MeSCs) reside in the hair follicle bulge adjacent to hair follicle stem cells (HFSCs) [5]. MeSCs of the hair repeatedly proliferate and differentiate during each hair cycle to pigment the hair follicles. It has been recently shown that quiescent melanocytes are a cell of origin for Melanoma [6], the most devastating type of skin cancer due to its highly metastatic potential. At the molecular level, activating mutations in RAS-RAF-MEK-ERK signaling pathway are found in the majority of the cutaneous melanomas[7]. For over 100 years, carcinogenesis has been coupled to metabolic changes, particularly the Warburg effect, whereby tumor cells take up high amounts of glucose and secrete lactate as a product of glycolysis[8]. Because of the near ubiquity of this observation across cancers, it was presumed that glycolysis and lactate secretion was critical for oncogenesis[4]. However, we previously showed that genetic deletion or promotion of the Warburg effect in nascent squamous cell carcinoma had no effect on tumorigenesis, except at the metabolic level where tumors exploited metabolic flexibility by increasing their utilization of glutamine through a process called glutaminolysis[9]. Over the last 10 years we have identified metabolic pathways that are

specifically enriched in hair follicle stem cells and showed that manipulation of these pathways can strongly regulate hair follicle stem cell activation[1]. We hypothesized that many adult stem cells in various tissues share enrichment for glycolytic metabolism that we observed in HFSCs, and therefore would respond to inhibition of pyruvate oxidation in a similar manner. As the key mediator of pyruvate oxidation, the mitochondrial pyruvate carrier is made up of multiple subunits of the proteins Mpc1 and Mpc2[10]. Genetic deletion of this complex during embryonic development is lethal, and many groups have used conditional deletion to remove this activity from a variety of tissues. In each tissue, loss of Mpc led to distinct effects, some beneficial, in others deleterious.

RESULTS

To determine the role of pyruvate oxidation in MeSC homeostasis we created transgenic animals bearing alleles for both Tyr-CreER and floxed Mpc1. At the start of the hair cycle, the first observable event macroscopically is pigmentation due to melanocytes generated from MeSCs, therefore measuring time to pigmentation is an accurate reflection of MeSC activation. As shown in Figure 1, deletion of Mpc1 before the start of the second adult hair cycle by Tamoxifen administration did not appear to affect the pigmentation, timing of the hair cycle, of follicular morphogenesis, or the number of melanocytes, suggesting that inhibition of pyruvate oxidation is not necessary for MeSC activation (Fig 1A-C). We confirmed that Mpc1 deletion did have an effect on metabolism in targeted cells by sorting MeSCs and performing metabolomics on mice pulsed with C13-Glucose (Fig 1D. In MeSCs with Mpc1 deletion, we did detect an increase in lactate production and inhibition of pyruvate oxidation as measured by C13 incorporation into TCA metabolites and amino acids (Fig 1D). The fact that Mpc1 deletion did not affect MeSC activation is not consistent with a similar deletion in HFSCs, which led to a strong activation and premature initiation of the hair cycle or ISCs and NSCs, which in both cases led to increased proliferation.

As MeSCs have been shown to be cells of origin for Melanoma, we next tested whether deletion of Mpc1 in MeSCs would affect their ability to initiate or propagate melanoma. We crossed mice to generate transgenic animals with Tyr-CreER, floxed-Mpc1, Lox-Stop-Lox BrafV600F, and floxed-Pten alleles, a combination that has become the accepted standard for murine melanoma GEMM. Remarkably, mice lacking Mpc1 in MeSCs showed reduced tumor burden, but no change in the time to tumor initiation (Fig 2A). Western blotting from these tumors confirmed deletion of Mpc1 (Fig 2B). Probing tumors histologically, we found that Mpc1 deleted tumors presented with a less invasive phenotype, and diminished proliferation as measured by expression of Sox10 and Mcm2 (Fig 2C and D). As another measure of tumor grade, we used FDG-PET imaging to examine glucose uptake in Braf/Pten driven tumors with and without Mpc1. In fact, Mpc1 KO tumors showed considerably less FDG uptake consistent with a lower tumor grade (Fig 2E). We also derived cell lines from these same melanoma described in Fig 2 to assess the effect of inhibition of pyruvate oxidation *in vitro*. In fact, cell lines derived from Mpc1 KO tumors still demonstrated a lower proliferation rate, as shown *in vivo* (Fig 2F and G). Furthermore, treating wildtype melanoma tumors with UK5099, an established small molecule inhibitor of Mcp1 (IC50 = 50nM), also slowed cell division *in vitro*, consistent with the Mpc1 deleted tumors *in vitro* and *in vivo* (Fig 2F and G).

To summarize, inhibition of pyruvate oxidation did not appear to have an effect on the self-renewal or differentiation of melanocytes, but did show an effect on melanoma formation from melanocyte stem cells. Despite the fact that Mpc inhibition in associated with elevation of glycolysis which is thought to drive cancer formation, we found just the opposite to be true, namely that inhibition of pyruvate oxidation in fact led to diminished melanoma aggressiveness both *in vivo* and *in vitro*.

FIGURES

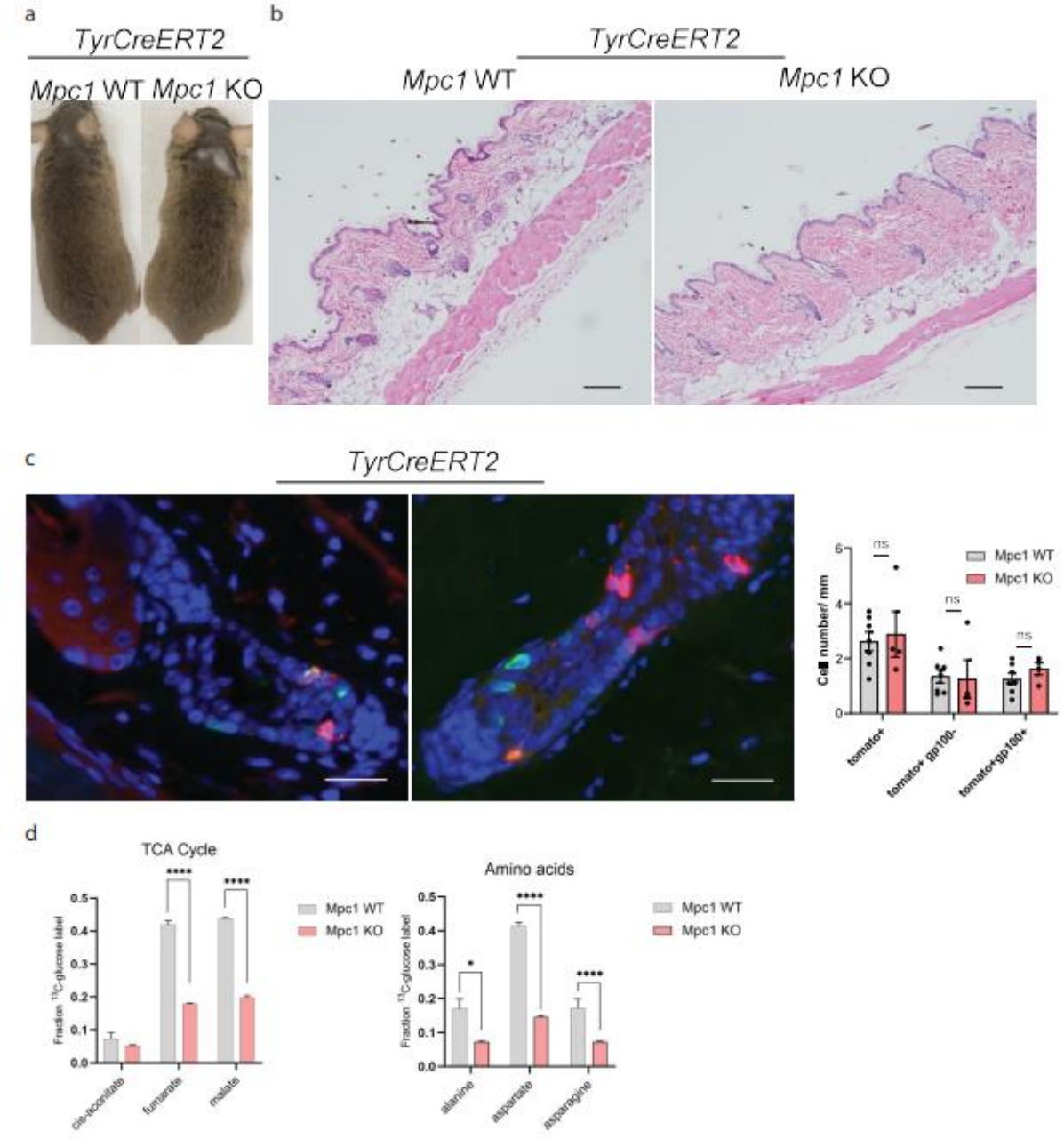

Figure 1. Deletion of Mpc1 in MeSCs does not affect melanogenesis or pigmentation

A, Macroscopic images of mice 2 months after deletion of Mpc1 via recombination under the control of the inducible TyrCreER transgene showed no effect on pigmentation in hair. **B**, Histological images of wildtype and Mpc1 deletion animals did not show microscopic effects on melanogenesis. **C**, Microscopic imaging of Tomato allele combined with Mpc1 deletion under

TyrCreER did not lead to altered numbers of MeSCs as shown and quantified. **D**, Metabolomics on sorted MeSCs (via Tomato expression) showed diminished TCA cycle intermediates and amino acids as would be expected if pyruvate oxidation is blocked by the loss of Mpc1.

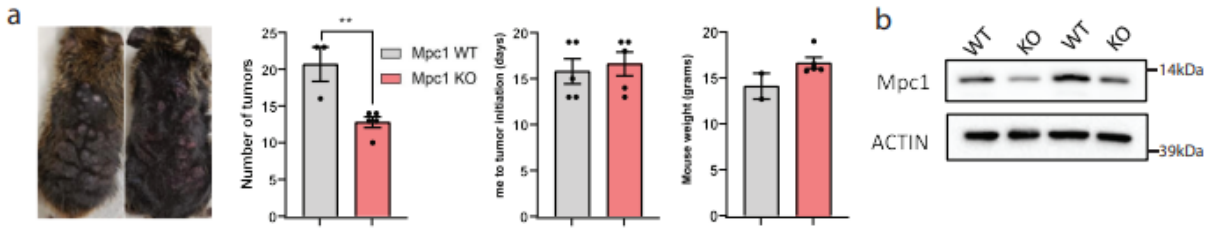

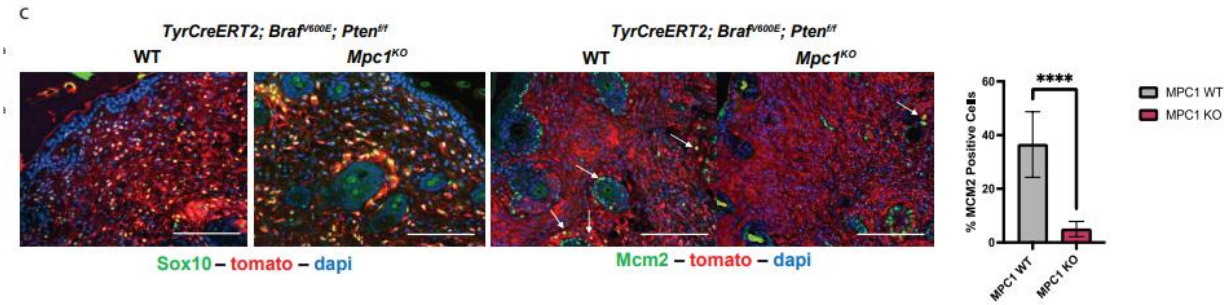

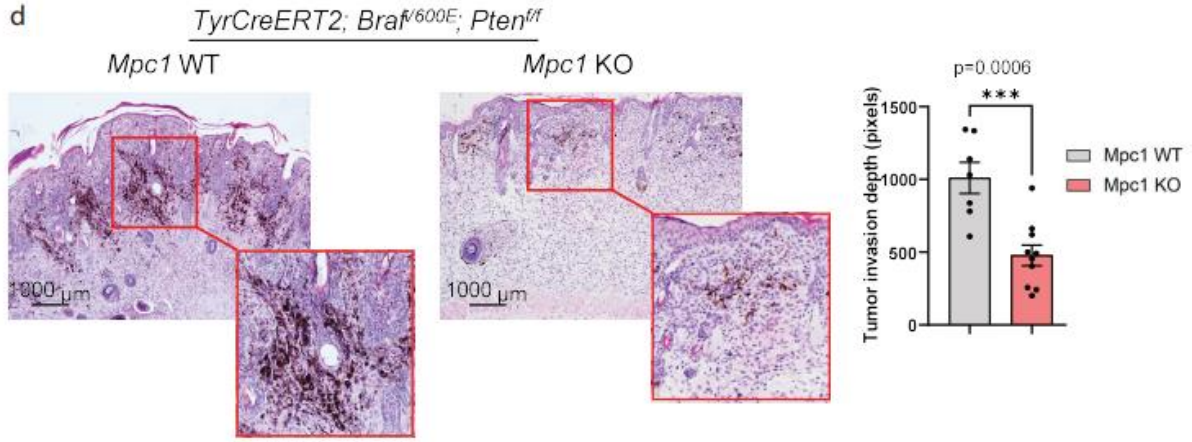

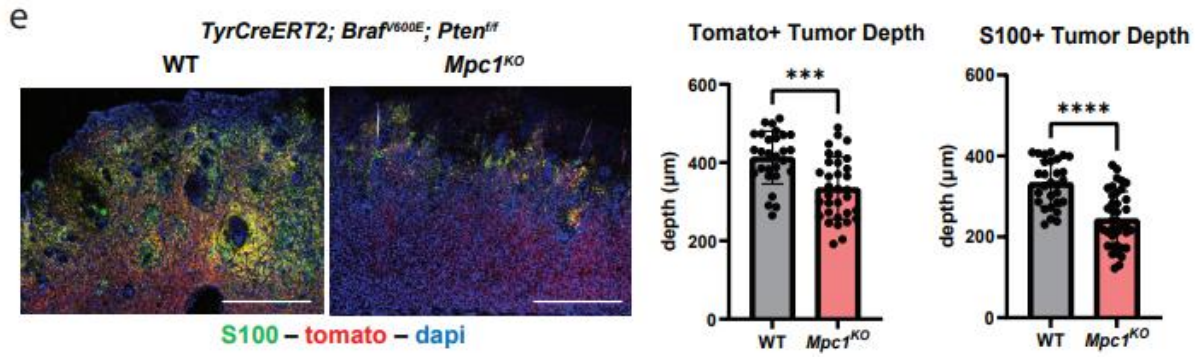
e
TyrCreERT2; Braf V600E; Pten f/f
WT
Mpc1 KO
S100 – tomato – dapi
Tomato+ Tumor Depth
S100+ Tumor Depth
depth (µm)
***
****
WT
Mpc1 KO

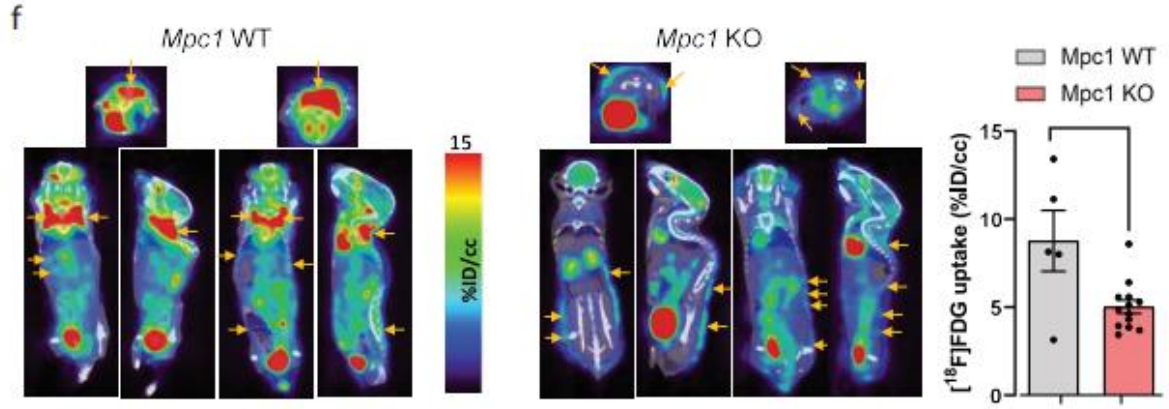
f
Mpc1 WT
Mpc1 KO
15
%ID/cc
Mpc1 WT
Mpc1 KO
[18F]FDG uptake (%ID/cc)

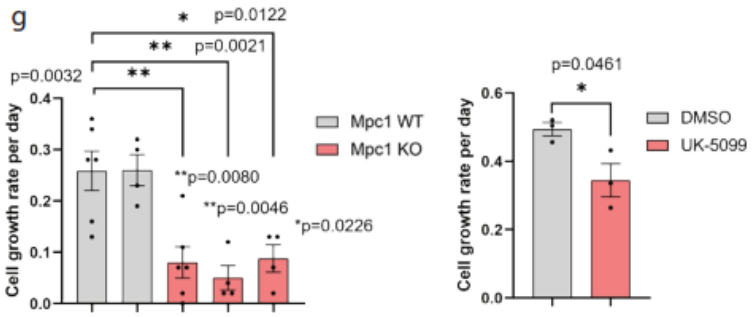
g
p=0.0122
p=0.0021
p=0.0032
**p=0.0080
**p=0.0046
*p=0.0226
Cell growth rate per day
Mpc1 WT
Mpc1 KO
p=0.0461
DMSO
UK-5099

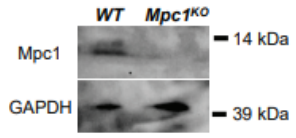
h
WT
Mpc1 KO
Mpc1
GAPDH
14 kDa
39 kDa

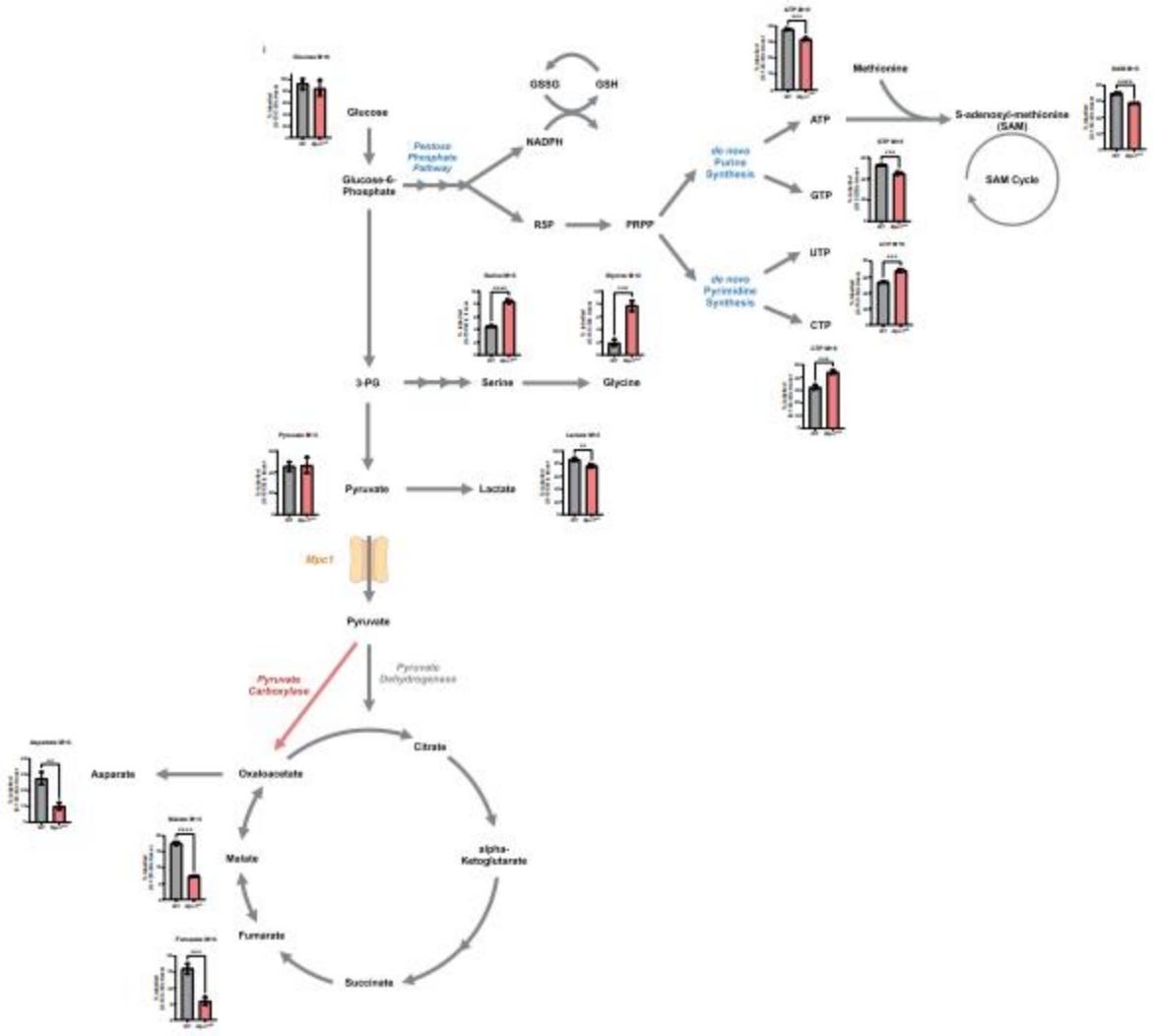

Figure 2. Deletion of Mpc1 during melanonamgenesis abrogates tumor progression
A, Macroscopic images and quantification of mice with (left) and without Mpc1 (right) in MeSCs after induction of expression of Braf and loss of Pten. The number of tumors was diminished in the Mpc1 KO mice compared to control, but the time to tumor formation was not affected. **B,** Western blotting with tumor tissue with and without Mpc1 was performed to validate the deletion in the tumors. **C**, Microscopic imaging of tumor tissue showed that Mpc1-deleted tumors had reduced proliferation of the melanoma compared to wildtype. **D**, Histological staining of tumors suggested reduced invasion and progression in the absence of Mpc1. **E**, Immunostaining with markers of melanoma and recombination (tdTomato) confirmed that Mpc1 tumors show diminished invasion. **F**. Live animal FDG-PET imaging showed a diminished overall tumors as

measured by FDG uptake, confirming the macroscopic analysis in **A**. **G**, left, Cell lines isolated from the tumors described showed reduced proliferation in the absence of Mpc1. Right, treatment of wildtype cell lines with UK5099, which blocks Mpc1 function, suppressed proliferation of melanoma cells *in vitro*. **H**, Metabolomics with c13-glucose to compare glucose utilization in wildtype and Mpc1-KO tumors showed evidence of both diminished pyruvate oxidation (malate and fumarate labeling), and increased one carbon metabolism (serine and glycine) and effects on the Pentose Phosphate Pathway

REFERENCES

1. Flores, A., et al., Lactate dehydrogenase activity drives hair follicle stem cell activation. Nat Cell Biol, 2017. 19(9): p. 1017-1026.PMC5657543
2. Schell, J.C., et al., Control of intestinal stem cell function and proliferation by mitochondrial pyruvate metabolism. Nat Cell Biol, 2017. 19(9): p. 1027-1036.PMC6137334
3. Petrelli, F., et al., Mitochondrial pyruvate metabolism regulates the activation of quiescent adult neural stem cells. Sci Adv, 2023. 9(9): p. eadd5220.PMC9977184
4. Warburg, O., On the origin of cancer cells. Science, 1956. 123(3191): p. 309-14,
5. Schell, J.C., et al., A role for the mitochondrial pyruvate carrier as a repressor of the Warburg effect and colon cancer cell growth. Mol Cell, 2014. 56(3): p. 400-13.PMC4268416
6. Steingrimsson, E., N.G. Copeland, and N.A. Jenkins, Melanocyte stem cell maintenance and hair graying. Cell, 2005. 121(1): p. 9-12,
7. Moon, H., et al., Melanocyte Stem Cell Activation and Translocation Initiate Cutaneous Melanoma in Response to UV Exposure. Cell Stem Cell, 2017. 21(5): p. 665-678 e6.PMC9004284
8. Warburg, O., On respiratory impairment in cancer cells. Science, 1956. 124(3215): p. 269-70,
9. Flores, A., et al., Increased lactate dehydrogenase activity is dispensable in squamous carcinoma cells of origin. Nat Commun, 2019. 10(1): p. 91.PMC6327029
10. Zhong, Y., et al., Application of mitochondrial pyruvate carrier blocker UK5099 creates metabolic reprogram and greater stem-like properties in LnCap prostate cancer cells in vitro. Oncotarget,2015. 6(35): p. 37758-69.PMC4741963
11. Patterson, J.N., et al., Mitochondrial metabolism of pyruvate is essential for regulating glucosestimulated insulin secretion. J Biol Chem, 2014. 289(19): p. 13335-46.PMC4036342

12. Hildyard, J.C., et al., Identification and characterisation of a new class of highly specific and potent inhibitors of the mitochondrial pyruvate carrier. Biochim Biophys Acta, 2005. 1707(2-3):p. 221-30,

CHAPTER 5

CONCLUSION

These projects have identified metabolic flexibility, limits to flexibility, and therapeutic targets in SCC and melanoma. Although both skin cancers exhibit differences in their response to altering metabolism, our data potentially point toward therapeutic combinatorial strategies to target cancer initiation and progression. In SCC, targeting LDHA or GLS alone is not effective in preventing SCC formation because cancer cells adapt and use other metabolic pathway to grow. However, targeting both LDHA and GLS in combination is effective to starve cancer cells from their carbon sources and prevent SCC formation. These results elucidate the effectiveness of targeting glycolysis, lactate metabolism, or glutaminolysis in combination. Using this, we can identify metabolic targets, such as transporters and enzymes, associated with these processes in combination moving forward. In melanoma, we did see a single knock out of Mpc1 was effective in decreasing progression of the cancer. Although it did not fully eliminate the cancer, using a combination of Mpc1 inhibition and other enzymes or transporters like GLS, ASCT2, GLUT1, MCT4 would be of interest moving forward to completely abolish tumorigenesis.

While previous studies argued that blockade of individual metabolic nodes could be an effective treatment strategy, our data argue otherwise. It is worth speculating that the difference between these outcomes could be due to the cancer models being used, namely, *in vitro* versus *in vivo*. Our data in SCC are consistent with studies showing that instead multiple metabolic pathways must be targeted to overcome metabolic flexibility of cancer cells, including a previous *in vivo* study in lung cancer showing that tumors that are insensitive to inhibition of glycolysis or GLS alone, are sensitive to the combination of both glycolysis and GLS inhibition (1-3). *In vivo*, cancer cells have access to the tumor microenvironment, circulation, and immune cells, so it is possible that targeting one pathway *in vitro* can be effective because it does not have access to other nutrients or cell types that are present *in vivo*. As a result, therapeutic abrogation of cancer progression will probably require pharmacological targeting of more than

one pathway as our genetic data presented here suggest. Fortunately, extensive effort has been devoted to creating small-molecule inhibitors of various metabolite uptake and utilization pathways such as CB839 (GLS), GSK2837808A (LDHA), UK5099 (Mpc1), and AZD0095 (MCT4). All these compounds show good safety profiles; however, none of these compounds by themselves effectively block tumor progression but perhaps could be more efficacious in combination. It is worth noting that another approach with the drug 6-Diazo-5-oxo-l-norleucine (DON) is beginning to show promise in clinical trials (4-6). However, this compound appears to target many proteins in the glutamine utilization pathway and perhaps has targets outside of the glutamine pathway, in which case would be consistent with the hypothesis that it is necessary to target multiple metabolic nodes to treat cancer.

While our study to target melanoma through metabolism is focused on one metabolic target, Mpc1, this alone was enough to impact tumorigenesis and lead to a less aggressive melanoma. On the same theme as SCC, it is likely targeting Mpc1 in melanoma will need to be combined with another therapeutic or metabolic target to fully diminish the cancer. Since melanoma is so deadly due to its aggressiveness, our results highlight the importance to continue to study Mpc1 inhibition in melanoma. Future studies include treating melanoma with UK5099, Mpc1 inhibitor, chronically over time at different time points *in vivo* to track when Mpc1 inhibition is most effective. UK5099 can be formulated in chow and fed to mice as early as post weaning exhibiting a chronic treatment of Mpc1 inhibition. Additionally, it would be interesting to combine UK5099 treatment with another metabolic target, or another therapeutic for melanoma such as immunotherapy or radiation therapy. To extend that study, focusing on melanoma that is resistant to other therapies would be interesting to treat with Mpc1 inhibition to observe if targeting metabolism in melanoma is most effective pre- or post-therapeutic intervention by other approaches.

Of the many striking results, the *GLS*^{KO}*LDHA*^{KO} mice that failed to generate SCC was very exciting and led to question exactly how these double knock out mice regress or become necrotic. Since we have a general timeline of when papilloma do form in these mice, we can generate these mice, begin the chemical carcinogenesis, and at the timepoint we observe these papilloma begin to form or regress, we collect the papilloma and characterize them for metabolomics, RNAseq, immunoblotting, and histology. It can be that the papilloma might not rely on the generation of lactate or glutamine being used for TCA, and solely grow using glucose metabolism for TCA cycle derived ATP. However, as they try to transform, their machinery required the use of enzymes like LDHA and GLS to facilitate the transformation. It would be interesting to specifically focus on the immune cells during this process. Since we did observe a presence of macrophages in the wildtype and knock out SCCs, its likely they are also present during the papilloma development in the *GLS*^{KO}*LDHA*^{KO} mice. The macrophages observed, however, were not infiltrating the tumor, instead they were in the tumor mesenchyme. Macrophages have elevated glutamine metabolism to sustain their growth (7), so it's possible they are driven to the tumor for glutamine since cancer cells can't use the glutamine in either *GLS*^{KO} or *GLS*^{KO}*LDHA*^{KO} mice. In the double knock out specifically, it could be the immune cells take up all the nutrients that the cancer cells can't use because their machinery to metabolize them is knocked out. This could then create more powerful immune cells that could potentially infiltrate tumors at the papilloma phase and cause regression. Specific promoters that target certain immune cells could also be used down the line to knock out GLS or LDHA alone or in combination with the HFSC knockouts which only target the epithelial cells in the tumor. Nonetheless, characterizing the role of immune cells during this process is key to identify the crosstalk between cancer cells, immune cells, and regression.

Our data also point toward the need to inhibit multiple pathways to achieve effective cancer therapy and circumvent the metabolic flexibility. We hypothesize that in the double-mutant tumors deleted for LDHA and GLS, HFSCs failed to up-regulate alternative pathways to

substitute for the loss of glutaminolysis and lactate utilization as compensatory mechanisms and, as a result, failed to fuel the TCA cycle leading to tumor growth. As a test of these hypothesis, we showed that blocking the activity of a nutrient transporter (MCT4) specifically diminished tumorigenesis in *GLS*^{KO} tumors and had no effect on tumorigenesis in GLS-expressing cells. Therefore, it is worth speculating that inhibition of nutrient uptake could be an effective strategy to treat cancer. Future efforts will be devoted to both understanding the biochemical mechanisms underlying nutrient transporter expression at cancer cell membranes and developing methods to inhibit metabolic flexibility for the treatment of cancer.

As mentioned before, there are various small molecule inhibitors that target the enzymes or transporters that we focused on in our SCC studies. To that end, ongoing experiments focus on recapitulating our genetic results with pharmacological inhibitors. First, we aim to recapitulate the *GLS*^{KO}*LDHA*^{KO} results by using inhibitors to target GLS, such as CB839, and LDHA, such as GSK2837808A in combination. Additionally, we are treating mice with AZD0095, MCT4 inhibitor, and CB839 to recapitulate the findings were observed in *GLS*^{KO} mice treated with AZD0095. Because we did observe nutrient transporters to play a key role during metabolic flexibility, we are also interested in treating mice with combinations of transporter inhibitors or different combinations of enzyme + transporter inhibitors to identify effective targets.

When setting up these experiments, the timing of when to begin treatment is important. During the DMBA/TPA skin chemical carcinogenesis, there is an initiation phase, where we treat with DMBA, progression phase, which consists of contiguous TPA treatment, and then the development of SCCs. If deciding to treat with inhibitors right after the initiation phase and continue to treat until the end of the experiment, that will show the effectiveness of the inhibitor combination as a preventative. If treating with inhibitors when a papilloma forms, which typically takes 10-15 weeks, that can represent a benign tumor in the clinic and effectiveness of inhibition can translate to the treatment of lower stage SCCs in patients. Moreover, treating with inhibitors when SCCs develop can translate inhibitor combinations being used for treatment of patients

with SCC that are already developed. All these experiments will provide valuable information for a translational purpose. The concentration of inhibitors and frequency of inhibitor application will also play a crucial role in the effectiveness of these future experiments.

Studies have shown that metabolites themselves can act as signaling molecules by directly binding to protein targets to regulate their activity. Perhaps lactate is the best example of this phenomenon, where proteins can be covalently modified by lactylation on lysine residues. Probing for lactylation in our skin cancer models and different knock out conditions will begin to explore the crosstalk between metabolites and downstream signaling. However, it is possible that instead of altered levels of particular metabolites, metabolites trigger a distinct signal that then changes the level of TXNIP protein levels to regulate the glucose transporter or EGFR at the membrane to regulate ASCT2. TXNIP has been shown in different contexts to be regulated at the RNA level by zinc finger protein 36 (ZFP36) and by microRNAs or at the transcriptional level by oncogenes, cytokines, and growth factors, but our initial efforts to demonstrate a similar mechanism did not yield substantial results. Until there are better described pathways for nutrient expression as a regulator of metabolic flexibility, perhaps small-molecule manipulation of these transporters would be the best way to circumvent metabolic flexibility to treat cancer. For EGFR and ASCT2 regulation, it would be interesting to treat tumors with EGFR inhibitors to determine if that can also influence glutamine transport and metabolism in our models. Vast studies on EGFR in cancer have led to significant effort to create effective EGFR inhibitors to treat cancer, however, these inhibitors alone as a therapeutic have failed. With our results in SCC, it would be interesting to test a combination of LDHA inhibitors with EGFR inhibitors and see if that also recapitulates the same changes in EGFR localization and glutamine transporter levels.

In the coming years, these findings can give a clear insight to new metabolic targets, combination treatments, and ultimately using inhibitors combinations to treat patients in the clinic. Because these cancers are on the skin and likely visible, topical treatments with these

inhibitors in a gel or lotion can specifically treat the cancer without too much worry of normal cells being drastically targeted. Another approach to establish these future goals is collaborating with laboratories that can do high throughput drug screenings to test multiple combinations of inhibitors. An effective way to study this can be by generating three-dimensional organoid models derived from human cancers, primarily SCC and melanoma, and testing our metabolic inhibitor combinations on these. Ultimately this can then be translated to other different types of cancers to understand how universal these targets are. The media in which these organoids is extremely important when addressing these questions of flexibility and effectiveness of inhibitors. Many medias contain high glucose concentrations and either no or low levels of glutamine or lactate. Organoids will ideally first need to be cultured and adapted to a system where all nutrients are present, and then treated with inhibitors to determine if cells adapt to single to double metabolic manipulation.

REFERENCES

1) M. Momcilovic, S. T. Bailey, J. T. Lee, M. C. Fishbein, D. Braas, J. Go, T. G. Graeber, F. Parlati, S. Demo, R. Li, T. C. Walser, M. Gricowski, R. Shuman, J. Ibarra, D. Fridman, M. E. Phelps, K. Badran, M. St John, N. M. Bernthal, N. Federman, J. Yanagawa, S. M. Dubinett, S. Sadeghi, H. R. Christofk, D. B. Shackelford, The GSK3 signaling axis regulates adaptive glutamine metabolism in lung squamous cell carcinoma. *Cancer Cell* **33**, 905–921 e905 (2018).
2) M. Momcilovic, D. B. Shackelford, Dual targeting of EGFR and glutaminase in lung cancer. *Mol. Cell. Oncol.* **5**, e1297883 (2018).
3) M. Momcilovic, S. T. Bailey, J. T. Lee, M. C. Fishbein, C. Magyar, D. Braas, T. Graeber, N. J. Jackson, J. Czernin, E. Emberley, M. Gross, J. Janes, A. Mackinnon, A. Pan, M. Rodriguez, M. Works, W. Zhang, F. Parlati, S. Demo, E. Garon, K. Krysan, T. C. Walser, S. M. Dubinett, S. Sadeghi, H. R. Christofk, D. B. Shackelford, Targeted inhibition of EGFR and glutaminase induces metabolic crisis in EGFR mutant lung cancer. *Cell Rep.* **18**, 601–610 (2017).
4) W. Yu, X. Yang, Q. Zhang, L. Sun, S. Yuan, Y. Xin, Targeting GLS1 to cancer therapy through glutamine metabolism. *Clin. Transl. Oncol.* **23**, 2253–2268 (2021).
5) R. Rais, K. M. Lemberg, L. Tenora, M. L. Arwood, A. Pal, J. Alt, Y. Wu, J. Lam, J. M. H. Aguilar, L. Zhao, D. E. Peters, C. Tallon, R. Pandey, A. G. Thomas, R. P. Dash, T. Seiwert, P. Majer, R. D. Leone, J. D. Powell, B. S. Slusher, Discovery of DRP-104, a tumor-targeted metabolic inhibitor prodrug. *Sci. Adv.* **8**, eabq5925 (2022).
6) Y. Yokoyama, T. M. Estok, R. Wild, Sirpiglenastat (DRP-104) induces antitumor efficacy through direct, broad antagonism of glutamine metabolism and stimulation of the innate and adaptive immune systems. *Mol. Cancer Ther.* **21**, 1561–1572 (2022).
7) Ma, G., Zhang, Z., Li, P. *et al.* Reprogramming of glutamine metabolism and its impact on immune response in the tumor microenvironment. *Cell Commun Signal* **20**, 114 (2022).

APPENDIX

Materials and Methods

Animals

Chapter 2 and 3: All animal experiments and related procedures were performed and maintained in accordance with protocols set forth and approved by University of California, Los Angeles (UCLA) Animal Resource Committee and the Institutional Animal Care and Use Committee at UCLA in facilities run by the UCLA Department of Laboratory Animal Medicine. Animal strains came from the Jackson Laboratory (K15-CrePR, GLS1 fl/fl, LDHA fl/fl, and MPC1 fl/fl).

Chapter 4: All animals were maintained in UCLA's division of Laboratory Medicine (DLAM)-approved pathogen-free facilities and procedures were performed according to the UCLA Animal Research Committee. TyrCreERT2; BRAFV600E/+; Pten+/- and Rosa26tdtomato mice on C57BL/6J background were obtained from Jackson laboratories. Mpc1 flox mice were obtained from Rutter lab. They were crossed to obtain the following genotypes: TyrCreERT2; BRAFV600E; Pten -/-; Mpc1 f/+; Rosa26td-tomato (Mpc1 WT) and TyrCreERT2; BRAFV600E/+; Pten -/-; Mpc1f/f; Rosa26td-tomato (Mpc1 KO). Cre-loxP recombination of floxed sites was induced by intraperitoneal injection of Tamoxifen (Sigma, T5648) prepared in corn oil (Sigma, C8267). Animals were treated with 2 mg Tamoxifen daily for 5 consecutive days.

Primary Cells and Cell Lines

Chapter 4: Melanoma cells were isolated from primary skin tumors of mice and cultured in 2D conditions. For this, tumors were dissected from skin of mice, cut into small pieces with scissors, and incubated in 1.5 mL of 5mg/ml 1:1 Collagenase I/IV mixture for 45 minutes in 5% CO_2 at 37°C. The cells were centrifuged for 5 minutes at 1100 rpm with wash buffer consisting of, 10X Hanks Balanced Salt Solution (Gibco; 14025092) and 20% FBS. The supernatant was discarded and cells were incubated in 2 mL of cell dissociation buffer (Gibco; 13150016) for 10

minutes in 5% CO_2 at 37°C. The cells were aspirated with an 18G syringe various times and then centrifuged at 1100 rpm for 5 minutes with wash buffer. The supernatant was discarded, medium was added, and the cells were counted with hemocytometer and trypan blue. Cells were plated at 1,000,000 cells per well (GenClone 25-105) and fed every other day. Medium consists of Ham's F-12 (Gibco; 11765054), 10% FBS, and 1mL of Primocin (Invivogen, NC9392943).

Growth Rate Experiments

Chapter 4: Cells were counted with a hemocytometer and trypan blue and seeded at 50,000 cells/well (GenClone 25-105). The following day 2-3 wells were trypsinized for 5 minutes, centrifuged for 5 minutes at 1100 rpm with media, and counted to obtain the initial cell seeding. Cells were discarded. Four days later the remaining wells were trypsinized, centrifuged for 5 minutes at 1100 rpm with media, and counted to obtain the final cell count. The following equations were used to obtain growth rate and fold change [Fold Change (4 days)= (Cf - Ci)/ Ci] [Growth Rate (k): ln(Cf/Ci)= k (Tf-Ti)]. Data were analyzed in Microsoft Excel, formatted in GraphPad Prism, and error bars represent ±SEM. An unpaired, two-tailed student's t-test determined significance, with $P < 0.05$ considered statistically significant, denoted by $*P < 0.05$ and $**P < 0.01$.

Two-stage tumorigenesis in mouse skin

Chapter 2 and 3: Tumors were induced on genetically engineered mice using K15-CrePR animals floxed for either GLS or GLS and LDHA by a cutaneous two-stage skin chemical carcinogenesis. Transgenic animals were shaved and treated with mifepristone (200 µl of 10 mg/ml dissolved in filtered sunflower seed oil) daily for 3 days by intraperitoneal injection to delete GLS or GLS and LDHA. After 1 week of treatment with mifepristone, mice were topically treated with a tumor-initiating agent, DMBA (400 nmol dissolved in acetone). After 1 week of

DMBA application, mice were topically treated with a tumor growth–promoting agent, TPA (20 nmol dissolved in 100% ethanol), twice a week 3 to 4 days apart until time of harvest and 25 to 35 weeks after the initial DMBA treatment. Papilloma began to form 10 to 20 weeks post-DMBA treatment, and SCCs began to form 20 to 35 weeks post-DMBA treatment.

Histology, immunofluorescence, IHC, and immunoblotting

Chapter 2-4: Tumors were harvested from dorsal skin for each indicated genotype and embedded in unfixed optimal cutting temperature (OCT) compound. Tumors in OCT were cut at 10 μm on a Leica 3200 Cryostat for immunostaining and hematoxylin and eosin staining. For immunofluorescence staining, slides were briefly fixed in 10% buffered formalin and washed in phosphate-buffered saline (PBS) twice for 10 min. Slides were blocked with 10% goat serum/0.25% Triton X-100 for 1 hour at room temperature while rotating. Primary antibodies were diluted into blocking buffer, added to samples, and incubated overnight. The next day, slides were washed in PBS/Tween. Secondary antibodies were added at 1:500 dilution and were incubated on slides rotating at room temperature for 1 hour. Slides were then washed in PBS/Tween, mounted with Prolong Gold with 4′,6-diamidino-2-phenylindole (DAPI; Invitrogen), and sealed with clear nail polish. IHC was performed on formalin-fixed paraffin-embedded tissue sections. Slides underwent antigen retrieval with citrate, were incubated in hydrogen peroxide for 30 min at 4°C, blocked with 10% goat serum/0.25% Triton X-100 for 1 hour at room temperature, and incubated with primary antibodies overnight. For detection, we used a secondary horseradish peroxidase–labeled polymer (Dako) and 3-amino-9-ethylcarbazole (AEC) Substrate Chromogen (Vector Laboratories). For Western blot, the total protein concentration was determined using the bicinchoninic acid (BCA) assay kit (Pierce) per the manufacturer's protocol with a microplate reader. Ten micrograms of protein was loaded per well for each tumor lysate. Gel was run, transferred, and blocked in 3% BSA. Primary antibodies were diluted in 3% BSA and incubated in membrane overnight. Membrane was washed,

incubated with goat anti-rabbit immunoglobulin G (H+L) secondary antibody (horseradish peroxidase; 1:20,000), and imaged using the SuperSignal West Pico PLUS Chemiluminescent Substrate. Table 1 lists the primary antibodies used for immunofluorescence (IF), IHC, and Western blot (WB):

TABLE 1: Antibodies used for IF, IHC, and WB.

Antibody	Source	Identifier	Technique
anti-rabbit KGA/GAC (GLS)	Proteintech	Cat #: 12855-1-AP	IF
anti-chicken KERATIN5	Biolegend	Cat #: 905901	IF
anti-rabbit CD45	abcam	ab10558	IF
anti-rat CD11b [M1/70]	abcam	ab197701	IF
anti-rabbit MCT1	Proteintech	Cat #: 20139-1-AP	IF
anti-rabbit MCT4	Proteintech	Cat #: 22787-1-AP	IF
anti-rabbit GLUT1 [EPR3915]	abcam	ab115730	IF, IHC
anti-rabbit TXNIP	Invitrogen	Cat #: yf3950376A	IHC
anti-rabbit ASCT2 (V501)	Cell Signaling	Cat #: 5345	IF
anti-rabbit EGFR (pY1068) [EP774Y]	abcam	ab40815	IF
anti-rat Ki67	eBioscience	Cat #: 41-5698-82	IF
anti-rabbit Cleaved-Caspase-3	Cell Signaling	Cat #: 9661S	IF
anti-rabbit p38 MAPK (pT180/pY182) (D3F9)	Cell Signaling	Cat #: 4511	WB
anti-rabbit AKT1 (pS473) + AKT2 (pS474) + AKT3 (pS472)	abcam	ab192623	WB, IF

anti-rabbit GSK-3β (pS9) (5B3)	Cell Signaling	Cat #: 9323	WB
anti-rabbit c-Jun (pS73) (D47G9)	Cell Signaling	Cat #: 3270	WB
anti-rabbit MEK1/2 (pS221) (166F8)	Cell Signaling	Cat #: 2338	WB
anti-rabbit ERK1 (pT202) + ERK2 (pT185)	abcam	ab201015	WB, IF
anti-rabbit STAT3 (pY705)	abcam	ab76315	WB
anti-rabbit CREB (pS133) (87G3)	Cell Signaling	Cat #: 9198	WB
anti-rabbit β-actin	abcam	ab8227	WB
anti-goat tdTomato	Arigo	ARG55724	IF
anti-rabbit Melanoma gp100 [EP4862(2)]	abcam	ab137078	IF
anti-rabbit MCM2	abcam	ab4461	IF
anti-rabbit Sox10 (H-140)	Santa Cruz	sc48824	IF
anti-rabbit S100	abcam	ab52642	IF
GAPDH	Cell Signaling	Cat #: 5174P	WB
anti-rabbit Mpc1	Cell Signaling	Cat #: 14462	WB

Tracing with $^{13}C_6$-d-glucose, $^{13}C_5$-l-glutamine, and $^{13}C_3$-sodium-l-lactate *in vivo*

Chapter 2: Before euthanasia, mice were intraperitoneally infused with $^{13}C_6$-d-glucose (Cambridge Isotope Laboratories, PR-31904), $^{13}C_5$-l-glutamine (Cambridge Isotope Laboratories, PR-30230), and $^{13}C_3$-sodium-l-lactate (Cambridge Isotope Laboratories, PR-31355) label for 10 min. $^{13}C_6$-d-glucose was infused at 2 g/kg, $^{13}C_5$-l-glutamine at 0.3 mg/g, and $^{13}C_3$-sodium-l-lactate at 200 µl of solution. After 10 min of tracing, tissues were dissected

within 3 to 5 min for metabolite extraction. Pulse labeling data represent fractional contribution of metabolites.

Metabolite extraction *in vivo*

Chapter 2: These experiments were performed as previously described in Flores *et al.* Nature Communications, 2019. Briefly, <8 mg of fresh tumors was momentarily rinsed in cold 150 mM ammonium acetate (pH 7.3) and then added into 1 ml of a cold solution of 80% methanol with 10 nM trifluoromethanosulfanate. Tumors samples were homogenized with a tissue homogenizer (BeadBug6 model: D1036, 5 cycles, 4000 speed, 30 times) for full homogenization. After removing insoluble material by centrifugation at 17,000*g* at 4°C for 10 min, the supernatant was added into a glass vial, and metabolites were dried down under vacuum or an EZ-2Elite evaporator. Mass spectrometry was performed as previously described in Flores *et al.* Nature Communications, 2019. Cell pellets were resuspended in radioimmunoprecipitation assay buffer (Pierce) with Halt protease and phosphatase inhibitors (Thermo Fisher Scientific) on ice. After removing insoluble material by centrifugation at 8000*g* at 4°C for 5 min, total protein concentration was determined using the BCA assay kit (Pierce) per the manufacturer's protocol with a microplate reader.

Metabolite extraction *in vitro*

Chapter 4: Cells were seeded in 6-well plates. For labeling and glucose consumption experiments, the media was replaced with DMEM containing 10 mM U-13C-gluose (Cambridge Isotypes), 10mM U-12C - glutamine and 10% dialyzed FBS 24h after seeding. The metabolites were extracted after 24h incubation in labeling media at 70-80% confluence. The labeling media was added to additional empty wells (without cells) for glucose consumption experiment. For metabolite extraction, the wells were washed twice with ice-cold 150 mM ammonium acetate, ph=7.3. 500 µl 80% methanol was added to each well and incubated at -80°C for 20 minutes.

The cells were scraped off the plate, vortexed and centrifuged at maximum speed. The resulting supernatant was dried under vacuum and dried metabolites were kept at -80°C until mass spectrometry analysis. Dried metabolites were reconstituted in 100µl of a 50% acetonitrile (ACN) 50% dH2O solution. Samples were vortexed and spun down for 10 minutes at >17,000g. 70 µl of the supernatant was then transferred to HPLC glass vials. 10 µl of these metabolite solutions were injected per analysis. Samples were run on a Vanquish (Thermo Scientific) UHPLC system with mobile phase A (20 mM ammonium carbonate) and mobile phase B (100% ACN) at a flow rate of 150 µl/min on a SeQuant ZIC-pHILIC polymeric column (2.1 3 150 mm 5 mm,EMD Milipore) at 35°C. Separation was achieved with a linear gradient from 20% A to 80% A in 20 min followed by a linear gradient from 80% A to 20% A from 20 min to 20.5 min. 20% A was then held from 20.5 min to 28 min. The UHPLC was coupled to a Q-Exactive (Thermo Scientific) mass analyzer running in a polarity switching mode with spray-voltage=3.2 kV, sheatgas=40, aux-gas=15, sweep-gas=1, aux-gas-temp=350°C and capillary-temp=275°C. For both polarities mass scan settings were kept at full-scan-range=(70-1000), ms1-resolution =70,000, max-injectiontime=250ms, and AGC-target=1E6. MS2 data was also collected from the top three most abundant singly-charged ions in each scan with normalized-collision-energy=35. Each of the resulting ‘’.RAW’’ files was then centroided and converted into two ‘’.mzXML’’ files (one for positive scans and one for negative scans) using msconvert from ProteoWizard. These ‘’.mzXML’’ files were imported into the MZmine 2 software package. Ion chromatograms were generated from MS1 spectra via the built-in Automated Data analysis pipeline (ADAP) chromatogram module and peaks were detected via the ADAP wavelets algorithm. Peaks were aligned across all samples via the Random sample consensus aligner module, gap-filled, and assigned identities using an exact mass MS1(+/-15ppm) and retention time RT (+/-0.5 min) search of our in house MS1-RT database. Peak boundaries and identifications were then further refined by manual curation. Peaks were quantified by area under the curve integration and exported as CSV files. If stable isotope tracing was used in the

experiment, the peak areas were additionally processed via the R package AccuCor 2 to correct for natural isotope abundance. Peak areas for each sample were normalized by the measured area of the internal standard trifluoromethanesulfonate (present in the extraction buffer) and by the number of cells present in the extracted well.

GLS activity assay

Chapter 2: Activity of GLS was measured by using a GLS activity fluorometric assay kit (Biovision, K455) according to the manufacturer's instructions.

FDG-PET imaging and analysis

Chapter 3 and 4: Small-animal PET/computed tomography scans were performed and analyzed as we described in Flores et al. 2019 on SCC mice., Standardized uptake value (SUV) was calculated using %ID/g. ID, injected dose. %ID/g = (SUV divided by animal weight in grams) × 100. Melanoma mice were fasted for 4h prior to procedure. They were placed on a heating pad and anesthetized with 1.5% vaporized isoflurane and injected with the [18F]-FDG via tail vein. Following 1-hour unconscious uptake, mice underwent micro-PET imaging (15 min static data acquisition) immediately followed by micoCT imaging using the Genisys8 PET/CT scanner (Sofie Biosciences). PET data was decay corrected, and attenuation correction was performed using the CT images. Co-registered PET/CT data were analyzed and quantified by drawing 3D regions of interest (ROI) using the AMIDE software.

Tumor quantification and scoring

Chapter 2 and 3: Each tumor developed was tracked over time, and fate was determined on the basis of appearance and histology of tumor. Tumors were scored using the following scoring system: 0 = papilloma regression; 1 = papilloma formation; 2 = papilloma grows; 1 = papilloma

gets smaller; 3 = papilloma turns into SCC; 4 = SCC grows; 3 = SCC gets smaller. Slope of each tumor score over time was quantified and noted as tumor rate.

Topical inhibitor treatments

Chapter 2 and 3: AZD0095 (MedChemExpress) was dissolved in dimethyl sulfoxide, and mice were treated at 10 times the maximal inhibitor concentration to penetrate the *in vivo* epidermal barrier. Inhibitor working solutions were then mixed into TPA and applied dorsally twice a week.

Statistics and reproducibility/statistical analysis

Chapter 2-4: All animals used come from a mixed C57BL6/FVB background with no preference in mouse gender for any studies. There was no statistical measure used beforehand to determine sample size. Data were analyzed in Microsoft Excel and GraphPad Prism, and error bars represent SD between two groups performed by a two-tailed *t* test analysis. Statistical significances were considered if $*P < 0.05$, $**P < 0.01$, and $***P < 0.001$. Sample size and statistical details can be found in the figure legends.